UNIVERSITY OF LONDON THESIS

Degree ᴘʰᴅ   Year 2006   Name of Author Gonzalez-Thomson

COPYRIGHT
This is a thesis accepted for a Higher Degree of the University of London. It is an unpublished typescript and the copyright is held by the author. All persons consulting the thesis must read and abide by the Copyright Declaration below.

COPYRIGHT DECLARATION
I recognise that the copyright of the above-described thesis rests with the author and that no quotation from it or information derived from it may be published without the prior written consent of the author.

LOANS
Theses may not be lent to individuals, but the Senate House Library may lend a copy to approved libraries within the United Kingdom, for consultation solely on the premises of those libraries. Application should be made to: Inter-Library Loans, Senate House Library, Senate House, Malet Street, London WC1E 7HU.

REPRODUCTION
University of London theses may not be reproduced without explicit written permission from the Senate House Library. Enquiries should be addressed to the Theses Section of the Library. Regulations concerning reproduction vary according to the date of acceptance of the thesis and are listed below as guidelines.

A.   Before 1962. Permission granted only upon the prior written consent of the author. (The Senate House Library will provide addresses where possible).

B.   1962 - 1974. In many cases the author has agreed to permit copying upon completion of a Copyright Declaration.

C.   1975 - 1988. Most theses may be copied upon completion of a Copyright Declaration.

D.   1989 onwards. Most theses may be copied.

This thesis comes within category D.

☑ This copy has been deposited in the Library of ___UCC___

☐ This copy has been deposited in the Senate House Library, Senate House, Malet Street, London WC1E 7HU.

The Role of Corner Angle

in Visual Physiology

and Brightness Perception

by

Xoana González Troncoso

B.Sc. Physics
Universidade de Santiago de Compostela (Spain) 2000

Gatsby Computational Neuroscience Unit
University College London
17 Queen Square
London WC1N 3AR, United Kingdom

THESIS

Submitted for the degree of Doctor of Philosophy
University of London

2006

UMI Number: U592849

UMI

Dissertation Publishing

ProQuest

Abstract

How do corners of different angles affect visual physiology and brightness processing in the brain? Some visual illusions show that corners can be more salient perceptually than edges, even when their physical luminance is equivalent. Combining several techniques (computational modeling, human psychophysics, and human fMRI) we have studied the relationship between corner angle, brightness perception, and visual physiology. Our psychophysical results show that corners appear quantifiably brighter for sharp than for shallow angles, and that the perceived brightness of the corner is linearly correlated to the corner's angle. Basic linear models of center-surround receptive fields predict the main result from the psychophysical experiments (that is, that sharp corners are brighter/more salient than shallow corners). Thus our data suggest that corners start to be processed from the very first stages of the visual system. Our human fMRI experiments furthermore show that BOLD signal response to corners increases parametrically with angle sharpness in all the retinotopic areas of the visual cortex, suggesting a general principle for corner processing throughout the visual hierarchy.

Acknowledgments

Contents

1. Chapter 1.

General Introduction

1.1. Visual system hierarchy

The process of "seeing" is complex and not well understood. What we do know is that neurons in the early visual system change their activity in response to stimuli with specific attributes (such as color, shape, brightness, etc) within a small range of visual space. The receptive field of a visual neuron is the area of the visual scene (or its corresponding region on the retina) that when stimulated (by light or electrical impulses) can influence the response of the neuron. Illumination outside the receptive field produces no effect on firing. Strictly defined "the term receptive field refers to the specific receptors that feed into a given cell in the nervous system, with one or more synapses intervening" (Hubel, 1995). Sherrington introduced the term "receptive field" in relation to reflex actions (Sherrington, 1906) and Hartline first applied it to the visual system (Hartline, 1940). Receptive fields at different stages in the visual system have different structure and properties. Studying the neuronal connectivity that gives rise to these different receptive fields will give us some insight into the role of specific circuits in visual processing. For instance, some early receptive fields have a spatial substructure while others do not. Stimulating different regions of these receptive fields can give rise to increases or decreases in neural activity. The interaction between the receptive field substructure and stimuli of

different types most likely underlies visual perception. Understanding the structure of the receptive field of a given neuron is therefore crucial to understanding and predicting the responses of a neuron to a given stimulus.

The responses of some cells can be modulated in a selective way by contextual stimuli lying far outside the classical receptive field (Blakemore and Tobin, 1972; Nelson and Frost, 1978; Allman et al., 1985; Gilbert and Wiesel, 1990; Levitt and Lund, 1997; Walker et al., 1999; Angelucci et al., 2002). Some of the extra-classical receptive field effects are suppressive. Several groups have proposed divisive models, in which the classical receptive field feeds into the numerator and the denominator is provided by a larger suppressive field. The classical receptive field would provide the basic selectivity for stimulus properties, whereas the suppressive field would modulate the responsiveness of the neuron (Levick et al., 1972; Albrecht and Geisler, 1991; Heeger, 1992; Carandini et al., 1997; Cavanaugh et al., 2002; Carandini, 2004; Bonin et al., 2005)

1.1.1 Retina

1.1.1.1 Anatomy

Vision starts in the retina: it is here where photons are first converted into electrical signals, and then into a series of neural responses interpreted by the brain to then construct our perception of the visual world.

The retina has the shape of a bowl (about 0.4mm thick in adult humans). It is a very well organized structure that has three main layers (called the nuclear layers) of neuronal bodies. These layers are separated by two layers containing synapses made by the axons and dendrites of these neurons (called the plexiform layers). The basic retinal cell classes and their interconnections were revealed by Ramón y Cajal over a century ago (Ramón y Cajal, 1893) (**Figure 1**).

A

Photoreceptor
layer

Outer plexiform
layer

Inner nuclear
layer

Inner plexiform
layer

Ganglion cell
layer

B
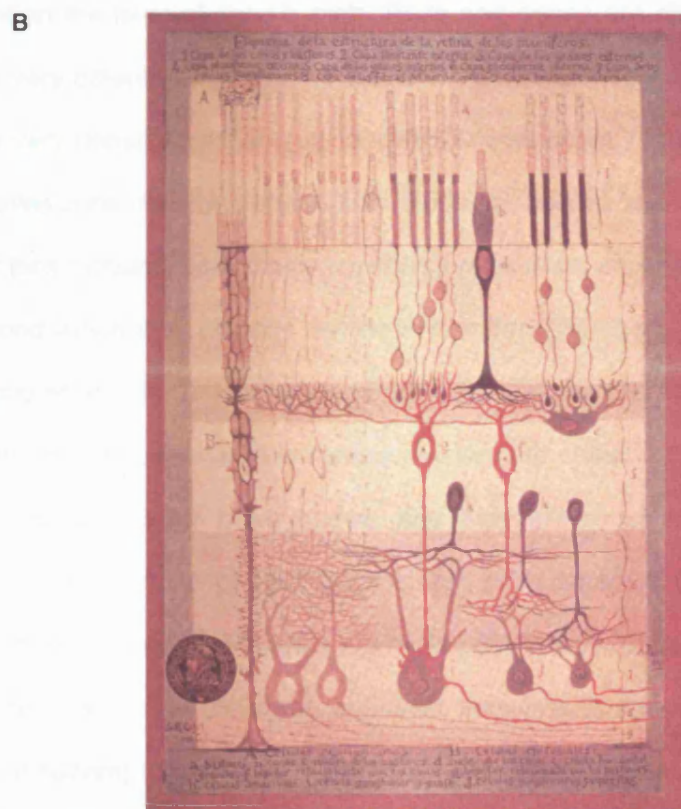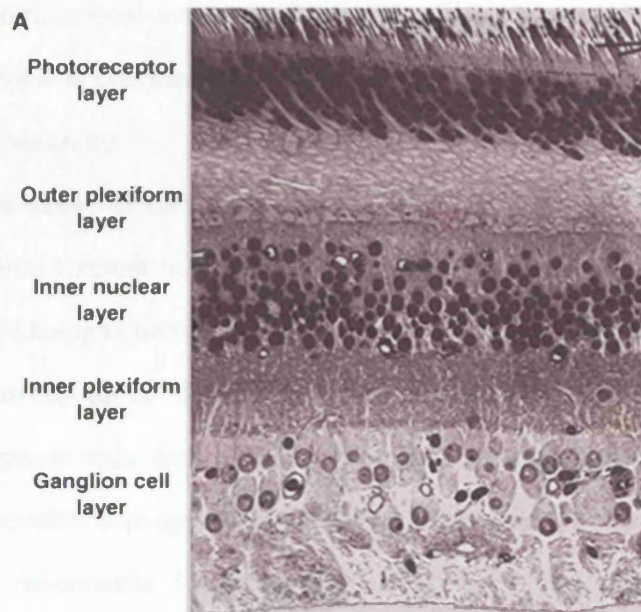
Figure 1. Retinal layers. **(A)** Light micrograph of a vertical section of the human retina from Boycott and Dowling (1969). **(B)** Cross-sectional microscopic drawing by Ramón y Cajal (reproduced from Hubel, 1995)

The functional anatomy of the retina is enormously rich and complicated. A short overview is provided here, to set a basis to understand the next few stages of the visual hierarchy.

The three nuclear layers are the photoreceptor layer (which lies on the back on the retina, furthest from the light coming in), the inner nuclear cell layer (in the middle) and the ganglion cell layer (nearest to the center of the eye).

Photoreceptor layer: light is transduced into electrical signals by photoreceptors: rods and cones. Cones are not sensitive to dim light, but under photopic conditions (bright light) they are responsible for fine detail and color vision. Rods are responsible for our vision under scotopic conditions (dim light), and saturate when the level of light is high. Rods and cones are distributed across the retina with very different profiles: in the fovea, where our fine vision is most detailed, cones are very densely packed (up to 160,000 cones/mm^2) but as we move away from the fovea cone density drops rapidly. Rods are absent from the fovea (Schultze, 1866), but their density rises quickly to reach a peak at an eccentricity between 5 and 7mm, beyond which they steadily decline in number (Østerberg, 1935; Curcio et al., 1987; Curcio et al., 1990). Humans have one type of rod and three types of cones. The 3 types of cones, responsible for color vision, are called L (or red) cones, M (or green) cones, and S (or blue) cones, and they are most sensitive to different segments of the spectrum of light: L cones are most sensitive to long wavelengths (peak sensitivity at 564nm), M cones are most sensitive to middle wavelengths (peak sensitivity at 533nm) and S cones are most sensitive to short wavelengths (peak sensitivity at 437nm) (Brown and Wald, 1963, 1964; Marks et al., 1964). L, M, and S cones are distributed in the retina in a particular way: only 10% of the cones are S cones, and they are absent from the fovea. Although L cones and M cones are randomly intermixed, there are ~2 times more L cones than M cones (Ahnelt et al., 1987; Cicerone and Nerger, 1989; Curcio et al., 1991; Mollon and Bowmaker, 1992; Roorda and Williams, 1999).

Inner nuclear layer: contains three classes of neurons: horizontal cells, bipolar cells, and amacrine cells. Horizontal cells have their bodies in the inner nuclear layer and connect to photoreceptors (through chemical synapses) and other horizontal cells (through gap junctions) in the outer plexiform layer (Wässle and Boycott, 1991). Horizontal cells receive input from photoreceptors, but they also give output to the same photoreceptors, providing lateral inhibition, which acts to enhance spatial differences in photoreceptor activation at the level of the bipolar cells (Dacey, 1999; Verweij et al., 1999). There are over 13 different types of bipolar cells (Boycott and Wassle, 1991; Kolb et al., 1992) and all of them have some dendritic processes in the outer plexiform layer, the soma in the inner nuclear layer and some axon terminals in the inner plexiform layer (Dowling and Boycott, 1966). The dendritic processes of a bipolar cell receive input from one type of photoreceptor (either from cones or from rods, but never from both) (Rodieck, 1998). Each bipolar cell then conveys its response to the inner plexiform layer, where it contacts both amacrine and ganglion cells (Dacey, 1999). Amacrine cells (over 30 different types), receive input from bipolar cells and other amacrine cells, and pass their messages onto bipolar cells, other amacrine cells, and ganglion cells (MacNeil and Masland, 1998; Dacey, 2000). Different types of amacrine cells may have different functions in retinal processing, but their specific roles remain unknown for the most part.

Ganglion cell layer: there are more than 20 different ganglion cell types (Kolb et al., 1992), and many of them are specialized on coding some particular aspect of the visual world such as contrast, color, movement... (Rodieck, 1998). Ganglion cells receive their input from amacrine and bipolar cells, and send their outputs to the brain (through the optic nerve) in the form of action potentials. These are the first cells in the visual pathway that produce action potentials (all-or-none) as their output; all the previous cell classes (photoreceptors, horizontal, bipolar and amacrine cells) release their neurotransmitters in response to graded potentials. Even though there are over 20 different types of ganglion cells, 2 of them account for

almost 80% of the ganglion cell population (Perry et al., 1984): the midget and the parasol ganglion cells, named by Polyak (1941). Near the fovea each midget ganglion cell receives direct input from only one midget bipolar cell (Kolb and Dekorver, 1991; Kolb and Marshak, 2003) and thus has a very small and compact receptive field (it collects input from a small number of cones). Parasol cells receive their direct input from diffuse bipolar cells, have larger dendritic fields, and thus receive input from many more cones (Watanabe and Rodieck, 1989). The dendritic field size increases with eccentricity for both types of cells (Watanabe and Rodieck, 1989; Dacey and Petersen, 1992; Dacey, 1993). Away from the fovea, the increase in dendritic field size with retinal eccentricity is more or less matched by a decrease in spatial density, so the amount of retina covered is approximately constant over most of the retina (Watanabe and Rodieck, 1989).

1.1.1.2 Physiology & Receptive Fields

The receptive fields of ganglion cells in the retina are approximately circular and have functionally distinct central and peripheral regions (called center and surround); stimulation of these two regions produces opposite and antagonistic effects upon the activity of the ganglion cells. Hartline first described retinal ganglion cell receptive fields as concentric using frog optic nerve recordings (Hartline, 1940). Kuffler recorded from ganglion cells in the cat's retina and was the first to report and fully characterize ganglion cells in mammals (Kuffler, 1952, 1953). Hubel and Wiesel found that optic nerve receptive fields in the spider monkey were very similar to the receptive fields of cat retinal ganglion cells (Hubel and Wiesel, 1960). Ganglion cells respond optimally to differential illumination of the receptive field center and surround. Diffuse illumination of the whole receptive field produces only weak responses. There are two main types of center-surround receptive fields: on-center receptive fields respond best to light falling on the center, and darkness falling on the surround; off-center receptive fields respond best to darkness on the center and light

on the surround (**Figure 2**). The properties of center-surround receptive fields change during scotopic conditions: the size of the receptive field center usually increases, the surround strength diminishes and there is a longer latency for the response (Barlow et al., 1957; Donner and Reuter, 1965; Masland and Ames, 1976; Bowling, 1980; Peichl and Wassle, 1983; Muller and Dacheux, 1997).
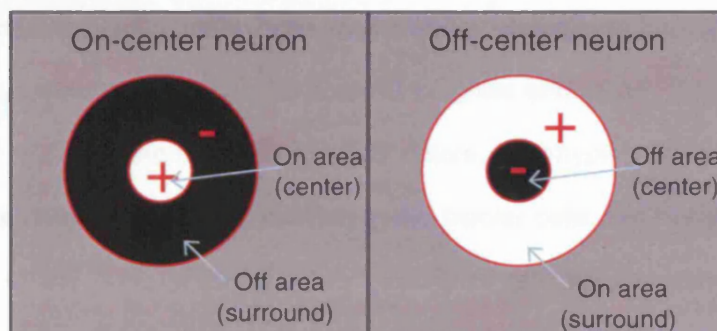
Figure 2. Concentric receptive fields of retinal ganglion neurons.

Once the center-surround receptive fields of ganglion cells were discovered and characterized, an important line of research was launched to discover the neural circuitry giving rise to the center-surround organization of receptive fields. Did bipolar cells also have center-surround receptive fields? If so, ganglion cells may just be inheriting this property from bipolar cells, and the underlying circuitry should be found earlier in the visual pathway.

Werblin and Dowling (Werblin and Dowling, 1969), and Kaneko (Kaneko, 1970) discovered, using intracellular recordings, that bipolar cells also have center-surround receptive fields. Therefore, center-surround receptive fields were presumed to be built-up in the previous synapse, where photoreceptors, horizontal cells and bipolar cells interact. The fact that there are on-center and off-center bipolar cells was also presumed to be explained at the level of this synaptic connection in the outer plexiform layer.

In the dark, photoreceptors are depolarized and continuously active (Trifonov, 1968), releasing glutamate to bipolar and horizontal cells. When light arrives and the photopigments bleach within a photoreceptor, that photoreceptor hyperpolarizes, and

the amount of glutamate released decreases in a graded manner, as a function of the amount of photons (Tomita, 1965). All photoreceptors use the same neurotransmitter, glutamate, and so on-center and off-center bipolar cells acquire their preference by having one of two types of glutamate receptor (Miller and Slaughter, 1986):

- On-center bipolar cells have metabotropic receptors that make the cell hyperpolarize when they receive glutamate (Slaughter and Miller, 1981; Nawy and Copenhagen, 1987). When light hits photoreceptors, they hyperpolarize and release less glutamate. This reduces the inhibition in the bipolar cells that therefore increase their activity. In the dark, photoreceptors depolarize and release more glutamate. Therefore the bipolar cells hyperpolarize.

- Off-center bipolar cells have ionotropic receptors that depolarize the cell when receiving glutamate (Nelson and Kolb, 1983; Slaughter and Miller, 1983). In this case, when light arrives to the retina, the photoreceptors hyperpolarize and release less glutamate. Consequently, the bipolar cells decrease their activity. In the dark, the photoreceptors depolarize and release more glutamate. As a consequence, the bipolar cells depolarize.

Both on- and off- bipolar cells make the same kind of contacts in the inner plexiform layer. All bipolar cells release glutamate as their neurotransmitter and all the ganglion cells have ionotropic receptors: therefore, ganglion cells that receive input from on-center bipolar cells are also on-center. Ganglion cells that receive input from off-center bipolar cells are off-center (Rodieck, 1998). In 1978 Nelson et al. discovered that there is a clear anatomical difference between on- and off- bipolar cells: they synapse onto ganglion and amacrine cells within different sublayers within the inner plexiform layer. The off-center bipolar dendrites make synapses closer to the inner nuclear layer whereas the on-center bipolar dendrites terminate closer to the ganglion cell layer (Nelson et al., 1978; Dacey et al., 2000).

The mechanism to construct the surround of the bipolar receptive field is not totally understood, but it is thought that horizontal cells are at least partly responsible, providing lateral inhibition to a large number of photoreceptors. It seems that the receptive field center of bipolar or ganglion cells results from the summed contributions of the photoreceptors in the absence of the influence of the horizontal cells. The receptive field surround would be the result from the action of horizontal cells on the same group of photoreceptors. There may also be an amacrine cell contribution to the surround, but not much is known about it (Rodieck, 1998; Dacey, 1999).

As described in **section 1.1.1.1** there are two predominant types of ganglion cells: midget and parasol (Polyak, 1941). Both types of ganglion cells have center-surround receptive fields with similar spatial organization, but physiological studies have described several differences between them: parasol cells respond more transiently to light onset or offset than midget cells (Gouras, 1968); parasol cells have larger receptive fields centers than midget cells at the same eccentricity (De Monasterio and Gouras, 1975); most midget cells have spectral selectivity and antagonism while most parasol cells do not (De Valois, 1960; Gouras, 1968; De Monasterio and Gouras, 1975); parasol cells respond much more vigorously than midget cells to small changes in luminance contrast (Kaplan and Shapley, 1986). The anatomical and functional differences between midget and parasol cells lead to two different visual pathways that keep segregated throughout the early visual system. The parvocellular pathway starts with the midget cells and it is very sensitive to color and spatial frequency. The magnocellular pathway starts with the parasol cells and it is most sensitive to luminance contrast and temporal frequency.

What information do the retinal ganglion cells send through the optic nerve? Due to the center-surround organization of their receptive fields, these neurons are quite insensitive to changes in overall levels of luminance. They signal differences within their receptive fields by comparing the degree of illumination between the

center and the surround. Meister and collaborators have shown that retinal ganglion neurons tend to fire synchronously and that the firing patterns represent specific messages about the visual stimulus that differ significantly from what one would derive by single-cell analysis. For example, synchronous spikes from ganglion cells may provide higher visual areas with a finer degree of spatial resolution than would be provided by spikes from individual neurons (Meister et al., 1995; Meister and Berry, 1999; Schnitzer and Meister, 2003).

1.1.2 LGN

All retinal ganglion cells send their axons to the brain via the optic nerve. Half of the axons decussate at the optic chiasm, so information from each temporal visual hemifield is sent to the contralateral hemisphere only. Retinal ganglion cells project to three major subcortical targets: the pretectum, the superior colliculus, and the lateral geniculate nucleus (LGN) of the thalamus. The LGN is the principal structure that sends visual information to the visual cortex. 90% of retinal ganglion cell axons terminate in the LGN. These projections happen in an orderly manner preserving the topographic representation of the visual word in the retina. Therefore, neighboring neurons in the LGN will be stimulated by adjacent regions in visual space. This property is called retinotopic organization.

In primates, the LGN contains 6 layers of cell bodies that can be classified in two groups according to their histological characteristics: the two bottom layers (ventral) contain large cell bodies and are called magnocellular layers; cells in the four upper layers (dorsal) are smaller and are called the parvocellular layers. The parvocellular layers receive their main inputs from the midget ganglion cells in the retina. The magnocellular layers receive their main inputs from parasol ganglion cells (Schiller and Malpeli, 1978; Leventhal et al., 1981; Perry and Cowey, 1981; Shapley and Perry, 1986; Conley and Fitzpatrick, 1989). Between each of the magno and parvo layers lies a zone of very small cells: the koniocellular layers. Konio cells are

functionally and neurochemically distinct from magno and parvo cells (Hendry and Yoshioka, 1994). The finest caliber retinal axons, presumably originating from retinal ganglion cells that are morphologically distinct from those projecting to magno and parvo layers (Leventhal et al., 1981), innervate the koniocellular layers (Conley and Fitzpatrick, 1989).

Each LGN receives input from the two eyes, but these inputs are segregated in different monocular layers: layers 1, 3, and 6 get input from the contralateral eye, and layers 2, 4, and 5 get input from the ipsilateral eye (Hubel and Wiesel, 1972).

Hubel and Wiesel discovered that LGN receptive fields have a similar center-surround configuration to retinal ganglion cells, although their center-surround is stronger (Hubel and Wiesel, 1961).

Virtually all parvocellular cells (99%) present linear spatial summation. That is, the response to two elements presented simultaneously to the receptive field equals the sum of the response to each of the elements presented separately. About 75% of magnocellular cells are also linear, the other 25% are not (Kaplan and Shapley, 1982).

The LGN is often called a relay nucleus because it is the only structure between the retina and the cortex. However, LGN neurons are part of a complex circuit that involves ascending, descending and recurrent sets of neuronal connections (Steriade et al., 1997; Sherman and Guillery, 2001; Alitto and Usrey, 2003). The major source of descending input comes from neurons in layer 6 of V1. These feedback connections can be excitatory (through direct monosynaptic connections) or inhibitory (through inhibitory interneurons in the LGN or the reticular nucleus of the thalamus) (Erisir et al., 1997; Guillery and Sherman, 2002). The functions the corticothalamic pathway are still under discussion (Alitto and Usrey, 2003). These connections could help to explain LGN neurons extra-classical receptive fields properties, like the effects of the suppressive field (Murphy and Sillito, 1987; Alitto and Usrey, 2003; Carandini, 2004; Bonin et al., 2005). It is generally

agreed that these feedback connections act by modulating the responsiveness of the LGN neurons, and not by driving the actual responses (Sherman and Guillery, 1998).

1.1.3 V1

1.1.3.1 Anatomy

LGN neurons send their axons through the optic radiations to the back of the brain, where the primary visual cortex, area V1, is located. V1 is virtually the only target of primate LGN neurons (Benevento and Standage, 1982; Bullier and Kennedy, 1983), The magnocellular and parvocellular pathways that started in the retina remain largely separated.

V1, like most cortical areas, has 6 main layers (Brodmann, 1909). Most of the LGN inputs arrive to layer 4, which is divided in four sublayers: sublayer 4Cα receives axons mostly from magnocellular neurons. Sublayer 4Cβ (and sublayer 4A to a lesser extent) receives axons mostly from parvocellular neurons. Layer 6 receives weak input from collaterals of the same LGN axons that provide strong input to layer 4C (Hubel and Wiesel, 1972; Lund, 1973; Hendrickson et al., 1978; Blasdel and Lund, 1983). Neurons from the koniocellular layers in the LGN send their axons to layer 1 and layers 2-3 (Livingstone and Hubel, 1982; Hendry and Yoshioka, 1994).

Layer 4Cα sends its output to 4B (Lund et al., 1977; Fitzpatrick et al., 1985; Callaway and Wiser, 1996). Axons from neurons in 4Cβ terminate in the deepest part of layer 3 (Fitzpatrick et al., 1985; Lachica et al., 1992; Callaway and Wiser, 1996). Layers 2, 3, and 4B project mainly to other cortical regions (Callaway, 1998) and also send axons to layer 5 (Blasdel et al., 1985). Layer 5 projects back to layers 4B, 2, 3 (Callaway and Wiser, 1996) and to the superior colliculus (Lund et al., 1975). Layer 6 projects to the LGN (Fitzpatrick et al., 1994; Wiser and Callaway, 1996) and also sends axons to several V1 layers (Lund et al., 1977; Wiser and Callaway, 1996). Many of the projection pyramidal cells have collaterals that connect locally. Layer 1

contains few cell bodies, but many axons and dendrites synapse there (Lund and Wu, 1997). **Figure 3** shows a schematic representation of the main connections.

In addition to the feedforward input coming from the LGN, V1 receives direct feedback from V2, V3, V4, V5 or MT, MST, FEF, LIP and inferotemporal cortex (Perkel et al., 1986; Ungerleider and Desimone, 1986b, 1986a; Shipp and Zeki, 1989; Rockland et al., 1994; Barone et al., 2000; Suzuki et al., 2000).
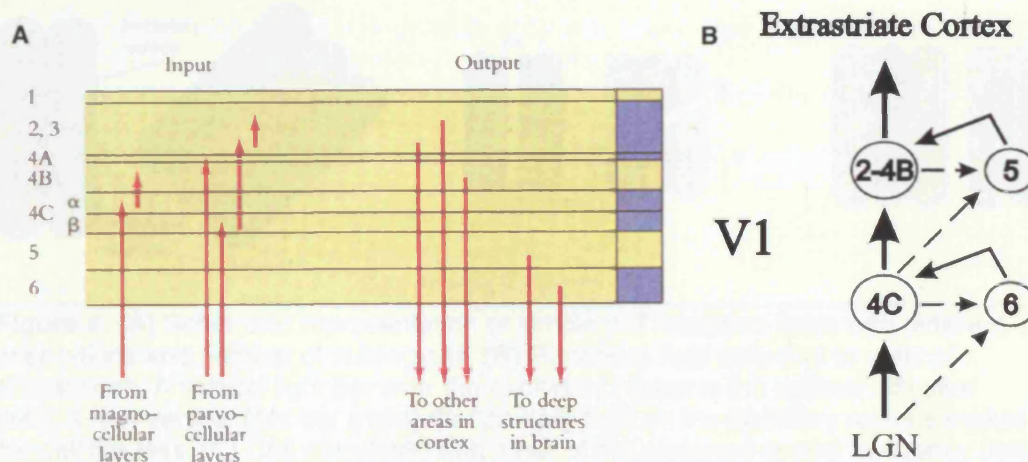
Figure 3. Schematic representation of V1 inputs, outputs and vertical interconnections. **(A)** From (Hubel, 1995). **(B)** From (Callaway, 1998).

1.1.3.2 Physiology & Receptive Fields

In primates, the receptive fields of most V1 input neurons (layer 4C) have the same center-surround organization as the LGN neurons they receive direct input from (Poggio et al., 1977; Bauer et al., 1980; Bullier and Henry, 1980; Blasdel and Fitzpatrick, 1984; Livingstone and Hubel, 1984). Outside of layer 4C, the receptive field structure is very different and we can distinguish two main groups of cells according to their receptive field type: simple cells and complex cells (Hubel and Wiesel, 1962).

Simple cells: Hubel and Wiesel first described the receptive fields of "simple cells" in area V1 (Hubel and Wiesel, 1959). The receptive fields of simple cells are organized in distinct elongated on and off antagonistic subregions, whose spatial arrangement determines the responses of the neuron to different stimuli. Simple cells

are selective to the orientation and spatial frequency of the stimulus (**Figure 4**). The response of simple neurons is reduced when there is a mismatch between the light and dark parts of the stimulus and the on- and off- regions of the receptive field. By testing the neuron's responses to different stimuli, it is possible to generate tuning curves for orientation and spatial frequency.
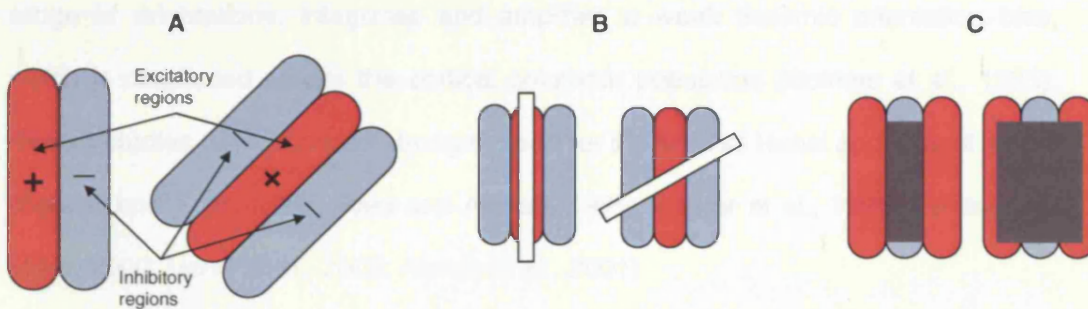
Figure 4. (A) Schematic representation of simple cell receptive fields with different orientations and number of subregions. **(B)** Receptive field selective to vertical orientations. A vertical light bar over the excitatory region is the optimal stimulus (left). A non-vertical light bar (right) that partially falls on the inhibitory regions makes the cell fire less. **(C)** Cell stimulated with a bar of the preferred spatial frequency (left) and with a bar that is too wide and thus falls on the opposite contrast subregions.

How are the elongated receptive fields of simple cells created? For many years two general models have attempted to explain how orientation selectivity is generated in the visual cortex (Alonso, 2002): feedforward excitatory models and inhibitory cross orientation models. The main feedforward model was proposed by Hubel and Wiesel shortly after discovering simple cells (Hubel and Wiesel, 1962): each simple cell gets its input from an array of center-surround receptive fields of the same sign that have their centers arranged along a straight line on the retina. The synapses from the center-surround receptive fields to the simple cell are excitatory and this gives the simple receptive fields its elongated shape and orientation selectivity (**Figure 5**). Inhibitory cross-orientation models propose that the feedforward connection from center-surround receptive fields establishes a weak orientation preference of simple cells, but that the narrow orientation selectivity comes from inhibitory inputs from cortical neurons with different orientations

preferences, which suppress the nonpreferred responses. There are several different models based on this principle: Koch and Poggio, 1985; Wehmeier et al., 1989; Worgotter and Koch, 1991; Carandini and Heeger, 1994... Somers et al. proposed a third type of model, a recurrent model: recurrent cortical excitation among cells preferring similar orientations, combined with iso-orientation inhibition from a broader range of orientations, integrates and amplifies a weak thalamic orientation bias, which is distributed across the cortical columnar population (Somers et al., 1995). Recent studies have provided strong support for the original Hubel and Wiesel model (Ferster and Koch, 1987; Reid and Alonso, 1995; Ferster et al., 1996; Ferster and Miller, 2000; Usrey et al., 2000; Alonso et al., 2001).
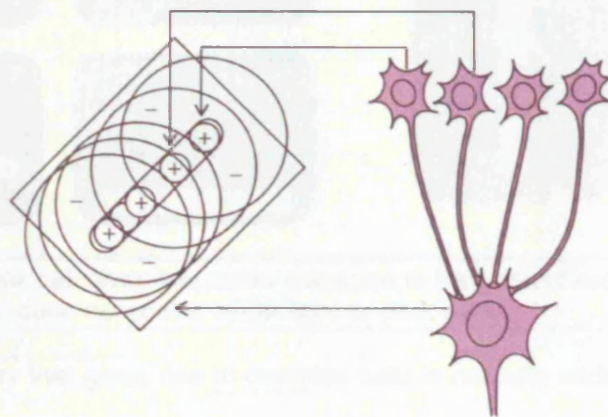
Figure 5. Schematic representation of the feedforward excitatory model proposed by Hubel and Wiesel in 1962. From Hubel (1995).

Complex cells: complex cells in the primary visual cortex, discovered by Hubel and Wiesel, are selective to the orientation and spatial frequency of stimuli (like simple cells) but their receptive fields do not have distinctive on and off subregions (Hubel and Wiesel, 1962). Consequently, complex cells receptive fields are invariant to the spatial phase (position of the stimulus within the receptive field) and contrast polarity of the stimulus. When a single bar is presented within the receptive field, complex cells respond equally well regardless of the bar's position

and contrast, as long as the bar has the preferred orientation and width (**Figure 6**). When pairs of bars are presented simultaneously within the receptive field, complex cells exhibit nonlinearity in spatial summation (Hubel and Wiesel, 1962): the response to simultaneous presentation of two stimuli cannot be predicted from the sum of the responses to the two stimuli presented individually. This is a fundamental property of complex cells; simple cells are more or less linear (Hubel and Wiesel, 1962; Movshon et al., 1978b; Carandini et al., 1997; Ringach, 2002b).

Position invariance

Contrast invariance
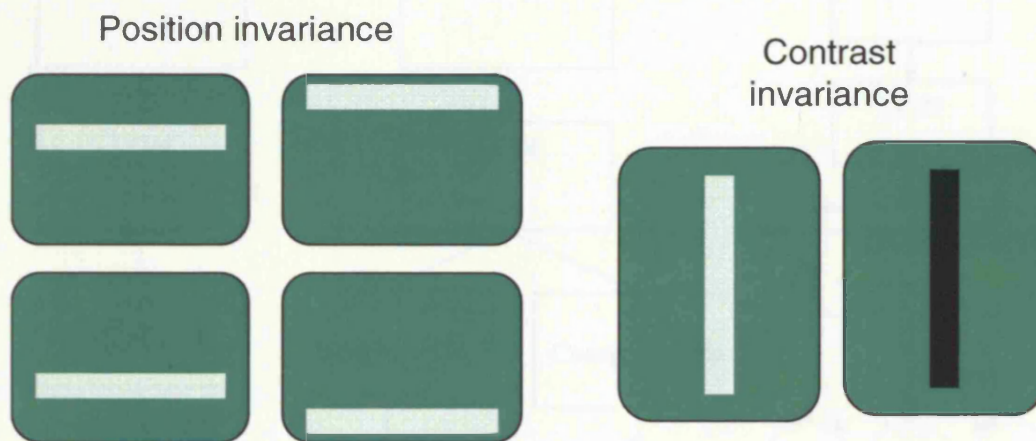
Figure 6. A complex cell gives the same response to bars anywhere within the receptive field, and does not prefer either light or dark bars.

The circuitry that gives rise to complex cells is not fully understood; there are several different hypothesis in the literature, some of which are shown in **Figure 7**. The "cascade model" (Hubel and Wiesel, 1962) suggests that simple cells and complex cells represent two successive stages in hierarchical processing: in a first stage, simple cells are created from the convergence of center-surround inputs that have receptive fields aligned in visual space. In the second stage, complex cells are then generated by the convergence of simple cells inputs with similar orientation preferences (**Figure 7**, left). "Parallel models" (Stone et al., 1979) propose that simple cells and complex cells are both constructed from direct geniculate inputs. Simple cells are created from the convergence of linear LGN inputs, and complex cells from the convergence of non-linear LGN inputs (**Figure 7**, middle). "Recurrent

models" (Chance et al., 1999) use a combination of weak simple cell inputs and strong recurrent complex cell inputs to generate complex cell nonlinearities (**Figure 7**, right). Martinez and Alonso (Alonso and Martinez, 1998; Martinez and Alonso, 2001; Martinez et al., 2005) published evidence supporting the Hubel and Wiesel cascade model.
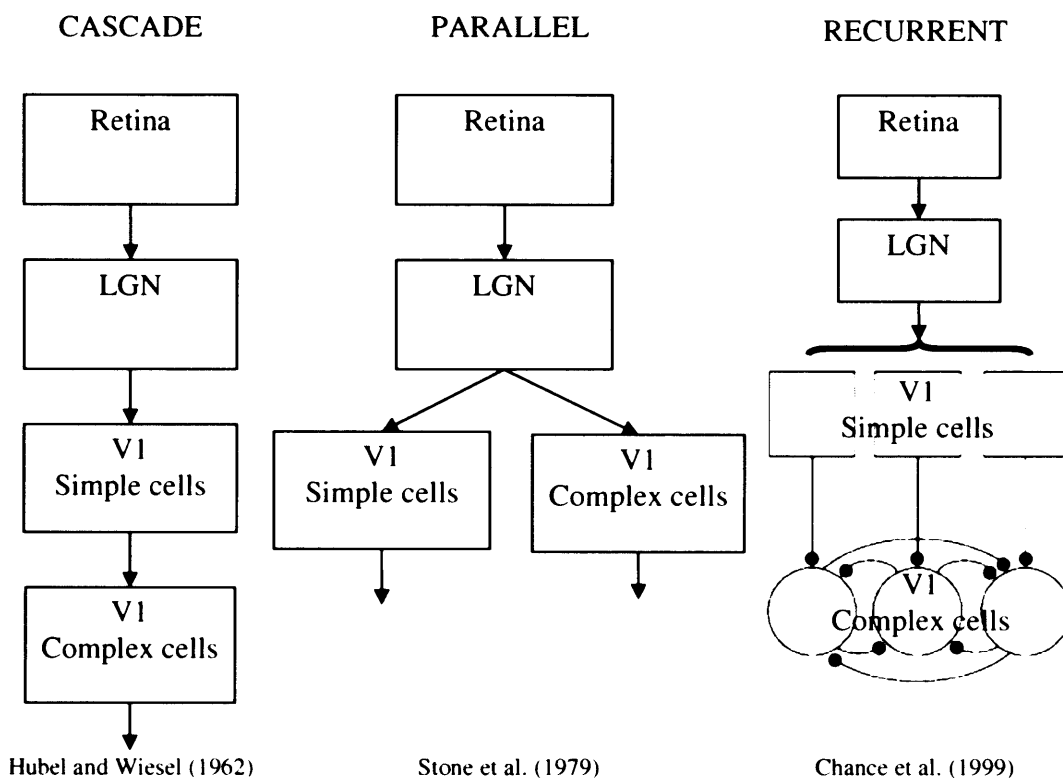
Figure 7. Different hypothesis about the connectivity of complex cells (after Martinez and Alonso, 2001).

End-stopped cells: ordinary simple and complex cells show length summation: the longer the bar stimulus, the better the response, until the bar is as long as the receptive field; making the bar even longer has no further effect. For end-stopped cells, lengthening the bar improves the response up to some limit, but exceeding that limit in one or both directions results in a weaker response. The same stimulus orientation evokes maximal excitation on the activating region and maximal inhibition on the outlying areas. Hubel and Wiesel discovered and characterized end-stopped cells in cat areas 18 and 19 and initially called them hypercomplex cells

(Hubel and Wiesel, 1965). Later Gilbert showed that some simple and complex cells in cat V1 are also end-stopped (Gilbert, 1977; Bolz and Gilbert, 1986). Several recent studies suggest that most primate V1 cells are somewhat end-stopped (Knierim and van Essen, 1992; Kapadia et al., 1999; Jones et al., 2001; Sceniak et al., 2001; Pack et al., 2003). The receptive field structure of end-stopped cells makes them especially sensitive to corners, curvature and terminators (Hubel and Wiesel, 1965; Hubel, 1995) (**Figure 8**).
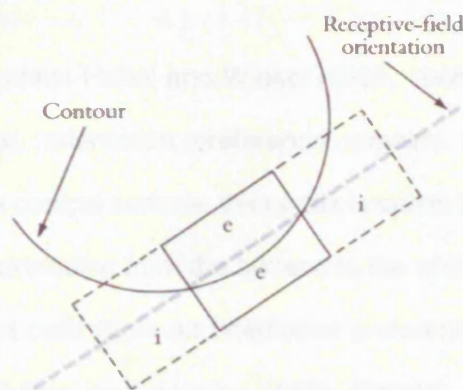
Figure 8. A curved border would be a good stimulus for the end-stopped cell represented in the diagram. From Hubel (1995).

Columnar organization: A fundamental feature of cortical organization is the spatial grouping of neurons with similar properties. V1 is functionally organized in layers and cortical columns, which are roughly perpendicular to the layers. The concept of cortical columns was introduced by Mountcastle in the somatosensory system (Mountcastle et al., 1955; Mountcastle, 1957; Powell and Mountcastle, 1959), although Lorente de Nó had envisaged their existence through his anatomical studies (Lorente de Nó, 1949). Hubel and Wiesel discovered columnar organization in area V1, first in the cat (Hubel and Wiesel, 1962) and then in the primate (Hubel and Wiesel, 1968, 1974; Wiesel et al., 1974). They showed that V1 cells with similar properties are grouped into columns: as they advanced an electrode in an orthogonal penetration from the cortex surface, they found that the neurons recorded by the

electrode had similar receptive field axis orientation, ocular dominance, and position in the visual field.

- Ocular dominance columns: the inputs from the two eyes are segregated in layer 4, where cortical neurons are driven monocularly. In any given column extending above and below layer 4, all the cortical neurons, even if driven by both eyes, share the same eye preference. Ocular dominance columns form an interdigitating pattern on the cortex (Hubel and Wiesel, 1962, 1968; Wiesel et al., 1974).

- Orientation columns: Hubel and Wiesel (1962, 1968, 1974) found that, just as with eye dominance, orientation preference remains constant in orthogonal penetrations through the cortical surface: the cortex is subdivided into narrow regions of constant orientation, extending from the surface to the white matter but interrupted by layer 4C, where most cells have no orientation preference (Poggio et al., 1977; Bauer et al., 1980; Bullier and Henry, 1980; Blasdel and Fitzpatrick, 1984; Livingstone and Hubel, 1984) (although some recent studies have found orientation selective cells in layer 4C (Ringach, 2002a; Shapley et al., 2003; Gur et al., 2005)). In a tangential electrode penetration, the orientation preference usually changes gradually.

Optical imaging studies have provided precise details about the columnar organization: orientation columns are arranged radially into pinwheel-like structures with orientation preference shifting gradually along contours circling the pinwheel center (Bonhoeffer and Grinvald, 1991; Blasdel et al., 1995). Each pinwheel center tends to occur near the center of an ocular dominance patch (Crair et al., 1997; Lowel et al., 1998), and iso-orientation contours tend to cross ocular dominance boundaries at right angles (Obermayer and Blasdel, 1993). Cortical columns where orientation preference changes smoothly or remains essentially constant are interspersed with regions containing orientation singularities where the orientation

changes abruptly by up to 90° (Blasdel and Salama, 1986; Ts'o et al., 1990; Bonhoeffer and Grinvald, 1991; Das and Gilbert, 1999).

Horizontal and feedback connections: many local connections in V1 have a wide lateral distribution, including long intralaminar connections spreading several millimeters (Callaway, 1998). Prominent horizontal connections are those originating from and terminating in layers 2-3 and 4B; these connections arise from neurons whose long-distance axon collaterals form periodic clusters (Gilbert and Wiesel, 1979, 1983; Rockland and Lund, 1983; McGuire et al., 1991; Anderson et al., 1993; Callaway and Wiser, 1996). These clusters tend to preferentially link columns of neurons with similar response properties: in cats, ferrets, and monkeys they preferentially link columns with similar orientation preference (Ts'o et al., 1986; Malach et al., 1993). Feedback connections from extrastriate cortex to V1 also show an orderly topographic organization and terminate in a patch-like manner within V1 (Angelucci et al., 2002). These two types of orderly connections (horizontal and feedback) may be involved in the generation of suppressive fields in V1 neurons, as well as other extra-classical receptive field modulations (Gilbert et al., 1996; Carandini et al., 1997; Angelucci et al., 2002; Levitt and Lund, 2002; Carandini, 2004). Intra cortical connections may be important to understand the neural computations carried out in V1. Zhaoping has proposed that V1 creates a saliency map using intra cortical mechanisms. This saliency map can be used to attract attention to a visual location without top-down factors, which may explain certain visual search properties (Zhaoping, 2005).

1.1.4 Extrastriate cortex: the dorsal and ventral visual pathways

The primate cortex has at least 32 distinct visual areas (Desimone and Ungerleider, 1989; Felleman and Van Essen, 1991). In the first two stages of cortical processing (V1 and V2), the magnocellular and the parvocellular pathways keep largely segregated: inputs from the LGN arrive to different sublayers in V1 according

to their magno/parvo origin and projections from V1 layer 4C are also fairly separated in V1 and V2 as revealed by cytocrome oxidase stainings (Livingstone and Hubel, 1984; Livingstone and Hubel, 1988; Van Essen and Gallant, 1994; Olavarria and Van Essen, 1997). After V1 there are two main processing streams, associated with different visual capabilities (Ungerleider and Mishkin, 1982; Maunsell and Newsome, 1987; Desimone and Ungerleider, 1989):

-The dorsal or parietal stream emphasizes motion analysis (with similar properties to the magnocellular pathway). After V2 the information flows to MT, MST and other intermediate areas. MT neurons are selective to the direction of stimulus motion, speed and binocular disparity (Zeki, 1974a, 1974b; Baker et al., 1981; Albright, 1984). The highest stages of this stream are clustered in the posterior parietal cortex. This stream is involved in assessment of spatial relationships and it is often called the "Where" pathway.

-The ventral or temporal stream emphasizes form and color analysis (similar properties as the magnocellular pathway). After V2 the information flows to V4 and other intermediate areas; many V4 neurons are selective to stimulus color (Zeki, 1978a, 1978b), orientation, width, and length of bars (Desimone and Schein, 1987), curvilinear and linear gratings (Gallant et al., 1993; Gallant et al., 1996), and contour features like angles and curves (Pasupathy and Connor, 1999). The highest stages of this stream are clustered in the inferotemporal cortex. This stream is concerned with visual recognition of objects as it is often called the "What" pathway.

The transformations of the visual image that occur along each of these pathways do not appear to result in increased selectivity for basic parameters (Maunsell and Newsome, 1987) such as direction or speed (Albright, 1984) in the dorsal pathway or wavelength (de Monasterio and Schein, 1982) or orientation (Desimone et al., 1985) in the ventral pathway. Also, retinotopic specificity decreases progressively in successive levels of each of the pathways: the average receptive field size in MT is 100 times larger than in V1 (Gattass and Gross, 1981). In MST

receptive fields can cover a full quadrant of the visual field (Desimone and Ungerleider, 1986). V4 receptive fields are about 30 times larger than V1 receptive fields (Van Essen and Zeki, 1978; Maguire and Baizer, 1984), and downstream in the ventral pathway they become over 100 times larger (Desimone and Gross, 1979). Rather than sharpening basic tuning curves, the transformation of information along each of the pathways appears to construct new, more complex response properties; both pathways may use similar computational strategies for processing information (Maunsell and Newsome, 1987).

The hypothesis of two distinct streams of processing was initially formulated by Ungerleider and Minsk (Ungerleider and Mishkin, 1982). Many different groups have provided anatomical, physiological, and behavioral support to this idea. In humans, clinical observations indicate that damage to the parietal cortex can affect visual perception of position, leaving object recognition unimpaired (Ratcliff and Davies-Jones, 1972; Damasio and Benton, 1979; Zihl et al., 1983). Temporal lobe lesions can produce specific deficits related to object recognition (Meadows, 1974b, 1974a; Pearlman et al., 1979; Damasio et al., 1982). Systematic lesions studies in primates have found a functional separation between the temporal and parietal cortices (Dean, 1976; Ungerleider and Mishkin, 1982; Mishkin and Ungerleider, 1983).

While it is widely accepted that information is computed in these two largely parallel visual pathways (as shown in schematic on **Figure 9** taken from Kandel et al., 2000), it is important to note that the separation between the two pathways is far from complete. There is anatomical and physiological evidence of substantial cross-talk between the two streams (Felleman and Van Essen, 1991; Van Essen et al., 1992; Merigan and Maunsell, 1993).
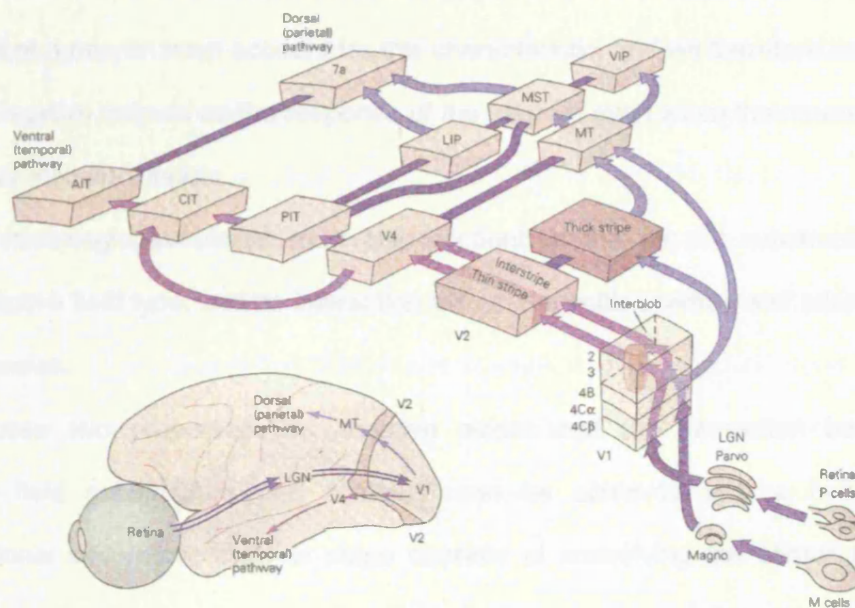
Figure 9. Schematic of the two visual pathways in the primate, showing the main connections between the different areas (from Kandel et al., 2000)

1.2. Center-surround receptive field simulations

1.2.1 Simulation of receptive fields

By understanding thoroughly the organization and properties of receptive fields at a given stage in the visual pathway, it becomes theoretically possible to predict their responses to any possible visual stimulus. The responses of early receptive fields can be predicted to some extent using computational models that simulates the receptive fields' output. One fundamental property of the neurons implemented in the computational model is that their unit of output is the action potential: neurons may integrate the graded excitatory and inhibitory inputs that they receive within their dendritic tree, but their output is a certain number of action potentials. Moreover, for our simulations we assume that a resting neuron produces no action potentials, so neuronal responses are only produced when the sum of inhibitory and excitatory inputs exceeds a certain threshold; if the sum is negative (the neuron is inhibited), or if the inputs fail to depolarize the neuron above threshold, then there is no output. The output of the neuron in the inhibited state is therefore

indistinguishable from the complete lack of inputs. Any computational simulation of the output of a neuron must account for this characteristic, and we therefore may not express negative outputs as the response of the neuron, even when the neuron may have highly inhibitory inputs.

A meaningful simulation must also account for the specific substructure of each receptive field type, and its interaction with the specific position and orientation of the stimulus.

These two properties (no negative output and the interaction between receptive field substructure and stimulus) can be achieved with a two-stage computational simulation: the first stage consists of convolving the stimuli with a linear filter that captures the receptive field spatial structure of the neuron being modeled. The second stage is a static non-linearity (such as half-wave rectification) that prevents the output of the model from being negative. We will explain the two stages shortly, but first we will describe two properties of early receptive fields that are key for these types of simulation: linearity and retinotopic organization.

Linearity: Most retinal ganglion and LGN center-surround receptive fields in the primate exhibit near-linear spatial summation properties (Kaplan and Shapley, 1982; Croner and Kaplan, 1995; Levitt et al., 2001). Simple cells in V1 also have this property (Hubel and Wiesel, 1962; Movshon et al., 1978b; Carandini et al., 1997; Ringach, 2002b). Linear spatial summation means that the response to the simultaneous presentation of two stimuli equals the sum of the responses to the two stimuli presented individually.

Retinotopic organization: As described in the General Introduction, the early visual system is retinotopically organized. This means that neighboring neurons have receptive fields that correspond to neighboring parts of the retina (and therefore to neighboring parts of the visual space). Since LGN neurons are retinotopically organized, and nearby neurons share similar receptive field properties and sizes, the output of an LGN cell to different parts of an image region is comparable to the global

output of an ordered array of LGN cells, with the same properties, looking at that region. This region should be small enough so that the receptive field properties of all neurons involved are similar (for instance, receptive field sizes increase with eccentricity, so neurons further apart would have different receptive field sizes).

Linear convolution: The output of linear, retinotopically organized neurons to a given image can be simulated by convolving a linear filter with the image (Marr, 1982; Wandell, 1995). The linear filter needs to capture the spatial structure of the receptive field. Therefore, filters representing retinal ganglion cells and LGN neurons must have a concentric center-surround organization, while filters representing V1 simple cells must have several elongated subregions. Basic models of neurons at the earliest stages of visual processing (retina, LGN, and V1 simple cells) typically include a single linear filter, whereas models of neurons at later stages of processing (V1 complex cells and beyond) require multiple filters (Enroth-Cugell and Robson, 1966; Movshon et al., 1978a; Adelson and Bergen, 1985; Touryan et al., 2002; Carandini et al., 2005). Convolving a linear filter with the image involves multiplying the intensities at each local region of the image (the value of each pixel) by the values of the filter and summing the weighted images intensities (Carandini et al., 2005). This output can be negative (when there is a mismatch between the sign of the filter and the sign of the image), so the model needs a second stage to describe how the filter outputs are transformed into a firing rate response (which is never negative).

Half-wave rectification: a half-wave rectification takes the negative values and makes them zero, without changing the positive values, thus simulating the effect of the non-linear threshold found in physiological neurons. This operation is called a static nonlinearity, because it depends only on the instantaneous outputs and it does not change with time. Other static nonlinearity functions, such as half-way squaring, can be used instead.

The two stages in the computational simulation (linear filtering and static nonlinearity) are followed in some models by a Poisson spike generator to transform the firing rate into spikes ("Linear – Nonlinear – Poisson" models) (Chichilnisky, 2001; Carandini et al., 2005). Other more realistic models, like the "Integrate-and-Fire" model, have also been proposed (Troyer and Miller, 1997; Reich et al., 1998; Shadlen and Newsome, 1998; Keat et al., 2001; Pillow et al., 2005). However, the "Linear – Nonlinear – Poisson" model is the simplest and most widely used model of linear responses.

1.2.2 Center-surround receptive fields as Difference of Gaussians filters

Center-surround receptive fields of retinal ganglion or LGN cells can be simulated with a Difference of Gaussians (DOG) filter (Rodieck, 1965; Enroth-Cugell and Robson, 1966). This model captures the spatial structure of concentric antagonistic receptive fields (Dayan and Abbot, 2001) and it is very widely used. The model assumes that Gaussian functions represent both the center and the surround of a concentric receptive field: the center is a narrow Gaussian, while the antagonistic surround is a much broader Gaussian. The subtraction of these two functions characterizes the response of the neuron (**Figure 10**).

We have developed software to implement the DOG model. The equation we used to represent the neuron's receptive field is:

$$N(x, y) = C(x, y) - S(x, y) = k_c e^{-\frac{x^2 + y^2}{\sigma_c^2}} - k_s e^{-\frac{x^2 + y^2}{\sigma_s^2}}$$

Where:

$$C(x, y) = k_c e^{-\frac{x^2 + y^2}{\sigma_c^2}} \rightarrow centre\ Gaussian$$

$$S(x, y) = k_s e^{-\frac{x^2 + y^2}{\sigma_s^2}} \rightarrow surround\ Gaussian$$

σ_c and σ_s, or the 'radius' of center and surround, represent the distance over which the sensitivities of center and surround fall to $1/e$ of the peak value, and k_c/k_s gives the relative strength of center and surround components.

Figure 11 shows the 3-dimensional plot of an on-center receptive field generated with this model.
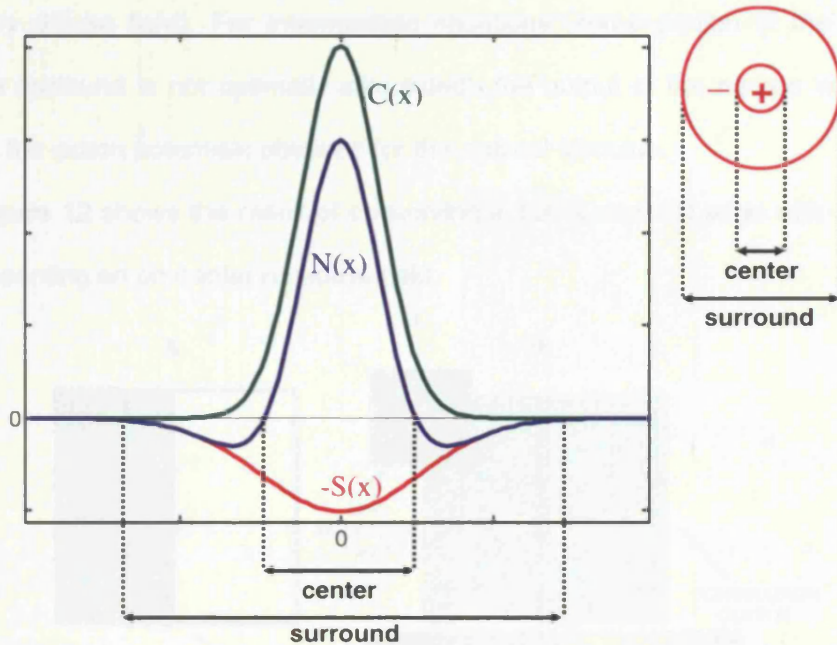
Figure 10. One-dimensional slice through the center of an on-center receptive field modeled as a DOG filter. C(x): excitatory center function; S(x): inhibitory surround function; N(x): resulting on-center receptive field.
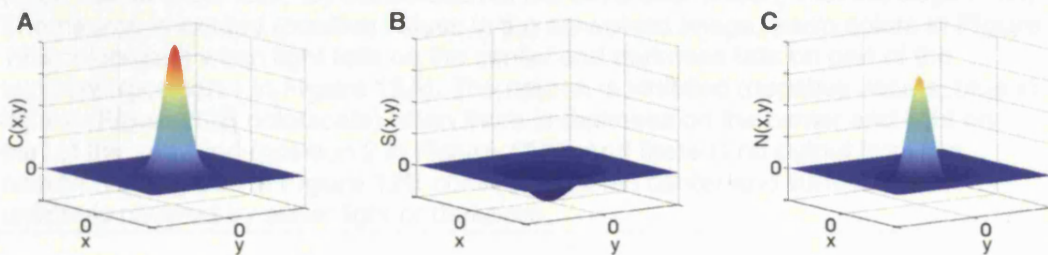
Figure 11. Three-dimensional plot of an on-center receptive field generated with the DOG model. **A)** Excitatory center. **B)** Inhibitory surround. **C)** On-center receptive field obtained as a Difference of Gaussians of the center and the surround.

We used the DOG model of center-surround receptive fields just described to simulate the output of linear retinal ganglion and LGN cells. When an on-center receptive field is stimulated with light on the center and darkness on the surround (the receptive field's preferred stimulus), the neuron responds with a certain number of action potentials. With opposite stimulation (darkness on the center and light on

the surround), the neuron is maximally inhibited and there is no output (the neuron is silent, as it also would be if not stimulated at all, or if whole receptive field was covered by diffuse light). For intermediate situations (some portion of the center and/or the surround is not optimally stimulated), the output of the neuron will be a fraction of the action potentials obtained for the optimal stimulus.

Figure 12 shows the result of convolving a 100% contrast edge with a DOG filter representing an on-center receptive field.
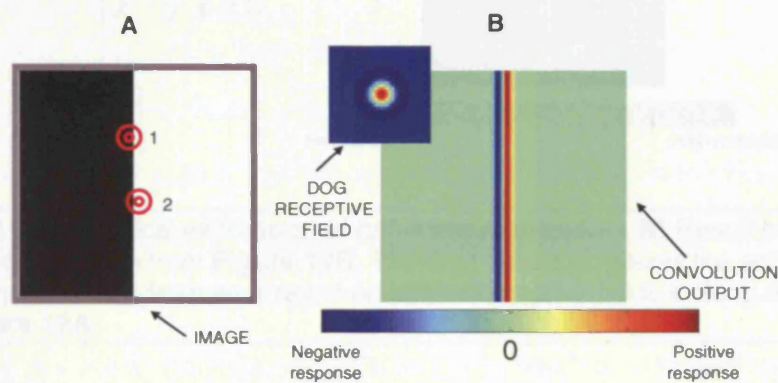
Figure 12. A) 100% contrast edge. The concentric red circles (1 and 2) represent the size of the DOG filter used with respect to the stimulus. Middle insert: Contour plot of an on-center DOG filter. B) Convolution of the DOG filter (Insert) with the edge in (A). The neuron is excited (positive values in the convolved image, warm colors in **Figure 12B** colorscale) when light falls on the center and darkness falls on part of the surround (position 1 in **Figure 12A**). The neuron is inhibited (negative values, blue in figure's **Figure 12B** colorscale) when there is darkness on the center and light on part of the surround (position 2 in **Figure 12A**). And there is no output from the neuron (zero, green in **Figure 12B** colorscale) when center and surround are uniformly covered by either light or darkness.

Now we can apply the second stage of the model, the half-wave rectification, to the result of the convolution (**Figure 13**).

For this simulation, and for the rest of center-surround simulations in this dissertation, the parameters for the DOG filter were chosen so that σ_s (the surround radius) was twice σ_c (the center radius), and both center and surround had the same weight ($k_c/k_s = 1$) towards the cell's output. These parameters may not match ideally the parameters for all neurons they represent, but they capture the fundamental essence of average LGN neurons in the primate (Derrington and Lennie, 1984; Irvin

et al., 1993; Tadmor and Tolhurst, 2000; Levitt et al., 2001). The parameters of the filter may be modified, changing the outputs of the simulation, but as long as they are kept within physiological limits, the fundamental results will remain qualitatively similar to the results presented throughout this thesis.
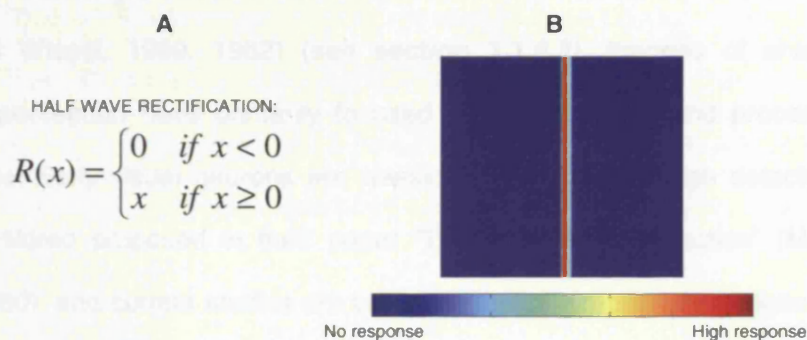
Figure 13. A) Mathematical expression of half-wave rectification. **B)** Result of rectifying the convolution from **Figure 12B**. The final output simulates the activity (extracellularly recorded) from an array of on-center receptive fields looking at the image in **Figure 12A**.

1.3. Corners/angles/junctions/points of maximum curvature

1.3.1 Fundamental visual features

Our perception of the visual world is constructed, step-by-step, by neurons in different visual areas of the brain (Hubel and Wiesel, 1962; Desimone et al., 1980; Shipp and Zeki, 1985; Felleman and Van Essen, 1991). While feedback certainly plays a role in the visual system (Alonso et al., 1993a, 1993b; Hupe et al., 1998; Martinez-Conde et al., 1999; Murphy et al., 1999), the visual system's overall tendency is towards a hierarchy, in which neurons in sequential levels extract more and more complicated features from the visual scene. These features include (but are not limited to) color, brightness, movement, shape, and depth.

In order to determine how visual perception is constructed in our brain, we need to establish what the fundamental visual features in a scene are. The current literature shows a certain degree of disconnect between physiological and psychophysical approaches, specifically concerning the relevance of corners and

curvature elements and the stage of the visual system where they are processed for the first time.

1.3.2 Corner physiology

Since Hubel and Wiesel's discovery of orientation selectivity in the early 60's (Hubel and Wiesel, 1959, 1962) (see **section 1.1.3.2**), theories of shape and brightness perception have primarily focused on the detection and processing of visual edges. Early visual neurons are classically considered "edge detectors", as Marr and Hildred proposed in their paper "Theory of edge detection" (Marr and Hildreth, 1980), and current studies are based on the assumption that edges are the most fundamental visual feature. The visual system's predisposition for edges versus diffuse light has been shown in physiological and perceptual studies (Mach, 1865; Hubel and Wiesel, 1959; Ratliff and Hartline, 1959; De Weerd et al., 1995; Livingstone et al., 1996; Paradiso and Hahn, 1996; Macknik and Haglund, 1999; Macknik et al., 2000).

Classical physiological experiments have suggested that shape perception is built up through a hierarchy of receptive field stages. The first stage of edge-detection is made up of center-surround neurons (Kuffler, 1952), which then converge to form the second stage of edge orientation-selective cells (Hubel and Wiesel, 1962). Orientation selective cells then converge onto the third stage of "end-stopped" (or hypercomplex) cells, which are curve and/or corner selective (Hubel and Wiesel, 1965; Dobbins et al., 1987; Versavel et al., 1990).

Various possibilities for subsequent (or alternative) corner-selective response properties in V1 have been proposed:

- Shevelev et al. reported that 1/3 of neurons in cat area V1 respond more strongly to corners than to edges or bars. 77% of the neurons selective to corners were selective to both the angle and the orientation of the corner, each of them having a specific preferred angle. Shevelev et al. suggested that corner selective

neurons play an important role in feature extraction and processing in V1. They considered it unlikely that these units get their "corner selectivity" by excitatory convergence of two neurons with different preferred orientation, as classical hierarchical models propose (Shevelev et al., 1998, 1999).

- Sillito et al. found evidence of cross-orientation facilitation in area V1, and suggested that V1 contains the neural machinery to detect local orientation discontinuities. V1 may therefore play a role in detecting the location and direction of a change in contour orientation, associated for example with junctions or corners (Sillito et al., 1995).

- Das and Gilbert combined optical imaging with simultaneous single cell recordings to study the role of short-range connections in V1. They reported a new set of response properties in V1 generated by local cortical interactions, that is, a set of graded specializations for processing locally complex visual features. As a result, V1 neurons may be functionally specialized for processing corners and junctions. Das and Gilbert further proposed that the corner processing properties of V1 neurons could form a functional map over the cortical surface, similar to and closely linked with orientation and spatial maps (Das and Gilbert, 1999).

Other studies suggest that most V1 cells are somewhat end-stopped and therefore sensitive to corners (Knierim and van Essen, 1992; DeAngelis et al., 1994; Kapadia et al., 1999; Jones et al., 2001; Sceniak et al., 2001; Pack et al., 2003).

In recent years the study of the physiological responses to corners, curves and terminators has generated a great deal of interest, and single-unit responses to curves and corners have been reported in striate and extrastriate cortex of cats and primates:

- Ito and Komatsu studied the responses of V2 neurons to corner outlines of different angles and orientations. They found that a large number of V2 neurons selectively responded to corner angles, and one fourth of them showed highly selective responses to a particular angle. They reported that for most angle selective

V2 neurons the response to the optimal angle reflected the specific combination of the two line components. Ito and Komatsu concluded that their results support the idea that signals encoding the orientation and location of individual line components converge on V2 neurons and that the extraction of angle features starts in area V2 (Ito and Komatsu, 2004).
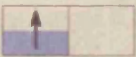
- Pack et al. studied the responses to terminators (any local region of the image that contains orientation discontinuities) and their role in encoding two-dimensional motion. They proposed that two-dimensional features, like end-points, corners, and intersections (terminators in general) allow accurate velocity measurements, even on very small spatial scales. Moreover, they showed that end-stopped V1 neurons are capable of encoding two-dimensional motion information independently of the orientation of the stimulus. They proposed that end-stopped V1 neurons measure two-dimensional correspondence in motion by responding preferentially to line endings. They also found that the majority of MT neurons are highly sensitive to the motion of two-dimensional terminators, and that the computation of two-dimensional motion occurs on a spatial scale that is much smaller than MT receptive field diameters: when information about two-dimensional motion is concentrated on a small region of the visual field, the resulting terminator signals exert a powerful effect on the responses of MT neurons (Pack et al., 2003; Pack et al., 2004).

- Pasupathy and Connor conducted a series of studies looking at contour features and shape representation in area V4 (Pasupathy and Connor, 1999, 2001, 2002). In their first study they presented single contour features (a corner or a curve) to the receptive field of a V4 neuron. They found that a substantial fraction of V4 cells exhibit specificity for individual corners or curvature segments, and suggested that responses to complex shapes may be understood in terms of their constituent contour features. They proposed that the systematic tuning for corners and curves (regarding their angle, convexity and orientation) cannot be explained in terms of

lower level factors such as edge orientation, spatial frequency or contrast direction (as almost all cells responded better to contour features than to any individual edge or line). They conclude that contour features are extracted as intermediate level shape primitives, that is, as an intermediate step toward complex shape recognition (Pasupathy and Connor, 1999). To explore the mechanisms of shape representation in V4, they then used moderately complex shapes that systematically combined convex and concave boundary elements. They found that many neurons in area V4 were sensitive to boundary information at a specific position relative to the object center; the most effective boundary pattern often comprised a sequence of adjacent curves and angles, with the tuning functions biased towards sharper convex curvature. The results suggested a parts-based representation of complex shape in V4, where the parts are contour segments defined by curvature and position relative to the rest of the object. Pasupathy and Connor concluded that shape representation in V4 is distributed, with individual cells encoding smaller parts of larger objects, and that boundary configurations at specific object-relative positions are important second-level shape features at intermediate processing stages (Pasupathy and Connor, 2001).

The studies mentioned above are based on the standard assumption that edges are the most fundamental visual feature, and that corner selective receptive fields develop subsequently to edge selective receptive fields. **Figure 14** shows a textbook example from Nichols et al. (2001).

However, some visual illusions show that corners can be perceptually more salient than edges, suggesting that corners may also be a more critical feature for shape and brightness perception. Visual illusions are a powerful tool to study the neural bases of perception because they allow us to dissociate our perception of a stimulus from its physical reality.

Type of cell	Shape of field	What is best stimulus?
Photoreceptor	⊕	Light
Ganglion		Small spot or narrow bar over center
Geniculate		Small spot or narrow bar over center
Simple (layers 4 and 6 only)		Narrow bar or edge (some end-inhibited)
Complex (outside layer 4)		Bar or edge
End-inhibited complex (outside layer 4)		Line or edge that stops; corner or angle

Ganglion cells and lateral geniculate cells

Simple cortical cells

Complex cells
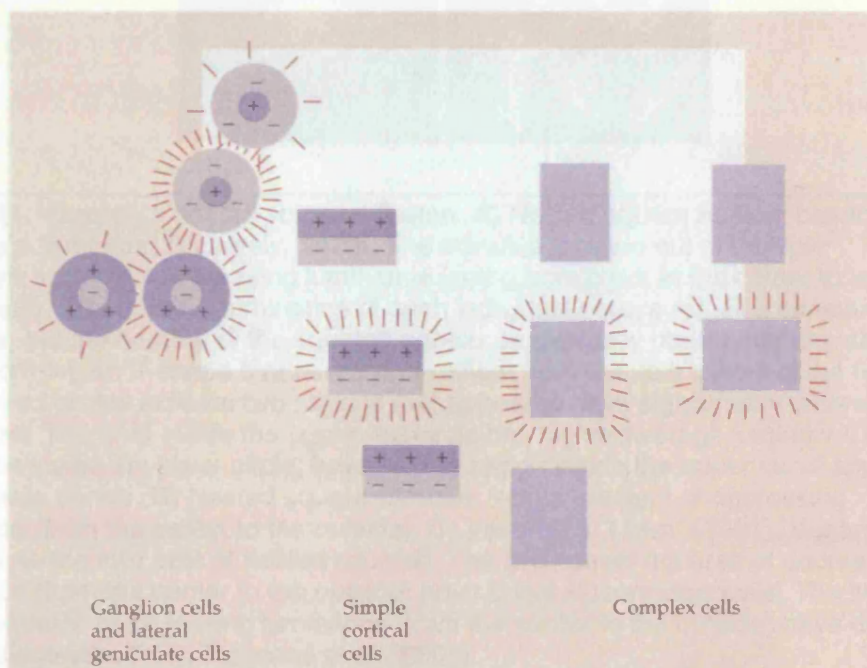
Figure 14. Corner processing is generally considered to be subsequent to edge processing Nichols et al. (2001).

Figure 15 shows Vasarely's "nested squares" illusion ("Arcturus", 1970). The image is made out of multiple concentric squares of decreasing luminance. The innermost square is white, and the outermost square is black. For each individual square, the physical luminance remains constant along the various regions of the

square. However, the corners of the squares appear perceptually brighter than the rest, forming a whitish X-shape that seems to irradiate from the very center of the figure. Our perception of corners being brighter than edges must have a neural correlate at some level of the visual pathway. Is it possible that corners are in fact a basic visual feature, even at the earliest stages of the visual system?
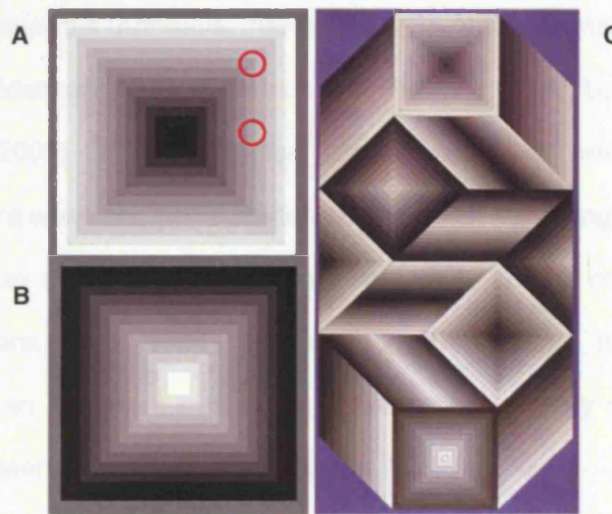
Figure 15. Vasarely's nested squares illusion. **A)** Nested square illusion, based in Vasarely's "Arcturus" (Vasarely, 1970). The stimulus is made out of multiple concentric squares of increasing luminance (going from black in the center to white in the outside). The physical luminance of each individual square remains constant at all points, but the corners of the squares appear perceptually darker than the straight edges, forming an X-shape that seems to irradiate from the very center of the figure. The two red circles indicate two regions that appear to have significantly different brightness. The area inside the upper red circle has higher average luminance than the region inside the lower circle; however the region inside the upper circle appears perceptually darker. **B)** Nested square stimulus, with a gradient of decreasing luminance (from the center to the outside). **C)** Vasarely's "Utem" (1981) (Vasarely, 1982). Note the four sets of nested squares. The two nested squares of decreasing luminance (from the center to the outside) have bright illusory diagonals. The two nested squares of increasing luminance (from the center to the outside) have dark illusory diagonals. From Troncoso et al. (2005)

1.3.3 Corners and psychophysics

Ibn Al-Haytham (also known as Al-Hazen) pointed out the importance of curvature in visual perception almost 1000 years ago when wrote in his treaty *Optics:* "For sight will perceive the figure of the surfaces of objects whose parts have different positions by perceiving the convexity, concavity or flatness of those parts, and by perceiving their protuberance or depression" (Al-Haytham, 1030/1989).

Although physiological studies consider that the processing of corners and curvature is subsequent to edge processing, psychophysical studies have shown that curvature and corner features are involved in numerous visual processes of varied complexity such as:

– Shape analysis. Many authors have discussed the role of corners and curvature in shape analysis (Attneave, 1954; Milner, 1974; Biederman, 1987; Ullman, 1989; Poggio and Edelman, 1990; Dickinson and Pentland, 1992; Loffler et al., 2003; Shevelev et al., 2003). Contour angles (discontinuities in orientation) remain qualitatively invariant when the point of view of the observer changes (although the size of the angle may change) being therefore very useful for the construction of 3D object representations (Watt, 1986). Discrete stimulus features (such as contour intersections) play an important role in the organization of early spatial vision by structuring the representation employed thereafter (Watt, 1985).

– Texture segmentation. Line terminators are critical for texture discrimination (Rubenstein and Sagi, 1996; Barth et al., 1998b).

– Filling-in and 3D shape perception. Locations that undergo abrupt curvature changes along a contour are particularly revealing about the shape of an object (Tse, 2002).

– Processing of motion signals. The human visual system relies heavily on pointlike object features such as line endings and terminators to compute the veridical direction of the motion of an object (Nakayama and Silverman, 1988; Loffler and Orbach, 1999).

– Attentional capture. A stimulus presented in a region of space adjacent to the corner of an object receives an enhancement of processing relative to a stimulus presented next to one of the object's straight edges (Cole et al., 2001).

– Saccade selection. Non-redundant, two-dimensional image features like curved lines and edge occlusions play an important role in the saccadic selection process (Krieger et al., 2000).

– Acuity. Sensitivity to angle acuity is greater than predicted by line orientation acuity (Watt, 1984; Chen and Levi, 1996; Heeley and Buchanan-Smith, 1996; Regan et al., 1996) , and observers are highly sensitive to corners and curvature in discrimination tasks (Bühler, 1913; Andrews et al., 1973; Watt and Andrews, 1982).

– Visual search. several form-based features will pop-out amongst a set of distracters, including:

- certain types of contour junctions: a major determinant of search is the presence of line junctions (Enns and Rensink, 1991).

- contour concavities: concavities can serve as basic features in visual search (Hulleman et al., 2000).

- contour curvature: curvature is a basic feature for visual search tasks (Wolfe et al., 1992).

- curvature discontinuities: the visual system quickly detects and analyzes abrupt changes in curvature in order to extract vital information about the 3D structure of the visual environment (Kristjansson and Tse, 2001).

It is commonly believed that features that exhibit pop-out during visual search are processed rapidly and in parallel across the visual field (Treisman and Gelade, 1980), although not all studies agree with this view (Duncan and Humphreys, 1989; Duncan and Humphreys, 1992; Li, 2002).

1.3.4 Corners and information theory

Our visual system is constrained physically by the amount of information it can process, such as by the relatively small number of axons available in the optic

nerve. It has been hypothesized that our visual system overcomes limitations such as this by extracting, emphasizing, and processing highly informative visual features (Barlow, 1961, 1989; Barenholtz et al., 2003; Hansen and Neumann, 2004; Feldman and Singh, 2005). Even a decade before Shannon founded the field of information theory (Shannon, 1948), Werner described angles as "those parts of contour which have stored within them the greatest amount of psychophysical energy", and proposed that "angles are especially intense parts of contour, and there is invested in them a central significance for the construction of optical figurations" (Werner, 1935). According to information theory, regions in the retinal image that include sudden changes or discontinuities contain more information about the spatiotemporal structure of the environment than uniform regions, simply because adjacent or subsequent values are unpredictable in discontinuous domains, whereas continuous regions are predictable by definition. Attneave proposed in the 1950's that "points of maximum curvature" (that is, discontinuities in edges, such as curves, angles and corners – any point at which straight-lines are deflected) contain more information than non- or low-curvature features and therefore they are more important for object recognition (Attneave, 1954) (**Figure 16**).

The visual system may have evolved to be especially sensitive to highly predictive cues, such as the various classes of contour discontinuity, because rapid detection and processing of these cues may provide the most efficient route to recovering world structure from the image (Gibson, 1950). The edge map is itself relatively predictable: from a computational point of view, the most useful information lies on the intersections and other discontinuities of the edge map (Watt, 1985).

Subsequent studies expanded on these results (Biederman, 1985; Resnikoff, 1985; Biederman, 1987; Norman et al., 2001), and Feldman and Singh have formally demonstrated that information is quantifiably higher at acute than obtuse corners (Feldman and Singh, 2005). Studies of natural scenes statistics have also recently begun to address the prevalence of corners and curves in our visual environment

(Krieger et al., 2000; Sigman et al., 2001; Yang and Purves, 2003; Howe and Purves, 2005).
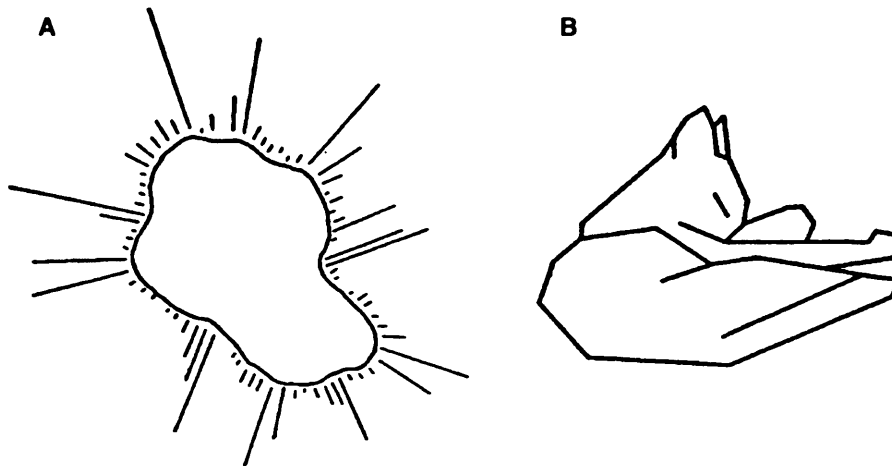
Figure 16. Attneave's studies on curvature. **(A)** Attneave showed this blob to subjects and asked them to choose 10 points to later reconstruct its shape. Radiating lines represent the frequency with which each of the points was chosen. The points chosen more often are those where the curvature of the contour is maximal. **(B)** This drawing of a sleeping cat was made by connecting the 38 points of maximum curvature with straight lines. The cat is perfectly recognizable. From Attneave (1954).

1.3.5 Literature review summary and conclusions

The corner literature offers different theoretical positions regarding corner processing:

- Information theory approaches and psychophysical experiments point out the relevance of corners in visual processing and their high information content, critical for object reconstruction.

- Physiological studies consider that edges are the most fundamental visual feature. Corner processing is a subsequent stage to edge processing and it happens for the first time in V1 or later. Curves and corners are "intermediate shape primitives".

Given the importance of corners and contour discontinuities for shape processing, it seems possible that the visual system may have evolved a specialized ability to detect these key features rapidly across the image. This suggests that

processing of corners and other informative contour discontinuities begins early in

the visual hierarchy. One of the goals of this thesis is to investigate the validity of this

new hypothesis.

2. Chapter 2.

Basic simulations

of center-surround responses

to corners

The purpose of this thesis is to explore the hypothesis that explicit corner processing (receptive field selectivity) begins at the earliest stages of the visual hierarchy and to quantify the perceptual and physiological contributions of corners of different angles. In this chapter we propose a new early receptive field model for corner processing, and we test it with computational simulations of center-surround receptive fields.

2.1. A new general early receptive field model for processing corners

Vasarely's nested squares illusion (**Figure 15**) shows that corners can be more salient perceptually than edges. As discussed in the General Introduction (**section 1.3**), physiological studies have proposed that corner processing starts in area V1 or later. Thus one might expect that the neural correlates of the nested squares illusion would be on area V1 or later.

However, some theoretical approaches have suggested that center-surround receptive fields can be responsible for Vasarely's nested squares illusion (Hurvich,

1981; Adelson, 1999; McArthur and Moulden, 1999). Nevertheless, this idea has never been quantified, with computational, physiological, or psychophysical approaches. Hurvich's basic idea (Hurvich, 1981) was that the contrast between the center and the surround regions of the receptive field would be stronger along the corner-gradients than along the edge-gradients in a nested-square pattern, resulting in increased perceptual salience at the corners (**Figure 17A**). Adelson (Adelson, 1999) applied center-surround filters to the nested squares and found that the output of the filters qualitatively matched the perception of the diagonals being brighter (**Figure 17B-C**).
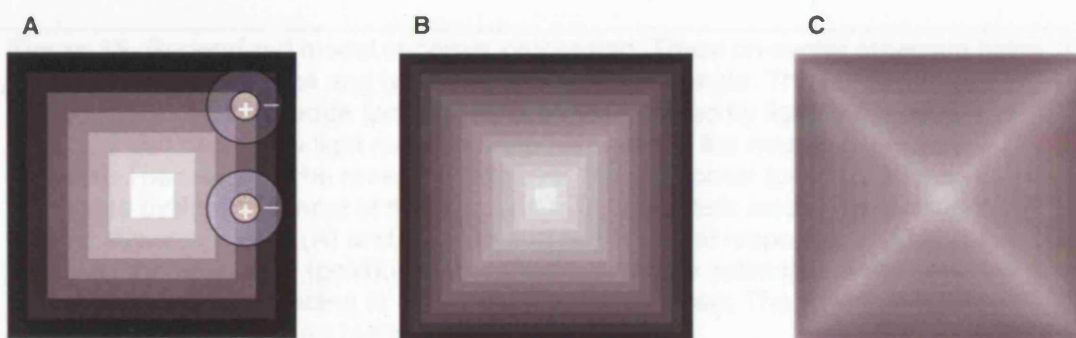
Figure 17. Hurvich's theoretical model of Vasarely's nested square illusion (Hurvich, 1981). **A)** Center-surround receptive fields are sufficient to explain the increased saliency of corners versus edges in Vasarely's square. The center-surround contrast is higher along the corner illusory-fold (upper receptive field) than along the edges of the nested squares (lower receptive field). Therefore the neural responses to the corner-fold will be higher, giving rise to a more salient percept. **B)** and **C)** Adelson's computational simulation of Hurvich's model (Adelson, 1999). A set of nested squares in a luminance gradient (B) is convolved (C) with a center-surround filter, in order to simulate the responses of a network of center-surround receptive fields. The output of the center-surround filter matches our subjective perception of the illusion.

Here we propose that Hurvich's and Adelson's models of Vasarely's nested squares illusion can be extended to a new generalized model of corner processing in the early visual system. We propose that the geometry of subcortical center-surround receptive fields makes them, in general, more sensitive to corners than to edges. This new hypothesis is not restricted to Vasarely's corner-gradients such as those addressed by Hurvich and Adelson (**Figure 17**), but applies to all corners.
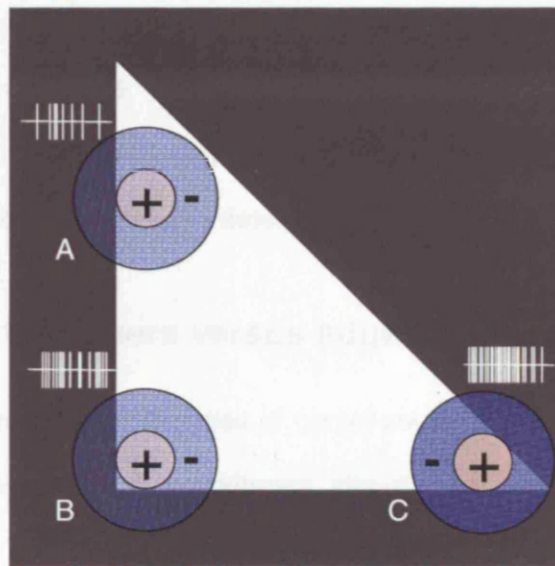
Figure 18. Generalized model of corner processing. Three on-center receptive fields are placed over one edge and two corners of a white triangle. The center of the receptive field over the edge (position A) is well stimulated by light, but most of the surround also falls in the light region, so the response of the neuron is partially inhibited. The center of the receptive field over the 90° corner (position B) is also stimulated by light and most of the surround falls in the dark area. This is a more optimal stimulus than in (A) and leads to a stronger neural response. The receptive field over the 45° corner (position C) receives even more optimal contrast between center and surround, leading to an even stronger response. The spiking responses depicted in the cartoon are hypothetical.

As illustrated in **Figure 18**, an on-center receptive field placed along an edge (position A) has light on the center, but most of the surround is also covered by light and the cell will not fire much. If we place the on-center receptive field over a 90° corner (position B in **Figure 18**), a higher proportion of surround will be covered by darkness, and the cell will fire more. When the on-center receptive field is over a sharper angle (position C in **Figure 18**) the proportion of surround covered by darkness is even higher and the cell will fire harder. We therefore propose that local contrast increases at corners, and that the sharper the corner angle, the higher the contrast. It follows that corners are hot spots for early center-surround receptive fields, and this could potentially account for the fact that corners are perceived as more salient and are more significant to shape perception.

Because subsequent receptive fields in the visual hierarchy (for instance, elongated simple-cell and complex-cell receptive fields in area V1) integrate visual

information from subcortical levels (Hubel and Wiesel, 1962; Tanaka, 1983; Ferster, 1986; Reid and Alonso, 1995; Ferster et al., 1996; Alonso and Martinez, 1998; Martinez and Alonso, 2001) we predict that cortical receptive fields will also be better tuned to corner-detection than to edge-detection.

2.2. Responses to corners versus edges

To study the response properties of center-surround neurons, we convolved DOG filters with images containing different stimuli (see **section 1.2**), and then quantified the results. To compare the strength of responses to corners versus edges in the early visual system, we applied the DOG receptive field simulations to edges and corners of different angles and contrasts.

Figure 19 shows the basic stimulus we used (100% contrast in this example); there is a corner at the top (30° in this example) and two vertical edges at the bottom. We measured the response from the computational simulations to this image, for different angles and/or contrasts of the stimulus.
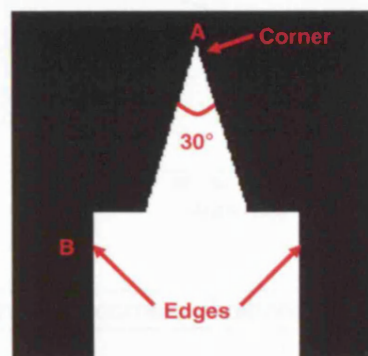
Figure 19. Stimulus containing a corner (A) and a vertical edge (B).

Figure 20 shows the DOG outputs results for 30° angles with 100%, 66% and 33% contrast. The DOG filter generates higher responses to the corner (white arrows, right column, **Figure 20**) than to the edges for all contrasts. The response of the filter decreases linearly with the stimulus contrast for both edges and corners.
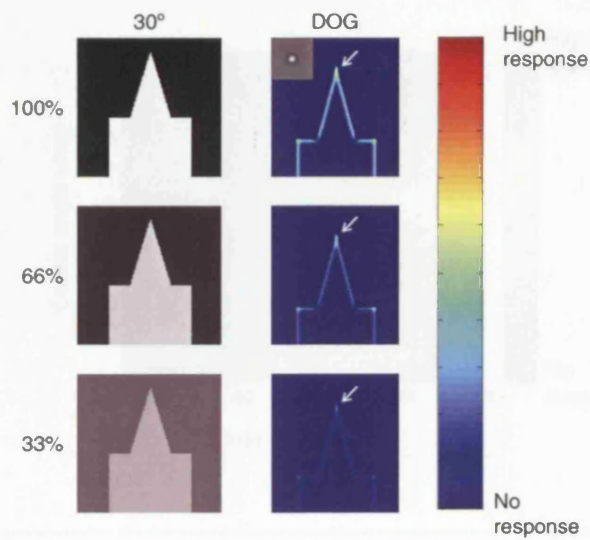
Figure 20. The stimuli in the left column are convolved with a DOG. Notice that responses to 30° corners (white arrows) are stronger than responses to edges.

Figure 21 shows the peak responses of DOG filters to all corner angles at 100% contrast (we changed the angle of the corner from 1° to 180° in 1° steps). Sharp corners generate stronger responses than shallow corners.
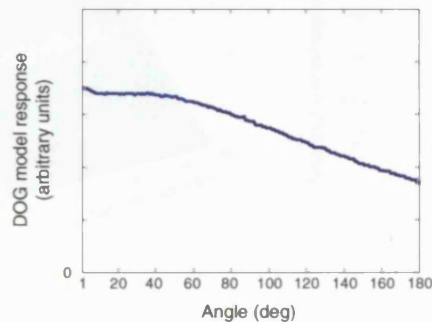
Figure 21. Predicted responses to corners of different angles (100% contrast).

If we analyze the results for all the different corner angles at all contrasts (**Figure 22**) we can see that the higher the contrast and the sharper the corner, the better the response.
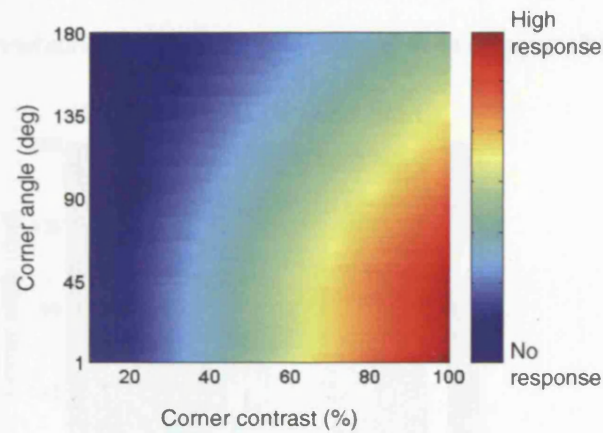
Figure 22. Predicted responses to corners of different angles and contrasts.

If we compare the response to corners against the response to edges for each contrast (**Figure 23**), we can see that the response to the corner is always higher than the response to the edge (ratio>1).
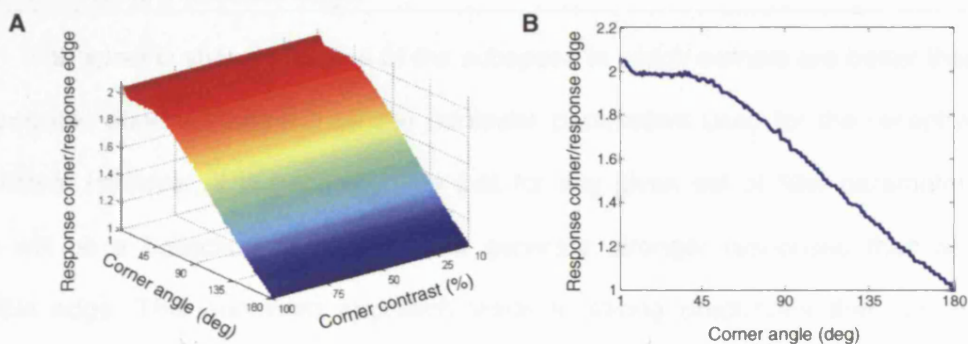
Figure 23. (A) Ratio response corner/edge for all contrasts. **(B)** Section at any value of contrast for the graph in (A).

How do responses to corners compare to responses to edges? To answer this question we calculated the level of contrast that an optimally oriented edge would need in order to evoke equivalent responses to those found for corners of all angles and contrasts (**Figure 24**). An edge could only evoke a response equivalent to the response generated by a 40° corner of 100% contrast, if the edge was about 200% contrast (dark red region in **Figure 24** colormap). However, because the contrast of a given stimulus can never be higher than 100%, equivalent contrast levels over 100%

(all warm colors in the colormaps of **Figure 24**) indicate the subspace of corner angles and contrasts in which corners are better stimuli than any possible edge.

EQUIVALENT EDGE CONTRAST
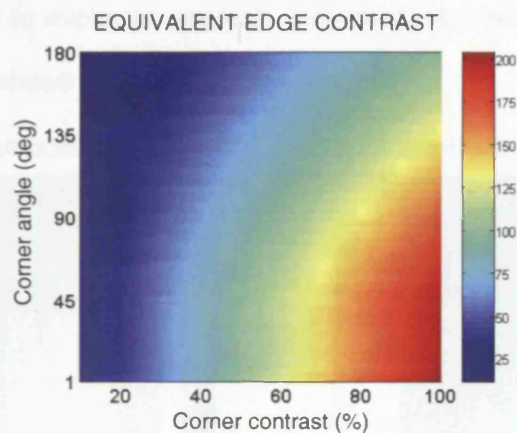
Figure 24. The colors encode the edge contrast that is necessary to evoke responses equal to corners of various angles and contrasts. Since one cannot physically raise the contrast of the edge above 100%, the warm colors (yellowish-reddish) indicate the corner parameters in which corners will generate stronger responses than any possible edge.

The specific shape and size of the subspace in which corners are better than any possible edge will depend on the particular parameters used for the receptive field filters. However, it is generally true that for any given set of filter parameters there will be a collection of corners that generate stronger responses than any possible edge. This principled approach leads to strong predictions that can be tested physiologically, and which can be used to validate different receptive field models, as well as the hypothesis that sharp corners are more salient than edges in the early visual system.

2.3. Responses to corners versus bars and spots

Kuffler showed that center-surround receptive fields give strong responses to spots (Kuffler, 1953); bars (slits of light) have also been suggested to be fundamental building blocks of vision (Hubel and Wiesel, 1959). Here we tested the theoretical responses of center-surround receptive fields to a bar of optimal width and to a spot

of optimal diameter against corners of various parameters. The analysis is similar to that in **Figure 24**, but here we calculated the level of contrast that an optimal bar/spot would need on order to evoke an equivalent response to corners of all angles and contrasts. **Figure 25** shows the results of this analysis.
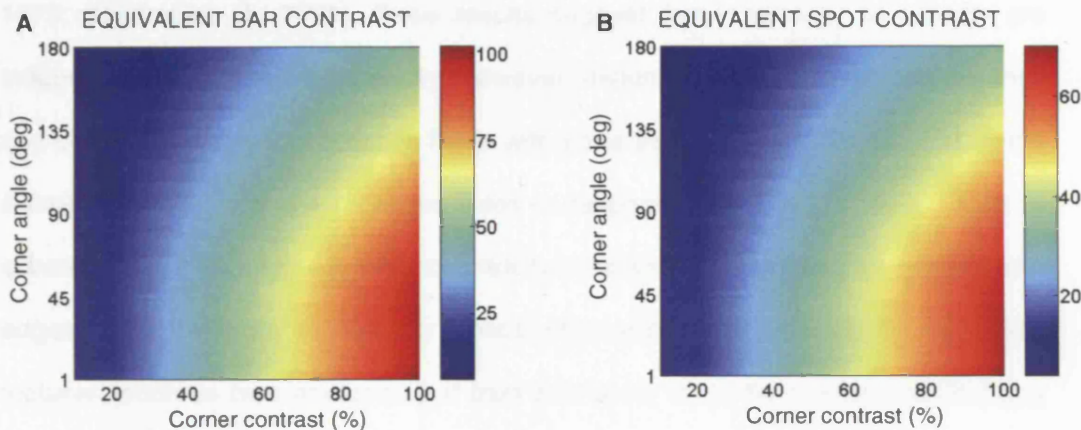
Figure 25. Comparison of responses to corners versus bars and spots. Color code as in **Figure 24**. **(A)** Sharp corners generate stronger responses than bars of optimal width (colorbar indicating equivalent bar contrast goes over 100%). **(B)** Responses to spots of optimal diameter are stronger than responses to corners.

We found that the simulated responses to sharp corners were better than the responses to bars of optimal width, but not better than responses to spots of optimal diameter. So spots are a better stimulus than corners for center-surround receptive fields. However if we consider the predominance of spots versus corners in nature, it is easy to see that spots are not very common features outside of the laboratory, whereas natural scenes contain plenty of corners (Krieger et al., 2000; Sigman et al., 2001; Yang and Purves, 2003; Howe and Purves, 2005). The next section proposes a general principle of corner perception that suggests that corners are more dependable visual stimuli than bars and spots for neurons of the early visual system.

2.4. Receptive field size independence

Receptive field responses to bars and spots are *dependent* on the interaction between the size (width) of the stimulus and the size of the receptive field. However,

responses to corners are independent of receptive field size. **Figure 26** illustrates this point.

Given that receptive field sizes increase gradually from the fovea to the periphery (Wilson and Sherman, 1976; Cleland et al., 1979; Peichl and Wassle, 1979; Kastner et al., 2001), these results suggest that responses to corners are independent of stimulus eccentricity. However responses to bars, spots, and gratings can be maximal only for receptive fields with sizes that closely match the size of the stimulus, that is, for those receptive fields corresponding to a very specific range of eccentricities. This suggests that eccentricity-invariant features (such as corners and edges) may be more reliable for shape processing than eccentricity-dependent features (such as bars and spots). If bars and spots were the fundamental building blocks of vision, we would expect objects to change brightness and shape drastically in different parts of the retina. Edges and corners are robust to eccentricity and so they may be more reliable building blocks of shape and brightness perception.

2.5. Summary and conclusions from basic simulations

In summary, our quantitative simulations suggest that:

1) Sharp corners generate stronger responses than edges for center-surround receptive fields (**Figure 24**).

2) Sharp corners generate stronger responses than bars, but not spots (**Figure 25**).

3) Responses to corners do not depend on receptive field size (and therefore eccentricity), whereas responses to bars, gratings and spots do (**Figure 26**).

Therefore, considering points 1), 2), and 3) above together, corners seem to be more dependable features than edges, bars or spots across different stimulation conditions.
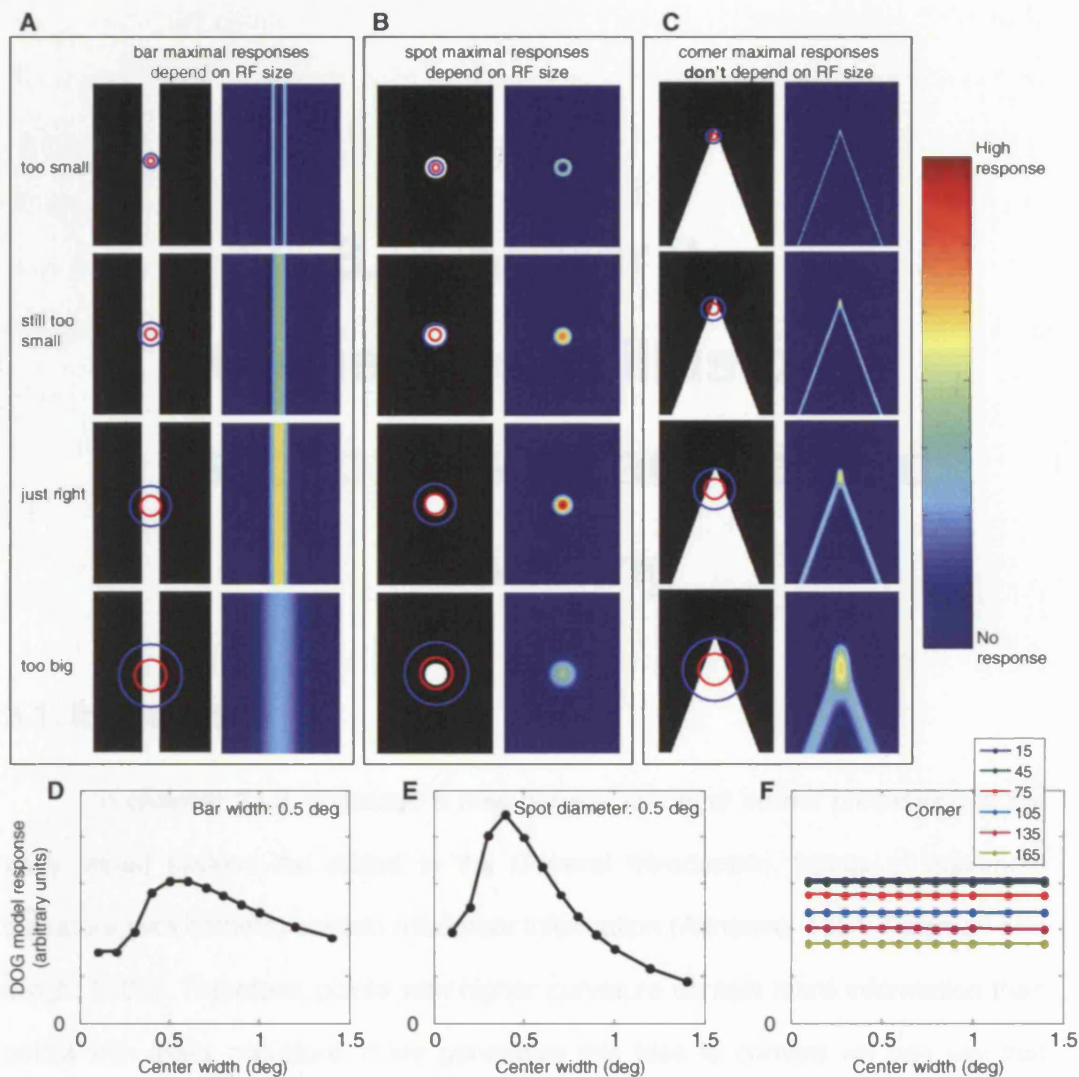
Figure 26. DOG responses to bars, spots, and corners for different receptive field sizes. **A)** The response to bars depends on the receptive field size. For a bar of a certain width (0.5 deg in the example) only a small range of receptive field sizes will generate maximum responses. **B)** The response to spots also depends on receptive field size. For a spot of a certain diameter (0.5 deg in the example) only a small range of receptive field sizes will generate maximum responses. **C)** The response to corners does not depend on receptive field size. For a corner of any given angle, all receptive field sizes will generate equivalent peak responses. Note that, although the responses generated by large filter sizes are blurrier than the responses generated by small filters, the peak of the responses remains unchanged through the different receptive field sizes (that is, the level of the red "hot spot" in each of the four convolutions is identical). **D)** Plot of maximal responses to a 0.5 deg bar for receptive fields with a center width from 0.1 to 1.4 deg. **E)** Plot of maximal responses to a 0.5 deg spot for receptive fields with a center width from 0.1 to 1.4 deg. **F)** Maximal responses of different receptive field sizes to corners of various angles. Although sharp corners generate stronger responses than shallow corners, all different receptive field sizes produce equivalent peak responses for any given corner angle.

3. Chapter 3.

Corner-based illusions: psychophysics and related modeling

3.1. Introduction

In **chapter 2** we proposed a new general model of corner processing in the early visual system. As stated in the General Introduction, points of maximum curvature (like corners) contain maximum information (Attneave, 1954; Feldman and Singh, 2005). Therefore, points with higher curvature contain more information than points with lower curvature. If we generalize this idea to corners we can say that sharp corners contain more information than shallow corners or edges. According to Barlow's Redundancy-Reducing Hypothesis (Barlow, 1961, 1989), the visual system is optimized to process the features that contain the most information. It is therefore possible that center-surround receptive fields may have evolved to make use of the reduced redundancy of corners versus edges and sharp corners versus shallow corners.

The high informational content of sharp corners, and our results that early visual modes respond more strongly to sharp than to shallow corners, led us to the prediction that sharp corners should appear more salient perceptually than shallow corners or edges. In this chapter we test this hypothesis.

As discussed in the General Introduction, Vasarely's "nested squares" illusion (Vasarely, 1970) shows that, in a luminance gradient composed of concentric squares, 90° corners generate illusory "folds", which appear as more salient (that is, either brighter or darker) than the adjacent flat (non-corner) regions of each individual square (**Figure 15**). However, one might argue that the corners of solid objects, like the red rectangle on **Figure 27**, do not appear to be more salient than the object's edges.

Figure 27. Red rectangle on a white background.

However, it also true that the edges do not appear as more salient than the interior of the rectangle, even though it is well established that early visual neurons respond to edges much more strongly than to uniform illumination (Mach, 1865; Hubel and Wiesel, 1959; Ratliff and Hartline, 1959; De Weerd et al., 1995; Livingstone et al., 1996; Paradiso and Hahn, 1996; Macknik and Haglund, 1999; Macknik et al., 2000). The reason why the edges of an object and the object's interior appear to have equivalent brightness is that "filling-in" processes in the extrastriate cortex use the information from the edges to fill in the inside (De Weerd et al., 1995; De Weerd et al., 1998; Pessoa and De Weerd, 2003; Komatsu, 2006). But under certain special stimulation conditions, like Mach bands (Mach, 1865; von Békésy, 1960; Ratliff, 1965), we can see that the edges of an object are in fact more salient than its inside. We propose that the same filling-in processes also normalize the apparent brightness of corners, explaining why corners do not generally appear as more salient than edges in most stimulation conditions (despite the fact early visual system neurons respond more strongly to corners). The geometry of the nested

square illusion partially counteracts filling-in processes, allowing us to see that corners are more salient than edges, in a similar way as the geometry of Mach bands makes it possible to see that the edges are more salient than the inside. We have developed several novel illusions that further demonstrate the perceptual saliency of corners.

3.2. Corners within luminance gradients: the Alternating Brightness Star

Vasarely's "nested squares" illusion (Vasarely, 1970) (**Figure 15**) is a classic illusion that has been described often (Hurvich, 1981; Kaiser, 1996; Morgan, 1996; Adelson, 1999; McArthur and Moulden, 1999). However, the strength of the effect has never been quantified or tested systematically with computational, psychophysical, or neurophysiological techniques. In this chapter we quantify the strength of Vasarely's nested squares illusion, and other related effects, with a psychophysical experiment (in a two-alternative-forced-choice brightness discrimination task). We also use the basic DOG models explained in **section 1.2** to explore whether our new general early receptive field model for processing corners (proposed in **section 2.1**) explains this phenomenon. Our results offer insights into the possible neural mechanisms responsible for these effects, and may help to explain corner perception in general. These experiments have been published on the journal *Perception* (Troncoso et al., 2005)

In Vasarely's artworks, each gradient fold is constructed from a series of nested squares. That is, the corner angle is exactly 90°. In order to test the strength of the illusory folds generated by Vasarely's corner-gradients, we started by varying the angles of the corners. In doing this, we discovered a novel visual illusion, which we called the Alternating Brightness Star (Martinez-Conde and Macknik, 2001; Troncoso et al., 2005). **Figure 28** shows several Alternating Brightness Stars, made

of concentric stars arranged in gradients of increasing or decreasing luminance. Bright or dark illusory folds can be perceived, depending on the polarity of the corner angle (whether the angles of the corners are concave or convex). We called this effect *Corner Angle Brightness Reversal*. An irregular version of the Alternating Brightness Star illusion (**Figure 28C**) furthermore shows that the strength of the illusion depends on how shallow or sharp the corner angle is. We called this effect *Corner Angle Salience Variation*: for shallow corner angles (**Figure 28C**, angle "2") the effect is weak, whereas for sharp corner angles (**Figure 28C**, angle "1") the illusory effect is strong (see http://smc.neuralcorrelate.com/demos/ABS-illusion.html for an interactive demonstration of these effects).

The Corner Angle Salience Variation and Corner Angle Salience Reversal effects may be related to a previous anecdotal observation by von Békésy, in which he briefly and qualitatively described the varying extents of apparent saturation in individual yellow gelatin wedges cut at different angles (von Békésy, 1968).
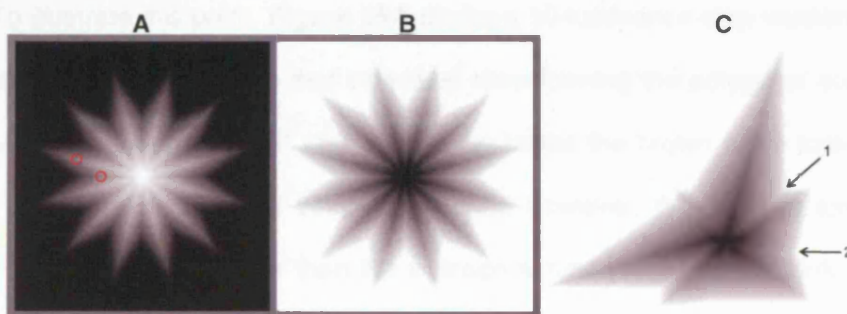
Figure 28. The Alternating Brightness Star illusion (Martinez-Conde and Macknik, 2001). **A, B)** The stimulus is made of concentric stars of graded luminance. In A), the innermost star is white; the outermost star is black. In B), the innermost star is black; the outermost star is white. The gradient from the center to the outside has 100 luminance steps. The illusory corner-folds that radiate from the center appear as light or dark depending on the polarity of the corner angle (Corner Angle Brightness Reversal effect), and on the direction of the luminance gradient. However, all illusory folds are physically equal to each other in luminance. The centers of the two red circles in A) indicate physically equivalent points in the luminance gradient. **C)** An irregular version of the Alternating Brightness Star illusion illustrates the Corner Angle Salience Variation effect. The illusory folds appear more salient with sharp corners (as in angle "1"), and less salient with shallow corners (as in angle "2"). Here the folds also appear perceptually light or dark depending on the polarity of the corner angle (concave or convex). From Troncoso et al. (2005).

These two effects are especially striking because they cannot be explained in terms of the physical luminance of the stimuli.
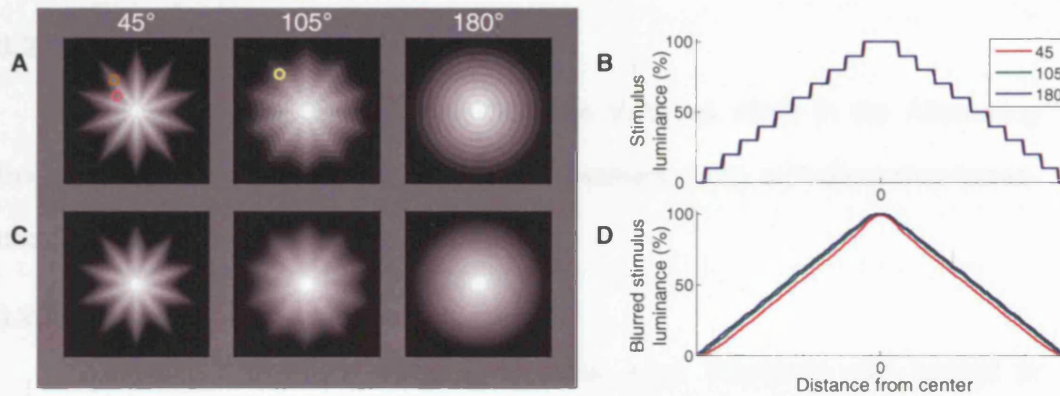
Figure 29. A) 10-luminance-step versions of Alternating Brightness Stars with 3 different angles: 45° (left column), 105° (middle), and 180° (right column). **B)** Luminance profile along one of the arms of the star for the stimuli in A), showing that the illusory have the same physical luminance in the 3 angle conditions (the three lines overlap). **C)** Blurred version of the stars in A) (Gaussian filtering). Note that the illusory folds become weaker. **D)** Luminance profile along one of the arms of the star for the stimuli in C), showing that the illusory folds cannot be explained by blurring: the luminance of the 45° star is the lowest, even though this is the condition where the illusory folds look brighter.

To illustrate this point, **Figure 29A** displays 10-luminance-step versions of the Alternating Brightness Star (so that individual stars forming the polygonal constructs are easy to identify). In the 45° star, the region inside the brown circle looks bright and the region inside the pink circle looks dark. However, the average luminance inside the brown circle is lower than the average luminance inside the pink circle! If we compare the brown circle (45° star) and the yellow circle (105° star), the region inside the brown circle looks brighter than the region inside the yellow circle, but again, the average luminance inside the brown circle is lower. This becomes evident when we blur the stimuli using a Gaussian (**Figure 29C**). **Figure 29B** shows the luminance profile of the Alternating Brightness Stars in **Figure 29A** along one of the arms of the star. The three angle conditions (45°, 105°, and 180°) have exactly the same profile. If we take the luminance profile along one of the arms of the star for the blurred stimuli (**Figure 29D**), we can see that the 45° condition (the one that looks brightest) has the lowest luminance! Blurring the stimuli works on the opposite

direction of the illusion, and therefore these effects cannot be explained by optical blurring due to the physical limitations of the eye.

3.2.1 Methods

To quantify the Corner Angle Salience Variation effect in the Alternating Brightness Star we ran a psychophysical experiment using a 2-alternative-forced-choice experimental design.

3.2.1.1 Subjects

12 naïve subjects (9 females, 3 males, adult volunteers with normal or corrected-to-normal vision) participated in 10 experimental sessions, of ~1 hour each, and were paid $15/session. Experiments were carried out under the guidelines of the Barrow Neurological Institute's Institutional Review Board (protocol number 04BN039).

3.2.1.2 Experimental Design

Subjects rested their head on a chin-rest, 57cm from a linearized video monitor (Barco Reference Calibrator V). Subjects were asked to fixate a small cross (1°x1°) within a 3.5° fixation window while visual stimuli were presented. To ensure proper fixation, eye position was measured non-invasively with a video-based eye movement monitor (EyeLink II, SR Research).

To test the magnitude of the illusory percept, subjects conducted a two-alternative-forced-choice brightness discrimination between the stimulus containing a corner gradient (Comparator stimuli) and non-illusory flat gradients (Standard stimuli). At the beginning of each trial, a red fixation cross was displayed on the monitor. Once the subject fixated the cross, two sets of stimuli appeared simultaneously: the Standard and the Comparator (one to the right and one to the left of the fixation cross, see **Figure 30**). The size of the Standard was 18° (h) x 0.5° (w). The Comparator stimulus was 18° (h) x 4° (w). Both Comparator and Standard stimuli were centered at 3° of eccentricity in both experiments.

The Comparator was a corner-gradient fold of 100 luminance steps with one of 13 possible angles: ±15°, ±30° (**Figure 30, Panel B**), ±45°, ±75° (**Figure 30, Panel C**), ±105°, and ±135° (for both illusory dark and bright folds), and 180°, which is a flat gradient (**Figure 30, Panel D**). Each step in the gradient was 0.04° high. To construct the Standard stimulus, we took a flat non-illusory gradient, we divided it into 11 luminance segments and we pseudorandomly scrambled the segments. To match the height of the Comparator we stacked 5 of these pseudorandomly scrambled gradients into a long vertical stripe that contained 55 segments total.
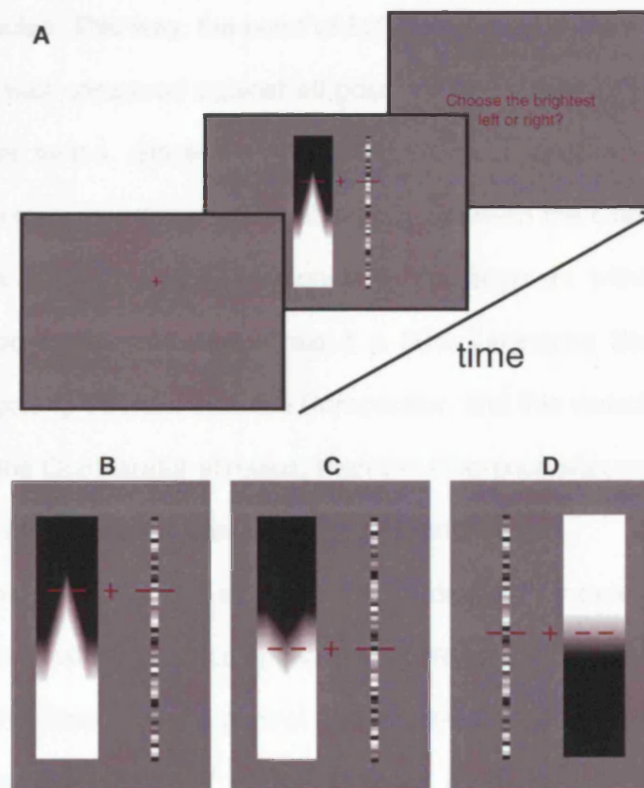
Figure 30. Experimental design. **A)** Monitor display during the time course of a single trial. **B, C, D)** Three different stimuli presentations of the brightness discrimination task (out of 572 possible conditions, see **section 3.2.2** for details). From Troncoso et al. (2005)

Red bars were displayed to the sides of the Standard and Comparator stimuli, to indicate precisely the parts of the stimuli to be compared. Red bars were always drawn at the same height as the point of 50% luminance of the corner gradient. Thus the vertical position of the red bars on the monitor varied as a function of the angle of

the corner gradient. The fixation point and the red bars on the Standard were drawn at the same vertical position as the red bars over the Comparator. The Standard stripe was drawn so that there was an equal chance of any one of the 11 possible luminance segments to be selected by the horizontal red bars. We made sure that the red bars were always in the center of one of the segments.

After 2 seconds, all stimuli disappeared. The subject's task was to compare the brightness of the pixel positioned precisely in the center between the inner ends of the red bars on the Standard stimulus, to the brightness of the same point on the Comparator stimulus. This way, the point of 50% luminance in the corner gradient of the Comparator was compared against all possible luminances of the Standard, for all corner angles tested. Since the discrimination point on the Comparator was always of 50% luminance, the physical difference between the Comparator and the Standard was a function of the luminance of the segment within the Standard stimulus indicated by the red bars. Thus if a 50% luminance Standard segment appeared perceptually different from the Comparator, and this varied as a function of corner angle of the Comparator stimulus, then the difference was not physical and it must have been caused by the illusory effects of corner angle.

Approximately half of the subjects (n=7) indicated, by pressing the left/right keys on a keyboard, which stimulus appeared *brighter* at the discrimination point (the Comparator or the Standard). To control for potential bias due to the choosing of a brighter stimulus, the other half of the subjects (n=5) indicated which stimulus appeared *darker*. These two groups were later averaged to control for criterion effects. The design was further controlled for effects of criterion, by giving subject's a bright-appearing Comparator in half the trials, and a dark-appearing Comparator in the other half of the trials. The experiment was counterbalanced for potential left/right and up/down criterion effects by ensuring that the Comparator was presented half the time on the left, and half the time on the right, with the bright half of the gradient on the upper half of the Comparator half the time. Subjects did not have to wait until the

stimuli turned off to indicate their decision, and could answer as soon as they were ready, in which case the stimuli were removed from the screen and the trial ended at the time of the subject's key-press. Standard and comparator had the same average luminance (50% gray) in all conditions. If the subject broke fixation (as measured by EyeLink II), the trial was aborted, and replaced in the pseudorandom trial stream to be re-run later.

The summary of all conditions (n = 572) was as follows:

- 2 screen positions: left and right

- 2 gradient directions: bright on top, dark on top

- 13 corner angles: ±15°, ±30°, ±45, ±75°, ±105°, and ±135° plus 180° (flat)

- 11 Standard luminances: 5%, 14%, 23%, 32%, 41%, 50%, 59%, 68%,

77%, 86%, and 95%

For each subject, each combination of gradient direction (bright-on-top versus dark-on-top) and corner angle was presented 20 times, over 10 sessions (2 trials per session per combination).

Psychometric curves were obtained fitting the data with logistic functions using a maximum likelihood procedure (Wichmann and Hill, 2001).

3.2.1.3 Center-surround simulations

As explained in **section 1.2.2**, we modeled center-surround receptive fields as Difference-Of-Gaussians (DOG) filters (Rodieck, 1965; Enroth-Cugell and Robson, 1966).

3.2.2 Results

3.2.2.1 Qualitative observations on the Corner Angle Brightness Reversal Effect

As predicted by the Corner Angle Brightness Reversal effect described earlier in the Alternating Brightness Star, the perceived sign of the illusory fold depended on the interaction between the polarity of the angle (concave, or upwards versus

convex, or downwards) and the direction of the gradient (black-to-white versus white-to-black). Black-to-white gradients (top-to-bottom) led to bright illusory folds when presented with upwards angles (as in **Figure 30A**), whereas the same gradient direction led to dark illusory folds when presented with downwards angles (as in **Figure 30B**). Conversely, white-to-black gradients (top-to-bottom) lead to bright illusory folds when presented with downwards angles, and to dark illusory folds when presented with upwards angles.

The summary of the qualitative perceptual effects with top-to-bottom gradients was as follows:

1) Black-to-white gradient + upwards angle = bright percept

2) White-to-black gradient + downwards angle = bright percept

3) Black-to-white gradient + downwards angle = dark percept

4) White-to-black gradient + upwards angle = dark percept

3.2.2.2 Alternating Brightness Star psychophysical test

We calculated the Point of Subjective Equality (PSE) for each Comparator (that is, its matching luminance in the non-illusory Standard) by determining the point on the psychometric curve (**Figure 31A**) in which the Comparator appeared more salient than the Standard in 50% of the trials (averaged over all subjects, and collapsed across conditions **1)**, **2)**, **3)**, and **4)** described above). The illusory enhancement for each corner angle was calculated as the difference between the point of subjective equality for a 180° non-illusory gradient and the point of subjective equality for the angle tested (**Figure 31B**). We found that the perceived salience of the corner varied linearly with the angle of the corner (independently of the interactions between angle polarity and gradient direction). Sharp angles generated stronger illusory salience than shallow angles (Corner Angle Salience Variation).
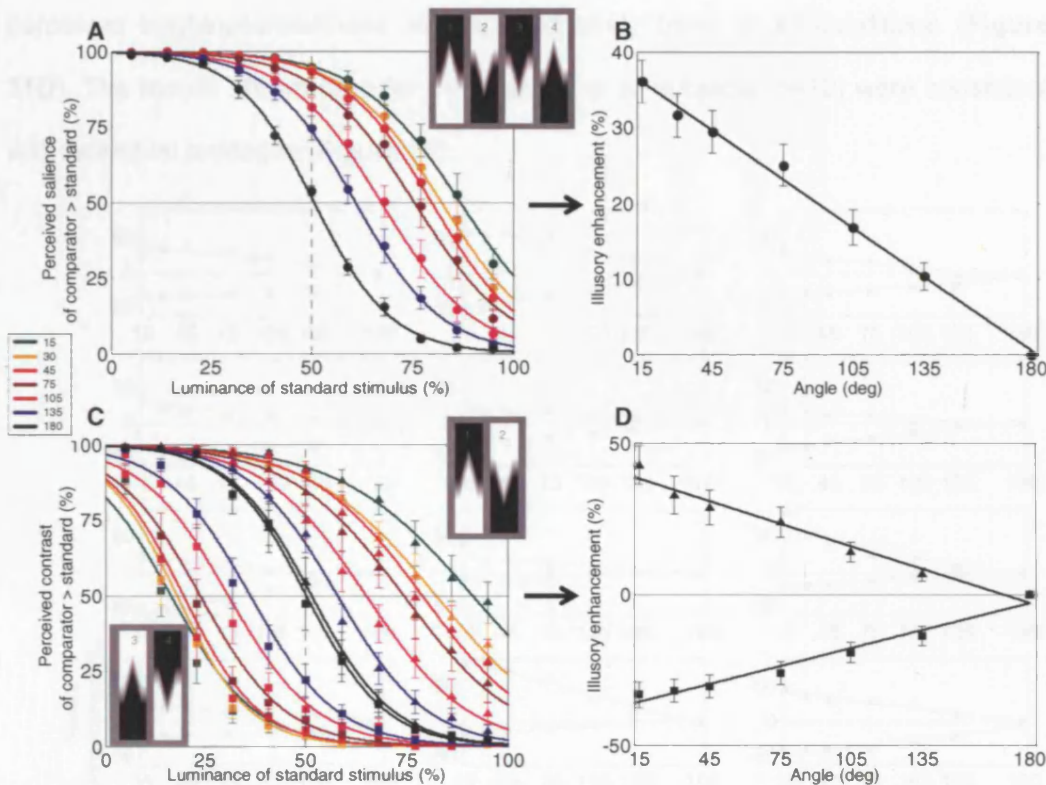
Figure 31. Psychophysical results for the Alternating Brightness Star experiment. **A)** Psychometric functions for the different corner angles are plotted in different colors. Gradient and angle polarities are collapsed: that is, we have averaged together the conditions where the illusory folds of the Comparator looked bright and the conditions where they looked dark (Insert: illustrations of the 4 collapsed conditions, for a 30° angle). **B)** Illusory enhancement of the PSEs with respect to the control condition (180° gradient) for the different Comparator corner angles. The illusory enhancement decreases linearly as the angle of the Comparator corner gradient becomes shallower (Corner Angle Salience Variation effect). **C)** Same data as in (A), but the conditions in which the illusory fold looked bright (triangles), and the conditions in which the illusory fold looked dark (squares) are presented separately (see inserts). The PSEs for conditions 1 and 2 (see insert) fall above the point of 50% luminance in the Standard stimulus. The PSEs for conditions 3 and 4 (insert) fall below the point of 50% luminance in the Standard stimulus (Corner Angle Brightness Reversal effect). **D)** Illusory enhancement of brightness (triangles) and darkness (squares) perception, as a function of corner angle. Error bars in A), B), C), D) represent the ± standard error of the mean for all subjects in each condition (n=12). From Troncoso et al. (2005).

Figure 31C shows the same results, but conditions **1)** and **2)** (triangle symbols) are plotted separately from conditions **3)** and **4)** (square symbols). PSEs for conditions **1)** and **2)** were higher than the PSE for the control, whereas PSEs for conditions **3)** and **4)** were lower than the PSE for the control (Corner Angle Brightness Reversal). The relationship between the angle of the corner and its

perceived brightness/darkness was approximately linear in all conditions (**Figure 31D**). The results shown here for the average of all subjects (n=12) were consistent with individual averages (**Figure 32**).
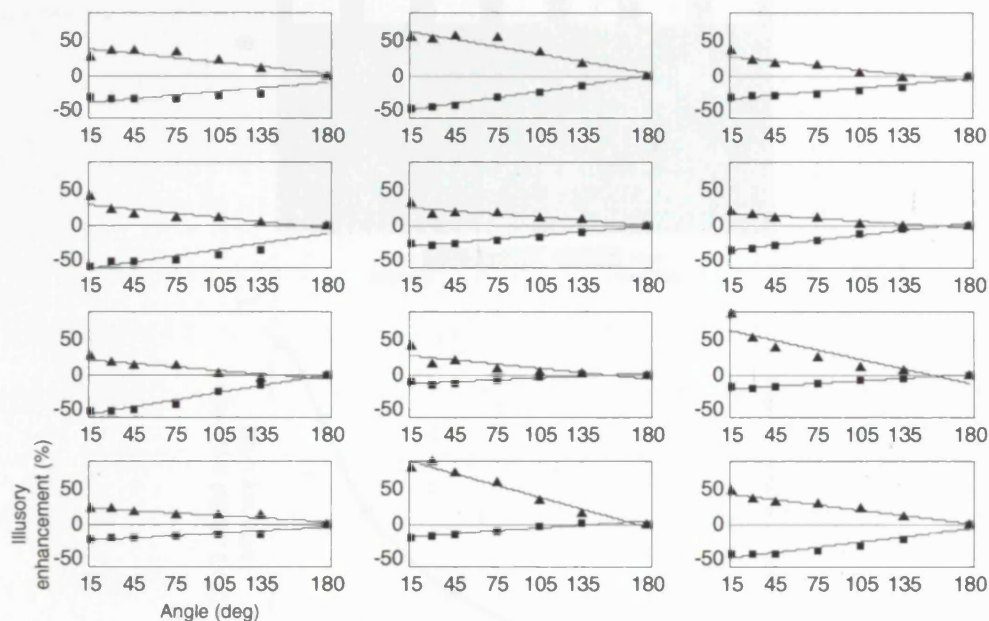
Figure 32. Individual subjects results. Each panel shows the result for an individual subject (axis and signs as in **Figure 31D**). Every single subject showed a parametric relationship between the angle of the corner and the perceived salience.

3.2.2.3 Center-surround simulations

Hurvich proposed that Vasarely's nested square illusion could be accounted for by center-surround receptive fields (Hurvich, 1981) (**Figure 17**). Center-surround receptive fields and lateral inhibitory processes have also been proposed to explain other classical brightness illusions, such as the Hermann grid (Hermann, 1870; Baumgartner, 1960, 1961; Spillmann and Levine, 1971), Mach bands (Mach, 1865; von Békésy, 1960; Ratliff, 1965), and Chevreul's staircase (Chevreul, 1839). We wondered whether the psychophysical results described here could be accounted for by an extension of Hurvich's center-surround model of Vasarely's nested square illusion, now applied to corner-gradients of all angles.
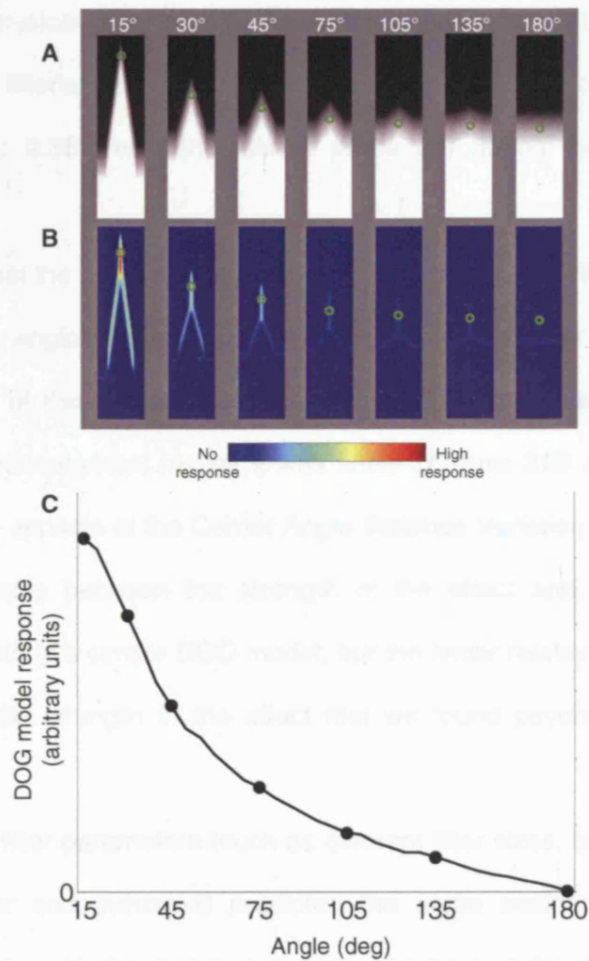
Figure 33. Computational simulations with a DOG filter. The filter parameters were chosen to match physiological center-surround receptive fields at the eccentricity used in the psychophysical experiments (3°). **A)** Examples of corner-gradient stimuli analyzed in the simulations (dark-to-bright gradients, upwards angles). These stimuli were equivalent to the Comparators (condition 1) in the psychophysical experiment. The green circles mark the point of 50% luminance. **B)** Convolving the DOG filter with the stimuli in (A) simulates the output of an array of center-surround neurons. The green circles indicate the responses of the model at the point of 50% luminance on the actual gradient. **C)** Predicted responses, at the point of 50% luminance on the corner gradient, for angles between 15° and 180° (in 5° steps). The data points indicate the angles used in the psychophysical experiment. From Troncoso et al. (2005).

To test this possibility, we modeled center-surround receptive fields as DOG filters (Rodieck, 1965; Enroth-Cugell and Robson, 1966); see **section 1.2.2** for details. We chose the size of the DOG filter to match a range of physiological center-surround receptive fields in the primate LGN (Derrington and Lennie, 1984; Irvin et al., 1993; Tadmor and Tolhurst, 2000; Levitt et al., 2001) at the eccentricity used

during the psychophysical experiments (3°). Both center and surround had the same weight towards the filter's output. **Figure 33** shows the results of convolving a DOG filter (σ_c: 0.18°; σ_s: 0.36°) with the stimuli presented during the psychophysical experiments.

We found that the predicted strength of the effect varied with the angle of the corner, with sharp angles producing stronger outputs. However, the relationship between the angle of the corner and the strength of the response was not linear, whereas in the psychophysical results it was linear (**Figure 31B** and **Figure 31D**). Thus the qualitative aspects of the Corner Angle Salience Variation effect (that is, the parametric relationship between the strength of the effect and the angle of the corner) are predicted by a simple DOG model, but the linear relationship between the corner angle and the strength of the effect that we found psychophysically is not accounted for.

Other DOG filter parameters (such as different filter sizes, or different weights between the center and surround) predicted the same basic result, with some variation in the shape of the curve, but none reproduced the linear relationship between corner angle and perceptual salience found psychophysically (**Figure 34A** and **Figure 34B**). Several other variations of the DOG model included using a half-wave squaring non linearity (instead of half wave rectification), applying local mean luminance normalization (Tadmor and Tolhurst, 2000), using Gabor filters, and using a quadrature energy model (Adelson and Bergen, 1985; Morrone and Burr, 1988). As shown in **Figure 34C** and **Figure 34D**, none of these alternative models predicted the linear relationship found in the experiment. Two main possibilities may account for this discrepancy: a) the psychophysical effects are not fully accounted for by center-surround neurons, or b) the psychophysical effects *are* fully explained by center-surround neurons, but simple DOG and other linear filters are not accurate models of center-surround receptive fields. These possibilities are moreover not mutually exclusive. Future experiments will obtain physiological recordings from LGN

neurons in the awake primate while presenting equivalent stimuli, in order to distinguish between these two alternatives.
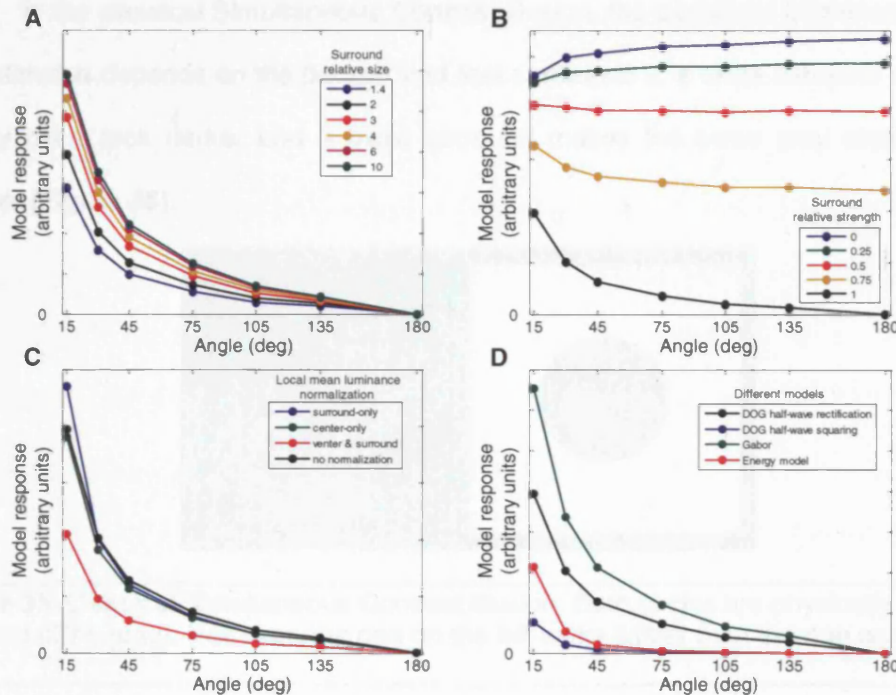
Figure 34. Predicted responses from several computational models. None of the variations plotted predicts the linear relationship between corner angle and corner salience found psychophysically. **(A)** DOG model with different surround sizes relative to the size of the center. **(B)** DOG model with different surround strengths relative to the strength of the center. **(C)** DOG model with local mean luminance normalization, as proposed by Tadmor and Tolhurst, (2000). **(D)** DOG with half-wave squaring as the nonlinearity, Gabor model, and energy model. In all plots the black line represents the results using the standard DOG model from **Figure 33**.

3.3. Solid corners: Flicker Augmented Contrast Corners

To ensure that the relationship between corner angle and corner salience (Corner Angle Salience Variation effect) is not limited to corners embedded in luminance gradients (as in the Alternating Brightness Star), we developed a new variant of the "Flicker Augmented Contrast" illusion (Anstis and Ho, 1998) that illustrates the perceptual saliency of solid corners. We then quantified the perceptual brightness of corners with different angles, using an experimental design equivalent

to the design used for the Alternating Brightness Star study. The results will be presented at the Visual Science Society 6th Annual Meeting (Troncoso et al., 2006).

In the classical Simultaneous Contrast illusion, the perceived brightness of a gray stimulus depends on the background that surrounds it: a white surround makes a gray circle look darker and a black surround makes the same gray circle look brighter (**Figure 35**).
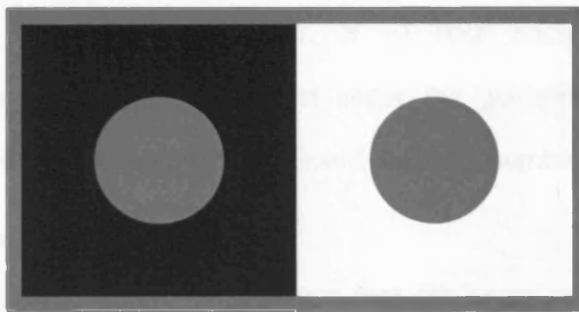
Figure 35. Classical Simultaneous Contrast Illusion. Both circles are physically identical (50% gray). However, the one on the left looks lighter than the one on the right.

Anstis and Ho discovered that Simultaneous Contrast is greatly enhanced if the grey circle flickers between white and black. They called this effect "Flicker Augmented Contrast": "a flickering test spot looks almost white on a dark surround and almost black on a light surround" (Anstis and Ho, 1998) (see at interactive demonstration of their illusion at http://www-psy.ucsd.edu/~sanstis/SAFAC.html). We created a variant of the Flicker Augmented Contrast illusion by introducing a corner as the flickering stimulus. If our general model of corner processing in the early visual system is correct, then the strength of the Flicker Augmented Contrast illusion should vary parametrically with the angle of the corner (Corner Angle Salience Variation). Here we quantify this effect: our results show that the Corner Angle Salience Variation effect is not restricted to corners embedded in luminance gradients (as in the Alternating Brightness Star), but it is a general and fundamental principle of corner perception, with potentially crucial implications for the brain mechanisms underlying early visual processing of shape and brightness.

3.3.1 Methods

To quantify the Corner Angle Salience Variation effect with the solid flickering corners we used the same 2-alternative-forced-choice design as in the Alternating Brightness Star experiment (see **section 3.2.1** for details)

3.3.1.1 Subjects

4 naïve subjects (adult volunteers with normal or corrected-to-normal vision) participated in 10 experimental sessions, of ~1 hour each, and were paid $15/session. Experiments were carried out under the guidelines of the Barrow Neurological Institute's Institutional Review Board (protocol number 04BN039).

3.3.1.2 Experimental Design

All the experimental set up and design was the same as in the Alternating Brightness Star experiment (see **section 3.2.1**)

The Comparator was a flickering corner with one of 13 possible angles: ±15°, ±30°, ±45°, ±75°, ±105°, and ±135°, and 180° (flat) (**Figure 36**). The corner flickered between 15% gray and 85% gray (50% luminance over time) at 15Hz (Anstis and Ho, 1998) against a black or a white background. At this flickering rate subjects had no difficulty lumping both phases of the flicker together and making judgments of the overall brightness of the flickering region (Anstis and Ho, 1998). To construct the Standard stimulus, we took a flat non-illusory gradient (100 steps, 0.06°/step), we divided it into 11 luminance segments and we pseudorandomly scrambled the segments. To match the height of the Comparator we stacked 4 of these pseudorandomly scrambled gradients into a long vertical stripe that contained 44 segments total. The size of the Standard was 24° (h) x 0.5° (w). The Comparator stimulus was 24° (h) x 4° (w). Both Comparator and Standard stimuli were centered at 3° of eccentricity.
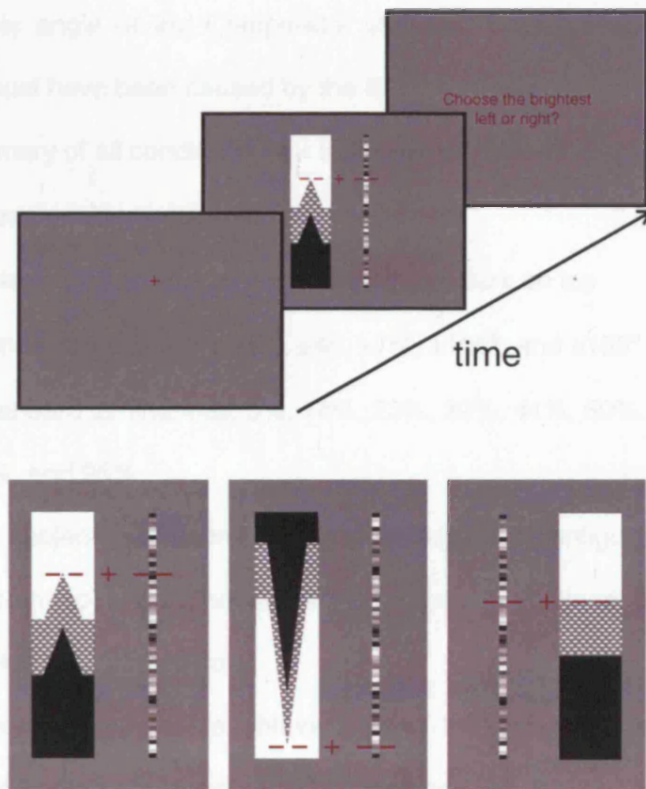
Figure 36. Experimental design. **A)** Monitor display during time course of a single trial. **B, C, D)** Three different stimuli presentations of the brightness discrimination task (out of 572 possible conditions, see Methods **section 3.2.2** for details). The patterned parts of the stimuli represent flickered between 15% and 85% gray at 15Hz during the experiments (50% luminance over time).

Red bars were displayed to the sides of the Standard and Comparator stimuli, to indicate precisely the parts of the stimuli to be compared. The red bars were always drawn at the same height as the tip of the flickering corner in the Comparator. Thus the vertical position of the red bars on the monitor varied as a function of the angle of the corner gradient.

The tip of the flickering corner was compared against all possible luminances of the Standard, for all corner angles tested. Since the discrimination point on the Comparator was always of 50% luminance, the physical difference between the Comparator and the Standard was a function of the luminance of the segment within the Standard stimulus indicated by the red bars. Thus if a 50% luminance Standard segment appeared perceptually different from the Comparator, and this varied as a

function of corner angle of the Comparator stimulus, then the difference was not physical and it must have been caused by the illusory effects of corner angle.

The summary of all conditions (n = 572) was as follows:

- 2 screen positions: left and right

- 2 background configurations: white on top, dark on top

- 13 corner angles: ±15°, ±30°, ±45, ±75°, ±105°, and ±135° plus 180° (flat)

- 11 Standard luminances: 5%, 14%, 23%, 32%, 41%, 50%, 59%, 68%,

77%, 86%, and 95%

For each subject, each combination of background configurations (white-on-top versus. black-on-top) and corner angle was presented 20 times, over 10 sessions (2 trials per session per combination).

Psychometric curves were obtained fitting the data with logistic functions using a maximum likelihood procedure (Wichmann and Hill, 2001).

3.3.2 Results

We determined the Point of Subjective Equality for each Comparator as in the Alternating Brightness Star experiment (**Figure 37A**). We calculated the illusory enhancement for each corner angle as the difference between the point of subjective equality for the 180° non-corner condition and the point of subjective equality for the angle tested (**Figure 37B**). We found that the perceived salience of the corner varied parametrically with the angle of the corner. Sharp angles generated stronger illusory salience than shallow angles (Corner Angle Salience Variation), as also found in the Alternating Brightness Star experiment. The average result (**Figure 37A** and **Figure 37B**) is consistent with the data for each individual subject (**Figure 37C**). Our results show that the Corner Angle Salience Variation effect is not limited to corners embedded within luminance gradients. Therefore we propose that the parametric relationship between corer angle and corner saliency is a general and fundamental principle of corner perception.
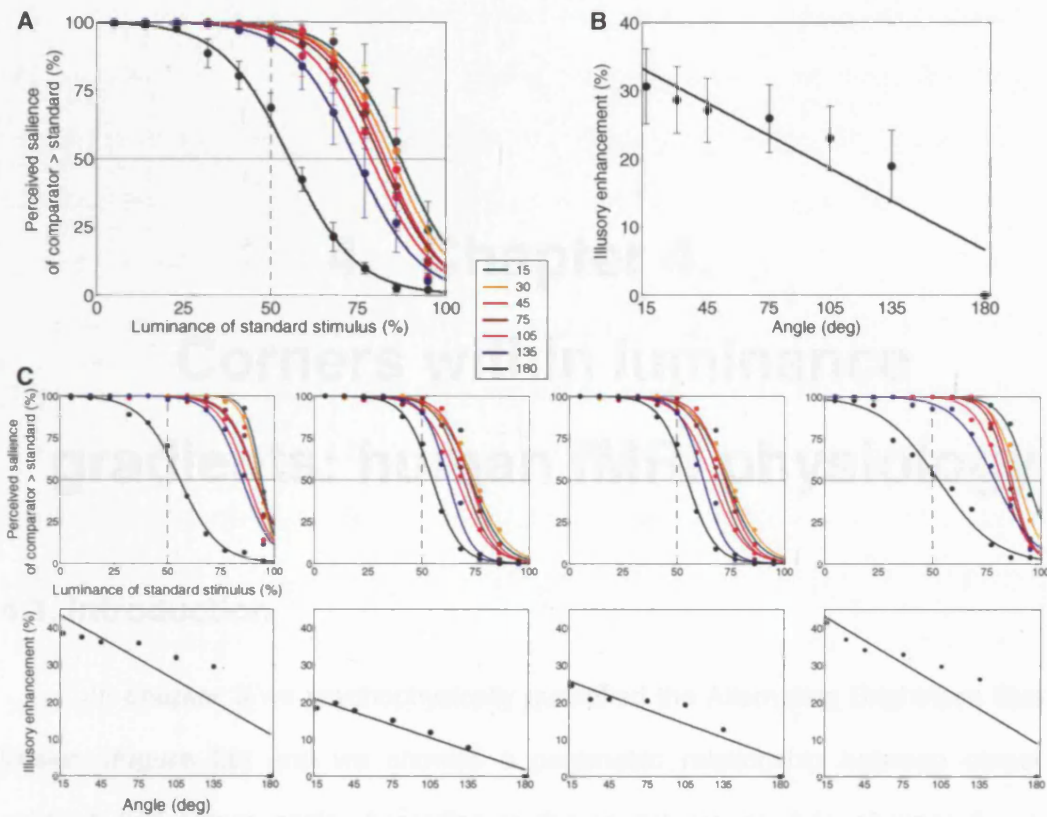
Figure 37. Psychophysical results for the flickering solid corner experiment. **A)** Psychometric functions for the different corner angles are plotted in different colors. The conditions where the tips of the corner of the Comparator looked bright and the conditions where they looked dark are collapsed. **B)** Illusory enhancement of the PSEs with respect to the control condition (180° corner) for the different Comparator corner angles. The illusory enhancement decreases parametrically as the angle of the Comparator corner gradient becomes shallower (Corner Angle Salience Variation effect). Error bars in A) and B) represent the ± standard error of the mean for all subjects in each condition (n=4). **C)** Results for the individual subjects: psychometric curves (top row) and illusory enhancement (bottom row).

4. Chapter 4.

Corners within luminance gradients: human fMRI physiology

4.1. Introduction

In **chapter 3** we psychophysically quantified the Alternating Brightness Star illusion (**Figure 28**) and we showed a parametric relationship between corner salience and corner angle. According to the model proposed in **chapter 2**, we suggested that the increase in perceived brightness at corners, curves, and other discontinuities, is due to the interaction between the shape of corners and the shape of early visual receptive fields. Previous models of corner processing suggested a primary role of specific extrastriate circuits in corner perception and processing (Hubel and Wiesel, 1965; Pasupathy and Connor, 1999; Ito and Komatsu, 2004). We conducted an fMRI experiment to test our hypothesis that all retinotopic receptive fields, may be equipped to locate corners on surfaces and encode their angle, whereas more specialized corner circuits, such as those found in V4 (Pasupathy and Connor, 1999), may encode specific features about corners, such as their orientation. If our hypothesis is correct, then all retinotopic areas in the occipital lobe should respond in a parametric way to corners of varying angles. If our hypothesis is incorrect, only those areas that are classically concerned with corner processing will preferentially activate in a differential manner to corner angle.

No previous studies of corner processing have been conducted in humans with whole brain fMRI imaging. The goal of our study was to determine the neural substrates of the Alternating Brightness Star illusion, particularly the Corner Angle Salience Variation effect, in the visual cortex of human subjects. We presented normal volunteers with Alternating Brightness Stars having equivalent angles to those used previously in the psychophysical experiments (see **chapter 3**), while acquiring fMRI data. We localized the retinotopic brain regions that modulated their activity in correlation with the angle of the corner. The BOLD correlates of the Alternating Brightness Star illusion matched the psychophysical results: BOLD signal responses were stronger for sharp angles than for shallow angles. A parametric relationship between corner angle and strength of BOLD signal was moreover observed in all individual retinotopic areas, and with similar magnitudes. This suggests that corner detection and corner angle salience processing are generalized properties of the early visual system, rather than the function of only a small subset of occipital circuits. Therefore we propose that specific corner-processing circuits, such as end-stopped cells in extrastriate areas (Hubel and Wiesel, 1965) and corner-processing neurons in area V4 (Pasupathy and Connor, 1999) serve to determine precise characteristics of corners, such as their orientation. These results offer insights into the neural mechanisms responsible for corner processing, and the stage(s) of the visual hierarchy in which it may first arise. This work has been presented at the flowing 2005 meetings: the European Conference on Visual Perception, the Society for Neuroscience Annual Meeting, and the Optical Society of America Vision Meeting (Troncoso et al., 2005a, 2005c, 2005b).

4.2. Methods

4.2.1 Subjects

24 healthy volunteers (of both genders between the ages of 18 and 40) participated in the study. Subjects were paid twenty dollars per session. All subjects were scanned on (at least) two separate days, with 1 session per day (1 session for retinotopic mapping and 1 or 2 sessions to measure BOLD responses under the different experimental conditions). Experiments were carried out under the guidelines of Dartmouth College's Institutional Review Board (protocol number 15782).

4.2.2 Stimuli

We drew Alternating Brightness Stars to extend across the entire monitor screen (**Figure 38**) and we presented them at 8 Hz counterphase flicker. Flickering the stimuli in this way had the dual benefit of counteracting luminance adaptation and maximizing the stimulation of the visual system.

Stimuli were projected onto a plexiglass screen outside the bore of the magnet, and viewed via a tangent mirror inside the magnet that permitted a maximum of 22° X 16° visible area. The projected image was smaller than this area and subtended approximately 17° X 12°. The monitor's luminance was linearized. In order to control for the potential effects of global luminance changes, we normalized the overall spatial luminance of the Alternating Brightness Star images with respect to the 180° condition. After luminance normalization, global luminance contrast (image luminance peak to image luminance trough distance) was highest in the 180° Alternating Brightness Star, and lowest in the 15° Alternating Brightness Star. This was a conservative control, as it was designed to work against our hypothesis that BOLD signal should increase with corner angle sharpness.

	A Alternating Brightness Star	B Same Contrast	C Opposite Contrast	D Contours
180 degrees				
105 degrees				
75 degrees				
45 degrees				
15 degrees				
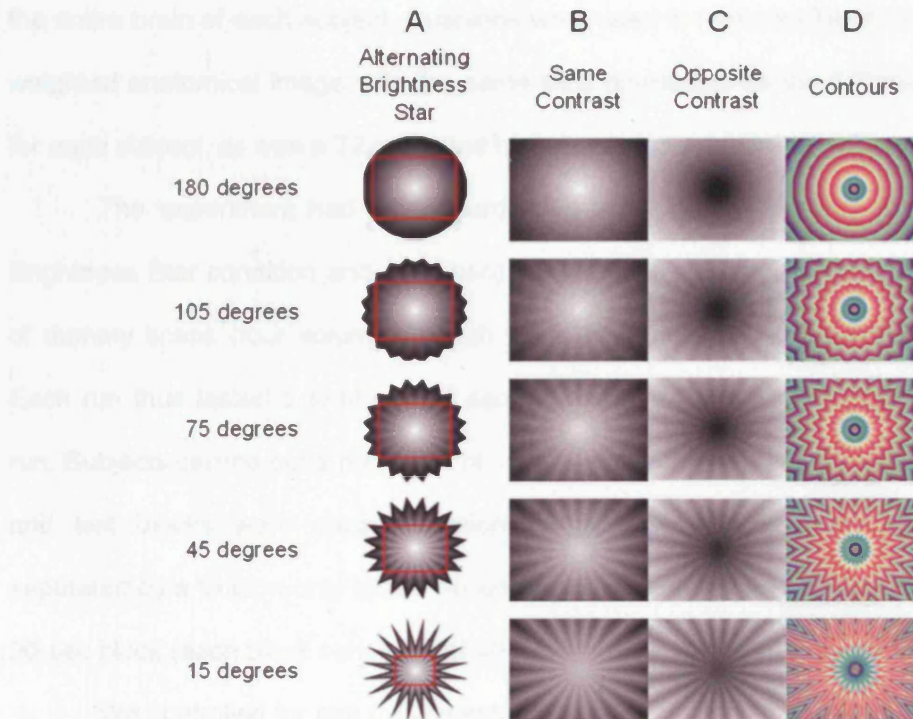
Figure 38. Alternating Brightness Star stimuli used during the fMRI experiment. **Column A)** Alternating Brightness Stars of different angle vertices. As the protruding vertices decrease in angle (lower rows), the brightness/salience effect grows stronger. Thus the peaks and troughs of each arm of the star look more salient with sharper angles, despite the fact that they have the same luminances as in lower angles. The red rectangle over each Alternating Brightness Star represents the part of the stimulus that was cropped and scaled to create the stimuli in columns B, C, and D. **Column B)** Same stimulus as in A, now zoomed in and normalized for overall luminance. The illusory effect remains stronger for the lower rows, which have sharper angles, even though their maximal overall contrast is lower than in the upper rows (due to the luminance normalization). **Column C)** Same as column B, but now sign-reversed. **Column D)** Same as in columns A-C, but now with a randomized color gradient, so that the angle of the contours in each row is more prominent. All stimuli presented during the experiment were from columns B and C.

4.2.3 Experimental Design

Continuous whole-brain BOLD signal was acquired at the Dartmouth Brain Imaging Center on a GE 1.5T signa scanner using a head coil. We collected standard T2*-weighted echoplanar functional images using 25 slices (4.5 mm thickness and 3.75-by-3.75 mm in-plane voxel resolution, inter-slice distance 1mm, TR = 2500 msec, flip angle = 90°, field-of-view = 240 X 240 X 256 mm, interleaved slice acquisition, matrix size=64x64) oriented approximately along the anterior-commissure posterior-commissure plane. These slices were sufficient to encompass

the entire brain of each subject. Cushions were used to minimize head motion. A T1-weighted anatomical image with the same slice orientation as the EPI was collected for each subject, as was a T2-weighted high resolution anatomical scan.

The experiment had a standard fMRI block design, with 11 (5 Alternating Brightness Star condition and 6 fixation) 20 sec blocks. Each run began with 10 sec of dummy scans (four volumes, which were discarded) to bring spins to baseline. Each run thus lasted a total of 230 sec. Condition order was randomized on each run. Subjects carried out a minimum of 10 runs each, and a maximum of 24. The first and last blocks were always fixation-only, and condition blocks were always separated by a fixation-only block. An entire cortical volume was scanned 8 times per 20-sec block (each block consisted of 40 cycles of the stimulus, duty cycle = 500ms).

We controlled for eye movements, wakefulness, and attention to the fovea by requiring subjects to perform a demanding reaction-time task, in which they had to respond (via button press) to a randomly-occurring change in fixation point color. The fixation point was approximately 0.2° X 0.2° and changed color on average about once every 1.5 sec. This color change occurred an equal number of times during each block. No motor areas were found to be activated differentially between conditions, corroborating that the motor task was equivalent across all conditions. This task could only be carried out successfully if the subject was fixating during both condition and fixation-only blocks, and attending to the fixation point carefully.

4.2.4 Data preprocessing

Data was analyzed offline using BRAIN VOYAGER (BV) 4.9.6 and custom MATLAB software. Effects of small head movements were removed using BV's motion correction algorithm. Slice scan time correction was carried out to correct for the fact that slices were not collected at the same time. Slices were corrected to have the same mean intensity. Functional data was not smoothed in the space domain, but any low-frequency temporal fluctuations whose wavelength was greater than 29

TRs were removed. This did not introduce correlations between a voxel and its neighbors.
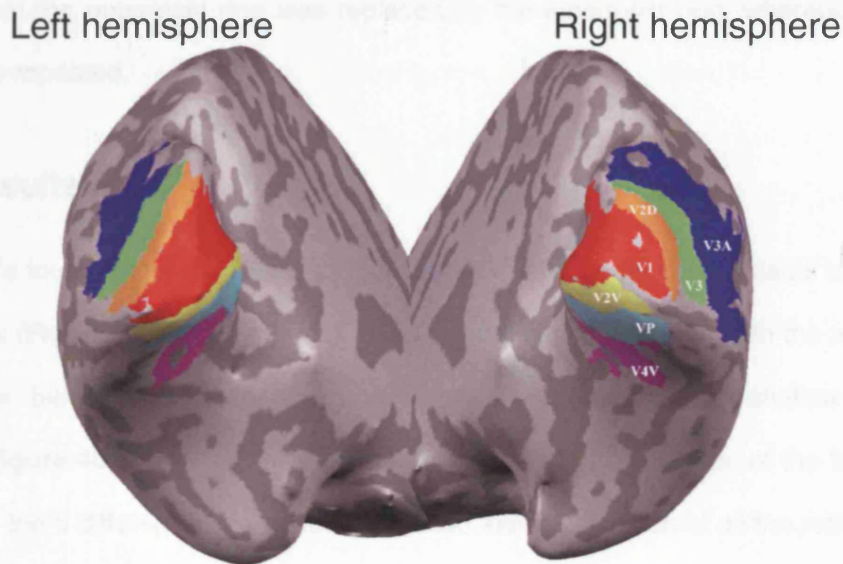
Figure 39. Retinotopic areas. Example of a single subject's right and left hemispheres with retinotopic areas marked.

4.2.5 Retinotopy

Retinotopy (**Figure 39**) was carried out using standard phase-encoding techniques (Sereno et al., 1995) (4.5 mm thickness and 3.75-by-3.75 mm in-plane voxel resolution, inter-slice distance 1mm, TR = 1600 msec, flip angle = 90°, field-of-view = 240 X 240 X 256 mm, interleaved slice acquisition, matrix size=64x64; 16 slices oriented along the calcarine sulcus) with the modification that two wedges of an 8Hz flicker black and white checkerboard grating were bilaterally opposite, to enhance signal to noise. Wedges occupied a given location for 2 TRs (3.2 secs) before moving to the adjacent location in a clockwise fashion. Each wedge subtended 18 degrees of 360 degrees. 9.6 secs (6 TRs of dummy scans) were discarded before each run to bring spins to baseline. 168 volumes were collected on each run. A minimum of 7 wedge runs were collected for each subject and then averaged to minimize noise before retinotopic data analysis in BV 4.9.6. A minimum of 3 runs were collected per subject using expanding 8Hz flickering concentric rings

that each spanned approximately one degree of visual angle in ring width. Each ring

was updated after one TR (1.6s) after which it was replaced by its outward neighbor,

except that the outermost ring was replaced by the innermost ring, whereupon the

cycle was repeated.

4.3. Results

We found angle-correlated BOLD activity in all the retinotopic visual areas of

the cortex (**Figure 40** and **Figure 41**). BOLD signal varied gradually with the angle of

the corner, being strongest for sharp corner angles and weakest for shallow corner

angles. **Figure 40** shows the average time-courses (n = 24 subjects) of the %BOLD

signal for the 5 different angle conditions tested, using the union of all the retinotopic

areas of each subject as the Region of Interest.
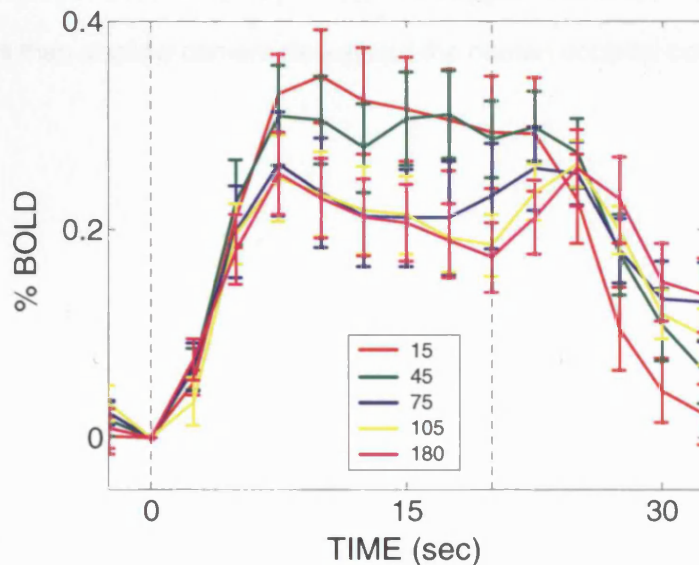
Figure 40. %BOLD responses to the Alternating Brightness Star stimulus, from all
retinotopic areas in 24 subjects. Response time-course plots from all 5 angle
conditions, color-coded for different corner angles. We used the union of all the
retinotopic areas in each subject as that subject's ROI. Dotted vertical lines indicate
Alternating Brightness Star stimulus onset and termination. Error bars represent
standard error of the mean between subjects.

Time courses for the individual retinotopic areas were also obtained. For each

retinotopic area, we calculated each subject's average response to each angle

condition (during times 5-20 secs after stimulus onset) and calculated the %BOLD signal z-score across the 5 conditions for that subject. Using z-scores allowed us to reduce a large fraction of variation in BOLD signal levels across subjects. When we plotted the %BOLD signal z-score (24 subjects average) against the angle of the corner, we found a parametric relationship, both for the union of all retinotopic areas and for each of the individual retinotopic areas (**Figure 41**). For each retinotopic area we performed a repeated measures ANOVA with a linear contrast based on the condition angle: the amount of variance in the z-scores that is accounted for by the linear contrast (partial eta squared: η_p^2) reached significance at a level of $p<0.01$ in all individual areas, as well as in the union of all retinotopic areas.

These results offer the first physiological correlates of the Alternating Brightness Star illusion. They moreover agree with our psychophysical measurements of this illusion (**chapter 3**), and suggest that sharp corners are more salient stimuli than shallow corners throughout the human occipital cortex.
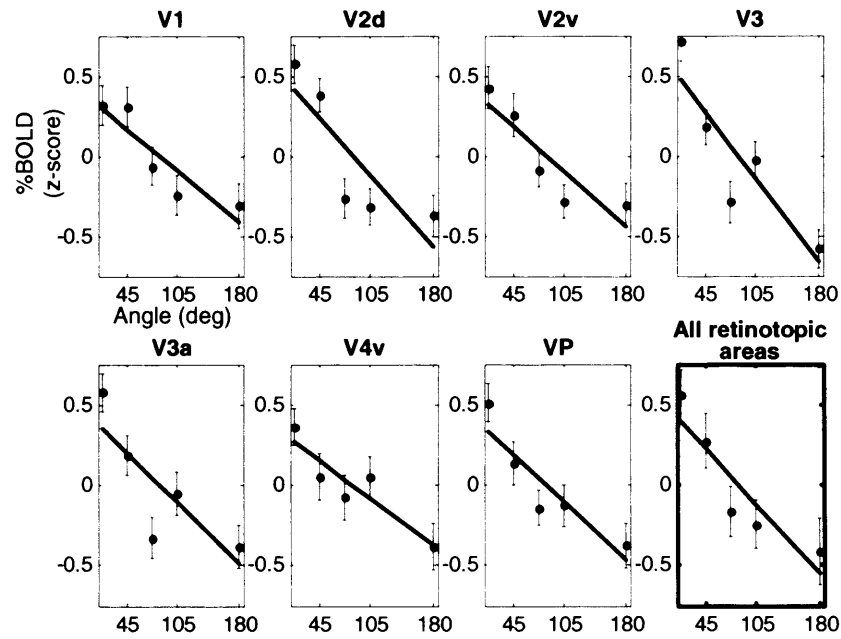
Figure 41. %BOLD signal (z-score) as function of corner angle in individual retinotopic areas and in the union of all retinotopic areas. Each data point was obtained by first averaging the responses between 5 and 20 secs after stimulus onset, for each subject's hemisphere, and then computing the z-score across the 5 angle conditions. Error bars represent standard error of the mean between subject hemispheres. The union of all retinotopic areas was calculated from the data in **Figure 40.**

5. Chapter 5.

Summary, discussion, and future directions

5.1. Summary and conclusions

The purpose of this dissertation project was to explore the hypothesis that corner processing begins at the earliest stages of the visual hierarchy and to quantify the contribution of corners of different angles to visual physiology and perception. Using human psychophysics, human fMRI, and computational simulations of center-surround receptive fields we have obtained the following results and conclusions:

- <u>From center-surround computational simulations</u> (**chapter 2**):

    - Computational simulations of center-surround receptive fields predict that responses to corners vary parametrically with the angle of the corner: the sharper the angle the higher the predicted response.

    - There is a subspace of angles and contrasts in which early neurons respond better to corners than to any possible edge.

    - Predicted responses to sharp corners are stronger than predicted responses to bars of optimal width.

    - Responses to corners do not depend on receptive field size, whereas responses to bars, gratings and spots do.

    - Corners are more dependable visual features than edges, bars or spots across different stimulation conditions.

- From human psychophysics of corner-based illusions (**chapter 3**):

  – We obtained the first psychophysical quantification of Vasarely's nested squares illusion and the Alternating Brightness Star illusion.

  – Perception of corners varies linearly with the angle of the corner.

  – The sharper the angle, the more salient the corner: Corner Angle Salience Variation effect.

  – When embedded in a luminance gradient, corners appear bright or dark depending on the interaction between the sign of the angle and the direction of the luminance gradient: Corner Angle Brightness Reversal effect.

  – Center-surround receptive field linear models qualitatively predict the perceptual result, but fail to predict the shape of the curve.

  – The results obtained with corners embedded in luminance gradients are applicable to solid corners as well.

- From human fMRI of corner-gradient illusions (**chapter 4**):

  – We obtained the first physiological correlates of the Alternating Brightness Star illusion.

  – BOLD signal strength is positively correlated with the sharpness of corner angle: the sharper the angle the stronger the BOLD response (physiological substrate of the Corner Angle Salience Variation effect).

  – Sharp corners are more salient than shallow corners in all retinotopic cortical areas.

  – This suggests a general principle for corner processing throughout the visual cortex.

5.2. Discussion

5.2.1 Corners and information

In 1961, Barlow proposed that the brain recodes visual data "so that their redundancy is reduced but comparatively little information is lost". This idea is known as the "Redundancy-Reducing Hypothesis" (Barlow, 1961, 1989). The redundancy-reducing hypothesis has been invoked as an explanation for why neurons at the early levels of the visual system are suited to perform "edge-detection", or "contour-extraction". However, redundancy reduction is not necessarily constrained to edges, but rather should theoretically apply to any feature in the visual scene (Rao et al., 2002). Just as edges are a less redundant feature than diffuse light, Attneave proposed in the 1950's that "points of maximum curvature" (i.e. discontinuities in edges, such as curves, angles and corners – any point at which straight-lines are deflected) are even less redundant than edges themselves, and thus contain more information (Attneave, 1954) (**Figure 16**). If points of high curvature are less redundant than points of low curvature, then sharp corners should also be less redundant than shallow corners. This led to our prediction that, following the redundancy-reducing hypothesis, sharp corners should appear to be perceptually more salient than shallow corners, which we demonstrated psychophysically in **chapter 3**.

5.2.2 Corner processing by center surround receptive fields

Theoretical and physiological models of vision have assigned the function of "edge detector" to early visual neurons (Marr and Hildreth, 1980), whereas corner detection has been considered a cortical process subsequent to edge detection (Hubel and Wiesel, 1965; Dobbins et al., 1987; Versavel et al., 1990; Knierim and van Essen, 1992; DeAngelis et al., 1994; Sillito et al., 1995; Shevelev et al., 1998; Das and Gilbert, 1999; Kapadia et al., 1999; Shevelev et al., 1999; Jones et al., 2001; Sceniak et al., 2001; Pack et al., 2003; Pack et al., 2004). In agreement with

this idea, several studies of shape processing have invoked curves and corners as intermediate shape primitives (Milner, 1974; Biederman, 1987; Ullman, 1989; Poggio and Edelman, 1990; Dickinson and Pentland, 1992; Pasupathy and Connor, 1999).

Vasarely's nested squares illusion and the related effects described in **chapter 3** show that corners are perceptually more salient than straight edges, and moreover that sharp corners are more salient than shallow corners. Hurvich's center-surround model of Vasarely's nested squares predicts that the 90° corner-gradient effects in Vasarely's artwork arise from subcortical center-surround receptive fields (Hurvich, 1981; see **section 2.1** for details). Moreover Marr's primal sketch has also been shown to highlight corners (Watt, 1988).

We proposed a new general model of corner processing in the early visual system, based on the fact that, due to the geometry of their center-surround receptive fields, retinogeniculate neurons should respond better to corners than to edges (**Figure 18**). It is possible that center-surround receptive fields may have evolved to make use of the reduced redundancy of sharp corners versus shallow corners and edges. Thus, while it seems likely that curves and corners play an important role during high-level object recognition and shape processing, corner and curve detection may first take place within the lowest levels of the visual system, rather than within mid-level circuits.

In his theoretical work Watt states that *"straight lines and curved lines are processed in parallel. There is a high curvature system (very little can be said about it) that could have great value as a feature detector"* (Watt and Andrews, 1982) and that *"It is possible to detect corners and intersections directly in the image, rather than calculating where lines intersect"* (Watt, 1988). Watt's theory remarks the importance of corners and proposes that corners can be detected directly on the image by Lapalcian operators. However, Watt did not make any suggestions as to where in the visual system these computations might take place, and did not relate

them to center-surround receptive fields in any way; he solely reflected that "very little can be said" about the "high curvature system" he proposed.

Our computational results (**chapter 3, Figure 33**) using center-surround receptive field simulations, predict the general trend of the perceptual observations (that the strength of the percept varies inversely with the angle of the corner). However, they fail to predict the exact shape of the quantitative psychophysical results.

Previous computational studies have proposed that linear receptive fields cannot process curvature features, since linear filtering, even if modified by common nonlinearities like thresholding or rectification, will generally confound straight lines with signals that show essentially two-dimensional variations (Zetzsche and Barth, 1990; Barth et al., 1998a; Mota and Barth, 2000). It has also been suggested that linear receptive fields cannot explain some simultaneous contrast illusions (Morrone et al., 1986; Ross et al., 1989). Thus it is possible that center-surround receptive fields do not fully account for the illusions studied, and that further cortical processing takes places after the retina/LGN levels. However, it is also possible that the basic DOG filters used here (despite the fact that we varied many of their parameters) are too rudimentary to completely simulate subcortical function. Linear DOG models account for the main properties of center-surround neurons, but they ignore many of the more complicated aspects, such as the influence of the suppressive field (see General Introduction), which could play a role on the illusions studied here through contrast gain control mechanisms (Shapley and Victor, 1978, 1981; Carandini, 2004; Bonin et al., 2005; Mante et al., 2005).

Future electrophysiological recordings from LGN neurons using stimuli equivalent to the ones presented here, will distinguish between these two possibilities.

5.2.3 Cortical neural correlates of corner perception

The study of the physiological responses to corners, curves and terminators has generated a great deal of interest in recent years (Shevelev et al., 1998; Pasupathy and Connor, 1999; Pack and Born, 2001; Pasupathy and Connor, 2001, 2002; Pack et al., 2003; Ito and Komatsu, 2004; Pack et al., 2004). Several electrophysiological studies have reported single-unit responses to curves and corners in striate and extrastriate cortex of cats and primates (Hubel and Wiesel, 1965; Shevelev et al., 1998; Pasupathy and Connor, 1999; Ito and Komatsu, 2004). However, many important questions remain. For instance, the neural correlates of corner perception in the human brain are unknown. Specifically, the BOLD correlates of corner perception have not been studied in any species to date. Finally, imaging and electrophysiological studies have yet to determine the contribution of angle sharpness to corner processing in any species.

In **chapter 4** we used the Alternating Brightness Star illusion as a tool to systematically investigate the physiological correlates of corner and angle processing in humans, through functional imaging. We found BOLD signal strength to be positively correlated with both the acuteness of corner angle and the strength of the Alternating Brightness Star illusion, since the strength of the Alternating Brightness Star illusion itself increases with angle acuteness. These results match the psychophysical data we collected while presenting equivalent stimuli (**chapter 3**). Just as Mach Bands, Chevreul's effect, and other edge-based illusions are significant to understanding the perception of all edges, the Vasarely and the Alternating Brightness Star effects studied here are significant to understanding corner perception in general.

Hurvich suggested that Vasarely's nested squares illusion (**Figure 15**) could be explained by contrast differences at the level of center-surround receptive fields (Hurvich, 1981). Following from this idea, we proposed more generally that *any* surface corner in the world will increase local contrast, and so sharp corners will be

perceptually more salient than shallow corners in general (**chapter 2**). Thus center-surround receptive fields may function as the first curvature detectors in the visual processing hierarchy, as the antagonism between center and surround should result in sharp corners generating stronger responses than shallow corners or flat edges. We also propose that the changes in BOLD signal observed in **chapter 3** are driven primarily by changes in local contrast at the corners (as local contrast, from the point of view of a single receptive field in the early visual areas, is higher at sharp versus shallow corners). Future single-unit studies will address the specific hypothesis that the physiological effects seen here are due to the interaction of corners and receptive field shape.

Our results agree with previous electrophysiological studies showing responses to corners in striate and extrastriate neurons (Hubel and Wiesel, 1965; Pasupathy and Connor, 1999). However, our findings were common to all retinotopic areas. The parametric relationship (described in **chapter 3)** between the amount of BOLD signal and the sharpness of the corner angle was not constrained to any given retinotopic brain region, as would be predicted by some models of corner processing, but it occurred in all retinotopic areas (as one would expect if the initial stages of corner processing take place subcortically). Some of the previous studies that found neuronal responses to corners in V1 (Shevelev et al., 1998) and in V2 (Ito and Komatsu, 2004) reported that the corner selective neurons have a preference for a particular angle (with all angles being represented in the population). Here we found that all cortical areas respond maximally to sharp corner angles. This result agrees with the study by Pasupathy and Connor which showed that over 70% of the V4 neurons that are tuned to corner angle respond more vigorously to sharp angles (Pasupathy and Connor, 1999).

Our fMRI results provide the first physiological evidence that corner angle plays an important role in stimulus salience throughout the visual system, including stages at least as early as area V1.

5.3. Future directions

Our results suggest that corners start being processed at the first stages of the early visual system (at the level of subcortical center-surround receptive fields), and not at the level of V1 or later, as currently suggested in the literature. We propose that corners are a fundamental visual feature for early visual neurons and that corners responses do not necessarily derive from the converging inputs from two neurons that are selective to two different edge orientations.

We have developed and quantified several visual illusions that show that corners are more salient than edges perceptually, and that corner salience depends parametrically on corner angle (Corner Angle Salience Variation effect). We have implemented computational simulations of center-surround receptive fields and found that the simulations predict the Corner Angle Salience Variation effect, with sharp corner angles eliciting the strongest responses. This suggests that center-surround neurons are in fact tuned to corners. However, even though the computational simulations predict the trend of the Corner Angle Salience Variation effect, they fail to capture the specific linear relationship between corner saliency and corner angle found psychophysically.

Future studies recording from center-surround neurons are needed to determine how these neurons actually respond to the illusion studied here. It is possible that center-surround responses do change linearly with the angle of the corner, which would show that the basic computational models used are not accurate enough to predict this property. The other possibility is that the responses match the computational predictions which would mean that the linear relationship arises after further processing by higher cortical areas.

We moreover found that BOLD signal strength is positively correlated with the acuteness of corner angle: sharp corners are more salient than shallow corners in all retinotopic areas, suggesting a general principle for corner processing throughout the

visual cortex. Even though we established that BOLD signal varies parametrically with corner angle in all cortical retinotopic areas, the fMRI experiment did not have enough power to ascertain whether the relationship was linear, or whether BOLD signal also varied parametrically with corner angle in the LGN. Further experiments recording from single cells in different areas will determine at what level of the visual hierarchy the relationship between corner salience and corner angle becomes linear and where the slope of the response matches the slope found psychophysically.

6. References

1) Adelson EH (1999). Lightness perception and lightness illusions. In The Cognitive Neurosciences, MS Gazzaniga, ed. (Cambridge, MA, MIT Press), pp. 339-351.

2) Adelson EH, and Bergen JR (1985). Spatiotemporal energy models for the perception of motion. Jourrnal of the Optical Society of America Serie A 2, 284-299.

3) Ahnelt PK, Kolb H, and Pflug R (1987). Identification of a subtype of cone photoreceptor, likely to be blue sensitive, in the human retina. Journal of Comparative Neurology 255, 18-34.

4) Al-Haytham I (1030/1989). Optics (London, The Warburg Institute, University of London).

5) Albrecht DG, and Geisler WS (1991). Motion selectivity and the contrast-response function of simple cells in the visual cortex. Visual Neuroscience 7, 531-546.

6) Albright TD (1984). Direction and orientation selectivity of neurons in visual area MT of the macaque. Journal of Neurophysiology 52, 1106-1130.

7) Alitto HJ, and Usrey WM (2003). Corticothalamic feedback and sensory processing. Current Opinion in Neurobiology 13, 440-445.

8) Allman J, Miezin F, and McGuinness E (1985). Stimulus specific responses from beyond the classical receptive field: neurophysiological mechanisms for local-global comparisons in visual neurons. Annual Review of Neuroscience 8, 407-430.

9) Alonso JM (2002). Neural connections and receptive field properties in the primary visual cortex. The neuroscientist 8, 443-456.

10) Alonso JM, Cudeiro J, Perez R, Gonzalez F, and Acuna C (1993a). Influence of layer V of area 18 of the cat visual cortex on responses of cells in layer V of area 17 to stimuli of high velocity. Experimental Brain Research *93*, 363-366.

11) Alonso JM, Cudeiro J, Perez R, Gonzalez F, and Acuna C (1993b). Orientational influences of layer V of visual area 18 upon cells in layer V of area 17 in the cat cortex. Experimental Brain Research *96*, 212-220.

12) Alonso JM, and Martinez LM (1998). Functional connectivity between simple cells and complex cells in cat striate cortex. Nature Neuroscience *1*, 395-403.

13) Alonso JM, Usrey WM, and Reid RC (2001). Rules of connectivity between geniculate cells and simple cells in cat primary visual cortex. Journal of Neuroscience *21*, 4002-4015.

14) Anderson JC, Martin KA, and Whitteridge D (1993). Form, function, and intracortical projections of neurons in the striate cortex of the monkey Macacus nemestrinus. Cerebral Cortex *3*, 412-420.

15) Andrews DP, Butcher AK, and Buckley BR (1973). Acuities for spatial arrangement in line figures: human and ideal observers compared. Vision Research *13*, 599-620.

16) Angelucci A, Levitt JB, Walton EJ, Hupe JM, Bullier J, and Lund JS (2002). Circuits for local and global signal integration in primary visual cortex. Journal of Neuroscience *22*, 8633-8646.

17) Anstis S, and Ho A (1998). Nonlinear combination of luminance excursions during flicker, simultaneous contrast, afterimages and binocular fusion. Vision Research *38*, 523-539.

18) Attneave F (1954). Some informational aspects of visual perception. Psychological Review *61*, 183-193.

19) Baker JF, Petersen SE, Newsome WT, and Allman JM (1981). Visual response properties of neurons in four extrastriate visual areas of the owl monkey (Aotus trivirgatus): a quantitative comparison of medial, dorsomedial, dorsolateral, and middle temporal areas. Journal of Neurophysiology *45*, 397-416.

20) Barenholtz E, Cohen EH, Feldman J, and Singh M (2003). Detection of change in shape: an advantage for concavities. Cognition *89*, 1-9.

21) Barlow HB (1961). Possible principles underlying the transformation of sensory messages. In Sensory Communication, WA Rosenblith, ed. (Cambridge, MA, MIT Press), pp. 217-234.

22) Barlow HB (1989). Unsupervised learning. Neural Computation *1*, 295-311.

23) Barlow HB, Fitzhugh R, and Kuffler SW (1957). Change of organization in the receptive fields of the cat's retina during dark adaptation. Journal of Physiology *137*, 228-254.

24) Barone P, Batardiere A, Knoblauch K, and Kennedy H (2000). Laminar distribution of neurons in extrastriate areas projecting to visual areas V1 and V4 correlates with the hierarchical rank and indicates the operation of a distance rule. Journal of Neuroscience *20*, 3263-3281.

25) Barth E, Zetzsche C, and Krieger G (1998a). Endstopped operators based on iterated nonlinear center-surround inhibition. In Human Vision and Electronic Imaging III, BE Rogowitz, and NP Pappas, eds. (SPIE), pp. 67-78.

26) Barth E, Zetzsche C, and Rentschler I (1998b). Intrinsic 2D features as textons. Jourrnal of the Optical Society of America *15*, 1723-1732.

27) Bauer R, Dow BM, and Vautin RG (1980). Laminar distribution of preferred orientations in foveal striate cortex of the monkey. Experimental Brain Research *41*, 54-60.

28) Baumgartner G (1960). Indirekte Größenbestimmung der rezeptiven Felder der Retina beim Menschen mittels der Hermannschen Gittertäuschung. Pflügers Archiv für die gesamte Physiologie *272*, 21-22(Abstract).

29) Baumgartner G (1961). Die Reaktionen der Neurone des zentralen visuellen Systems der Katze im simultanen Helligkeitskontrast. In Neurophysiologie und Psychophysik des visuellen Systems, R Jung, and HH Kornhuber, eds. (Berlin, Gottingen, Heidelberg, Springer), pp. 296-313.

30) Benevento LA, and Standage GP (1982). Demonstration of lack of dorsal lateral geniculate nucleus input to extrastriate areas MT and visual 2 in the macaque monkey. Brain Research *252*, 161-166.

31) Biederman I (1985). Human image understanding: Recent research and a theory. Computer Vision, Graphics, Image Proc, 29-73.

32) Biederman I (1987). Recognition-by-components: a theory of human image understanding. Psychological Review *94*, 115-147.

33) Blakemore C, and Tobin EA (1972). Lateral inhibition between orientation detectors in the cat's visual cortex. Experimental Brain Research *15*, 439-440.

34) Blasdel G, Obermayer K, and Kiorpes L (1995). Organization of ocular dominance and orientation columns in the striate cortex of neonatal macaque monkeys. Visual Neuroscience *12*, 589-603.

35) Blasdel GG, and Fitzpatrick D (1984). Physiological organization of layer 4 in macaque striate cortex. Journal of Neuroscience *4*, 880-895.

36) Blasdel GG, and Lund JS (1983). Termination of afferent axons in macaque striate cortex. Journal of Neuroscience *3*, 1389-1413.

37) Blasdel GG, Lund JS, and Fitzpatrick D (1985). Intrinsic connections of macaque striate cortex: axonal projections of cells outside lamina 4C. Journal of Neuroscience *5*, 3350-3369.

38) Blasdel GG, and Salama G (1986). Voltage-sensitive dyes reveal a modular organization in monkey striate cortex. Nature *321*, 579-585.

39) Bolz J, and Gilbert CD (1986). Generation of end-inhibition in the visual cortex via interlaminar connections. Nature *320*, 362-365.

40) Bonhoeffer T, and Grinvald A (1991). Iso-orientation domains in cat visual cortex are arranged in pinwheel-like patterns. Nature *353*, 429-431.

41) Bonin V, Mante V, and Carandini M (2005). The suppressive field of neurons in lateral geniculate nucleus. Journal of Neuroscience *25*, 10844-10856.

42) Bowling DB (1980). Light responses of ganglion cells in the retina of the turtle. Journal of Physiology *299*, 173-196.

43) Boycott BB, and Dowling JE (1969). Organization of the primate retina: light microscopy. Philosophical Transactions of the Royal Society of London, B *255*, 109-184.

44) Boycott BB, and Wassle H (1991). Morphological Classification of Bipolar Cells of the Primate Retina. Europena Journal of Neuroscience *3*, 1069-1088.

45) Brodmann K (1909). Vergleichende Lokalisationlehre der Grosshirnrinde in ihren Prinzipien Dargestellt auf Grund des Zellenbaues (Leipzig, Barth).

46) Brown PK, and Wald G (1963). Visual Pigments In Human And Monkey Retinas. Nature *200*, 37-43.

47) Brown PK, and Wald G (1964). Visual pigments in single rods and cones of the human retina. Direct measurements reveal mechanisms of human night and color vision. Science *144*, 45-52.

48) Bühler K (1913). Die Gestaltwahrnehumungen (Stuttgart, Spemann).

49) Bullier J, and Henry GH (1980). Ordinal position and afferent input of neurons in monkey striate cortex. Journal of Comparative Neurology *193*, 913-935.

50) Bullier J, and Kennedy H (1983). Projection of the lateral geniculate nucleus onto cortical area V2 in the macaque monkey. Experimental Brain Research *53*, 168-172.

51) Callaway EM (1998). Local circuits in primary visual cortex of the macaque monkey. Annual Review of Neuroscience *21*, 47-74.

52) Callaway EM, and Wiser AK (1996). Contributions of individual layer 2-5 spiny neurons to local circuits in macaque primary visual cortex. Visual Neuroscience *13*, 907-922.

53) Carandini M (2004). Receptive fields and suppressive fields in the early visual system. In The cognitive neurosciences, MS Gazzaniga, ed. (Cambridge, Massachusetts, MIT Press).

54) Carandini M, Demb JB, Mante V, Tolhurst DJ, Dan Y, Olshausen BA, Gallant JL, and Rust NC (2005). Do we know what the early visual system does? Journal of Neuroscience *25*, 10577-10597.

55) Carandini M, and Heeger DJ (1994). Summation and division by neurons in primate visual cortex. Science *264*, 1333-1336.

56) Carandini M, Heeger DJ, and Movshon JA (1997). Linearity and normalization in simple cells of the macaque primary visual cortex. Journal of Neuroscience *17*, 8621-8644.

57) Cavanaugh JR, Bair W, and Movshon JA (2002). Nature and interaction of signals from the receptive field center and surround in macaque V1 neurons. Journal of Neurophysiology *88*, 2530-2546.

58) Chance FS, Nelson SB, and Abbot LF (1999). Complex cells as cortically amplified simple cells. Nature Neurosciece *2*, 277-282.

59) Chen S, and Levi DM (1996). Angle judgement: is the whole the sum of its parts? Vision Research *36*, 1721-1735.

60) Chevreul (1839). De la loi du contraste simultané des couleurs, et de l'assortiment des objets colorés (Paris, Pitois-Levreault).

61) Chichilnisky EJ (2001). A simple white noise analysis of neuronal light responses. Network *12*, 199-213.

62) Cicerone CM, and Nerger JL (1989). The relative numbers of long-wavelength-sensitive to middle-wavelength-sensitive cones in the human fovea centralis. Vision Research *29*, 115-128.

63) Cleland BG, Harding TH, and Tulunay-Keesey U (1979). Visual resolution and receptive field size: examination of two kinds of cat retinal ganglion cell. Science *205*, 1015-1017.

64) Cole G, Gellatly A, and Blurton A (2001). Effect of object onset on the distribution of visual attention. J Exp Psychol Hum Percept Perform *27*, 1356-1368.

65) Conley M, and Fitzpatrick D (1989). Morphology of retinogeniculate axons in the macaque. Visual Neuroscience *2*, 287-296.

66) Crair MC, Ruthazer ES, Gillespie DC, and Stryker MP (1997). Ocular dominance peaks at pinwheel center singularities of the orientation map in cat visual cortex. Journal of Neurophysiology *77*, 3381-3385.

67) Croner LJ, and Kaplan E (1995). Receptive fields of P and M ganglion cells across the primate retina. Vision Research *35*, 7-24.

68) Curcio CA, Allen KA, Sloan KR, Lerea CL, Hurley JB, Klock IB, and Milam AH (1991). Distribution and morphology of human cone photoreceptors stained with anti-blue opsin. Journal of Comparative Neurology *312*, 610-624.

69) Curcio CA, Sloan KR, Jr., Packer O, Hendrickson AE, and Kalina RE (1987). Distribution of cones in human and monkey retina: individual variability and radial asymmetry. Science *236*, 579-582.

70) Curcio CA, Sloan KR, Kalina RE, and Hendrickson AE (1990). Human photoreceptor topography. Journal of Comparative Neurology *292*, 497-523.

71) Dacey D, Packer OS, Diller L, Brainard D, Peterson B, and Lee B (2000). Center surround receptive field structure of cone bipolar cells in primate retina. Vision Research *40*, 1801-1811.

72) Dacey DM (1993). The mosaic of midget ganglion cells in the human retina. Journal of Neuroscience *13*, 5334-5355.

73) Dacey DM (1999). Primate retina: cell types, circuits and color opponency. Progress in Retinal and Eye Research *18*, 737-763.

74) Dacey DM (2000). Parallel pathways for spectral coding in primate retina. Annual Review of Neuroscience *23*, 743-775.

75) Dacey DM, and Petersen MR (1992). Dendritic field size and morphology of midget and parasol ganglion cells of the human retina. Proceedings of the National Academy of Sciences of the United States of America *89*, 9666-9670.

76) Damasio AR, and Benton AL (1979). Impairment of hand movements under visual guidance. Neurology *29*, 170-174.

77) Damasio AR, Damasio H, and Van Hoesen GW (1982). Prosopagnosia: anatomic basis and behavioral mechanisms. Neurology *32*, 331-341.

78) Das A, and Gilbert CD (1999). Topography of contextual modulations mediated by short-range interactions in primary visual cortex. Nature *399*, 655-661.

79) Dayan P, and Abbot LF (2001). Theoretical neuroscience: computational and mathematical modeling of neural systems, 1 edn, (Cambridge, Massachusetts, MIT Press).

80) De Monasterio FM, and Gouras P (1975). Functional properties of ganglion cells of the rhesus monkey retina. Journal of Physiology *251*, 167-195.

81) de Monasterio FM, and Schein SJ (1982). Spectral bandwidths of color-opponent cells of geniculocortical pathway of macaque monkeys. Journal of Neurophysiology *47*, 214-224.

82) De Valois RL (1960). Color Vision Mechanisms in the Monkey. Journal of General Physiology *43*, 115-128.

83) De Weerd P, Desimone R, and Ungerleider LG (1998). Perceptual filling-in: a parametric study. Vision Research *38*, 2721-2734.

84) De Weerd P, Gattass R, Desimone R, and Ungerleider LG (1995). Responses of cells in monkey visual cortex during perceptual filling-in of an artificial scotoma. Nature *377*, 731-734.

85) Dean P (1976). Effects of inferotemporal lesions on the behavior of monkeys. Psychological Bulletin *83*, 41-71.

86) DeAngelis GC, Freeman RD, and Ohzawa I (1994). Length and width tuning of neurons in the cat's primary visual cortex. Journal of Neurophysiology *71*, 347-374.

87) Derrington AM, and Lennie P (1984). Spatial and temporal contrast sensitivities of neurones in lateral geniculate nucleus of macaque. Journal of Physiology *357*, 219-240.

88) Desimone R, Fleming J, and Gross CG (1980). Prestriate afferents to inferior temporal cortex: an HRP study. Brain Research *184*, 41-55.

89) Desimone R, and Gross CG (1979). Visual areas in the temporal cortex of the macaque. Brain Research *178*, 363-380.

90) Desimone R, and Schein SJ (1987). Visual properties of neurons in area V4 of the macaque: sensitivity to stimulus form. Journal of Neurophysiology *57*, 835-868.

91) Desimone R, Schein SJ, Moran J, and Ungerleider LG (1985). Contour, color and shape analysis beyond the striate cortex. Vision Research *25*, 441-452.

92) Desimone R, and Ungerleider LG (1986). Multiple visual areas in the caudal superior temporal sulcus of the macaque. Journal of Comparative Neurology *248*, 164-189.

93) Desimone R, and Ungerleider LG (1989). Neural mechanisims of visual processing in monkeys. In Handbook of neuropsychology, F Boller, and J Graman, eds. (Amsterdam, Elsevier), pp. 267-299.

94) Dickinson SJ, and Pentland AP (1992). From volumes to views: an approach to 3-D object recognition. CVGIP: Image understanding *55*, 130-154.

95) Dobbins A, Zucker SW, and Cynader MS (1987). Endstopped neurons in the visual cortex as a substrate for calculating curvature. Nature *329*, 438-441.

96) Donner KO, and Reuter T (1965). The dark-adaptation of single units in the frog's retina and its relation to the regeneration of rhodopsin. Vision Research *5*, 615-632.

97) Dowling JE, and Boycott BB (1966). Organization of the primate retina: electron microscopy. Proceedings of The Royal Society of London. Series B, Biological Sciences *166*, 80-111.

98) Duncan J, and Humphreys G (1992). Beyond the search surface: visual search and attentional engagement. Journal of Experimental Psychology: Human Perception and Performance *18*, 578-588; discussion 589-593.

99) Duncan J, and Humphreys GW (1989). Visual search and stimulus similarity. Psychological Review *96*, 433-458.

100) Enns JT, and Rensink RA (1991). Preattentive recovery of three-dimensional orientation from line drawings. Psychological Review *98*, 335-351.

101) Enroth-Cugell C, and Robson JG (1966). The contrast sensitivity of retinal ganglion cells of the cat. Journal of Physiology *198*, 517-552.

102) Erisir A, Van Horn SC, and Sherman SM (1997). Relative numbers of cortical and brainstem inputs to the lateral geniculate nucleus. Proceedings of the

National Academy of Sciences of the United States of America *94*, 1517-1520.

103) Feldman J, and Singh M (2005). Information along contours and object boundaries. Psychological Review *112*, 243-252.

104) Felleman DJ, and Van Essen DC (1991). Distributed hierarchical processing in the primate cerebral cortex. Cerebral Cortex *1*, 1-47.

105) Ferster D (1986). Orientation selectivity of synaptic potentials in neurons of cat primary visual cortex. Journal of Neuroscience *6*, 1284-1301.

106) Ferster D, Chung S, and Wheat H (1996). Orientation selectivity of thalamic input to simple cells of cat visual cortex. Nature *380*, 249-252.

107) Ferster D, and Koch C (1987). Neuronal connections underlying orientation selectivity in cat visual cortex. Trends in Neuroscience *10*, 487-492.

108) Ferster D, and Miller KD (2000). Neural mechanisms of orientation selectivity in the visual cortex. Annual Review of Neuroscience *23*, 441-471.

109) Fitzpatrick D, Lund JS, and Blasdel GG (1985). Intrinsic connections of macaque striate cortex: afferent and efferent connections of lamina 4C. Journal of Neuroscience *5*, 3329-3349.

110) Fitzpatrick D, Usrey WM, Schofield BR, and Einstein G (1994). The sublaminar organization of corticogeniculate neurons in layer 6 of macaque striate cortex. Visual Neuroscience *11*, 307-315.

111) Gallant JL, Braun J, and Van Essen DC (1993). Selectivity for polar, hyperbolic, and Cartesian gratings in macaque visual cortex. Science *259*, 100-103.

112) Gallant JL, Connor CE, Rakshit S, Lewis JW, and Van Essen DC (1996). Neural responses to polar, hyperbolic, and Cartesian gratings in area V4 of the macaque monkey. Journal of Neurophysiology *76*, 2718-2739.

113) Gattass R, and Gross CG (1981). Visual topography of striate projection zone (MT) in posterior superior temporal sulcus of the macaque. Journal of Neurophysiology *46*, 621-638.

114) Gibson JJ (1950). The perception of visual surfaces. American Journal of Psychology *63*, 367-384.

115) Gilbert CD (1977). Laminar differences in receptive field properties of cells in cat primary visual cortex. Journal of Physiology *268*, 391-421.

116) Gilbert CD, Das A, Ito M, Kapadia M, and Westheimer G (1996). Spatial integration and cortical dynamics. Proceedings of the National Academy of Sciences of the United States of America *93*, 615-622.

117) Gilbert CD, and Wiesel TN (1979). Morphology and intracortical projections of functionally characterised neurones in the cat visual cortex. Nature *280*, 120-125.

118) Gilbert CD, and Wiesel TN (1983). Clustered intrinsic connections in cat visual cortex. Journal of Neuroscience *3*, 1116-1133.

119) Gilbert CD, and Wiesel TN (1990). The influence of contextual stimuli on the orientation selectivity of cells in primary visual cortex of the cat. Vision Research *30*, 1689-1701.

120) Gouras P (1968). Identification of cone mechanisms in monkey ganglion cells. Journal of Physiology *199*, 533-547.

121) Guillery RW, and Sherman SM (2002). Thalamic relay functions and their role in corticocortical communication: generalizations from the visual system. Neuron *33*, 163-175.

122) Gur M, Kagan I, and Snodderly DM (2005). Orientation and direction selectivity of neurons in V1 of alert monkeys: functional relationships and laminar distributions. Cerebral Cortex *15*, 1207-1221.

123) Hansen T, and Neumann H (2004). Neural mechanisms for the robust representation of junctions. Neural Computation *16*, 1013-1037.

124) Hartline HK (1940). The receptive fields of optic nerve fibers. American Journal of Physiology *130*, 690-699.

125) Heeger DJ (1992). Normalization of cell responses in cat striate cortex. Visual Neuroscience *9*, 181-197.

126) Heeley DW, and Buchanan-Smith HM (1996). Mechanisms specialized for the perception of image geometry. Vision Research *36*, 3607-3627.

127) Hendrickson AE, Wilson JR, and Ogren MP (1978). The neuroanatomical organization of pathways between the dorsal lateral geniculate nucleus and visual cortex in Old World and New World primates. Journal of Comparative Neurology *182*, 123-136.

128) Hendry SH, and Yoshioka T (1994). A neurochemically distinct third channel in the macaque dorsal lateral geniculate nucleus. Science *264*, 575-577.

129) Hermann L (1870). Eine Erscheinung des simultanen Contrastes. Pflügers Archiv für die gesamte Physiologie *3*, 13-15.

130) Howe CQ, and Purves D (2005). Natural-scene geometry predicts the perception of angles and line orientation. Proceedings of the National Academy of Sciences of the United States of America *102*, 1228-1233.

131) Hubel DH (1995). Eye, brain and vision, 2 edn (New York, Scientific American Library).

132) Hubel DH, and Wiesel TN (1959). Receptive fields of single neurones in the cat's striate cortex. Journal of Physiology *148*, 574-591.

133) Hubel DH, and Wiesel TN (1960). Receptive fields of optic nerve fibres in the spider monkey. Journal of Physiology *154*, 572-580.

134) Hubel DH, and Wiesel TN (1961). Integrative action in the cat's lateral geniculate body. Journal of Physiology *155*, 385-398.

135) Hubel DH, and Wiesel TN (1962). Receptive fields, binocular interaction and functional architecture in the cat's visual cortex. Journal of Physiology *160*, 106-154.

136) Hubel DH, and Wiesel TN (1965). Receptive fields and functional architecture in two nonstriate visual areas (18 and 19) of the cat. Journal of Neurophysiology *28*, 229-289.

137) Hubel DH, and Wiesel TN (1968). Receptive fields and functional architecture of monkey striate cortex. Journal of Physiology *195*, 215-243.

138) Hubel DH, and Wiesel TN (1972). Laminar and columnar distribution of geniculo-cortical fibers in the macaque monkey. Journal of Comparative Neurology *146*, 421-450.

139) Hubel DH, and Wiesel TN (1974). Sequence regularity and geometry of orientation columns in the monkey striate cortex. Journal of Comparative Neurology *158*, 267-293.

140) Hulleman J, te Winkel W, and Boselie F (2000). Concavities as basic features in visual search: evidence from search asymmetries. Perception and Psychophysics *62*, 162-174.

141) Hupe JM, James AC, Payne BR, Lomber SG, Girard P, and Bullier J (1998). Cortical feedback improves discrimination between figure and background by V1, V2 and V3 neurons. Nature *394*, 784-787.

142) Hurvich LM (1981). Color vision (Sunderland, MA, Sinauer Associates).

143) Irvin GE, Casagrande VA, and Norton TT (1993). Center/surround relationships of magnocellular, parvocellular, and koniocellular relay cells in primate lateral geniculate nucleus. Visual Neuroscience *10*, 363-373.

144) Ito M, and Komatsu H (2004). Representation of angles embedded within contour stimuli in area V2 of macaque monkeys. Journal of Neuroscience *24*, 3313-3324.

145) Jones HE, Grieve KL, Wang W, and Sillito AM (2001). Surround suppression in primate V1. Journal of Neurophysiology *86*, 2011-2028.

146) Kaiser PK (1996). The joy of visual perception: A web book, http://www.yorku.ca/eye/thejoy.htm.

147) Kandel ER, Schwartz JH, and Jessell TM, eds. (2000). Principles of neural science, 4th edn (New York, McGraw Hill).

148) Kaneko A (1970). Physiological and morphological identification of horizontal, bipolar and amacrine cells in goldfish retina. Journal of Physiology *207*, 623-633.

149) Kapadia MK, Westheimer G, and Gilbert CD (1999). Dynamics of spatial summation in primary visual cortex of alert monkeys. Proceedings of the

National Academy of Sciences of the United States of America *96*, 12073-12078.

150) Kaplan E, and Shapley RM (1982). X and Y cells in the lateral geniculate nucleus of macaque monkeys. Journal of Physiology *330*, 125-143.

151) Kaplan E, and Shapley RM (1986). The primate retina contains two types of ganglion cells, with high and low contrast sensitivity. Proceedings of the National Academy of Sciences of the United States of America *83*, 2755-2757.

152) Kastner S, De Weerd P, Pinsk MA, Elizondo MI, Desimone R, and Ungerleider LG (2001). Modulation of sensory suppression: implications for receptive field sizes in the human visual cortex. Journal of Neurophysiology *86*, 1398-1411.

153) Keat J, Reinagel P, Reid RC, and Meister M (2001). Predicting every spike: a model for the responses of visual neurons. Neuron *30*, 803-817.

154) Knierim JJ, and van Essen DC (1992). Neuronal responses to static texture patterns in area V1 of the alert macaque monkey. Journal of Neurophysiology *67*, 961-980.

155) Koch C, and Poggio T (1985). The synaptic veto mechanism: does it underlie direction and orientation selectivity in the visual cortex? In Models of the visual cortex, DR Rose, and VG Dobson, eds. (New York, Wiley), pp. 408-419.

156) Kolb H, and Dekorver L (1991). Midget ganglion cells of the parafovea of the human retina: a study by electron microscopy and serial section reconstructions. Journal of Comparative Neurology *303*, 617-636.

157) Kolb H, Linberg KA, and Fisher SK (1992). Neurons of the human retina: a Golgi study. Journal of Comparative Neurology *318*, 147-187.

158) Kolb H, and Marshak D (2003). The midget pathways of the primate retina. Documenta Ophthalmologica *106*, 67-81.

159) Komatsu H (2006). The neural mechanisms of perceptual filling-in. Nature Review Neuroscience *7*, 220-231.

160) Krieger G, Rentschler I, Hauske G, Schill K, and Zetzsche C (2000). Object and scene analysis by saccadic eye-movements: an investigation with higher-order statistics. Spatial Vision *13*, 201-214.

161) Kristjansson A, and Tse PU (2001). Curvature discontinuities are cues for rapid shape analysis. Perception and Psychophysics *63*, 390-403.

162) Kuffler SW (1952). Neurons in the retina: organization, inhibition and excitatory problems. Cold Spring Harbor Symposia on Quantitative Biology *17*, 281-292.

163) Kuffler SW (1953). Discharge patterns and functional organization of mammalian retina. Journal of Neurophysiology *16*, 37-68.

164) Lachica EA, Beck PD, and Casagrande VA (1992). Parallel pathways in macaque monkey striate cortex: anatomically defined columns in layer III. Proceedings of the National Academy of Sciences of the United States of America *89*, 3566-3570.

165) Leventhal AG, Rodieck RW, and Dreher B (1981). Retinal ganglion cell classes in the Old World monkey: morphology and central projections. Science *213*, 1139-1142.

166) Levick WR, Cleland BG, and Dubin MW (1972). Lateral geniculate neurons of cat: retinal inputs and physiology. Investigative Ophthalmology *11*, 302-311.

167) Levitt JB, and Lund JS (1997). Contrast dependence of contextual effects in primate visual cortex. Nature *387*, 73-76.

168) Levitt JB, and Lund JS (2002). The spatial extent over which neurons in macaque striate cortex pool visual signals. Visual Neuroscience *19*, 439-452.

169) Levitt JB, Schumer RA, Sherma SM, Spear PD, and Movshon JA (2001). Visual responde properties of neurons in the LGN of normally reared and visually deprived Macaque monkeys. Journal of Neurophysiology *85*, 2111-2129.

170) Li Z (2002). A saliency map in primary visual cortex. Trends in Cognitive Sciences *6*, 9-16.

171) Livingstone M, and Hubel D (1988). Segregation of form, color, movement, and depth: anatomy, physiology, and perception. Science *240*, 740-749.

172) Livingstone MS, Freeman DC, and Hubel DH (1996). Visual responses in V1 of freely viewing monkeys. Cold Spring Harbor Symposia on Quantitative Biology *61*, 27-37.

173) Livingstone MS, and Hubel DH (1982). Thalamic inputs to cytochrome oxidase-rich regions in monkey visual cortex. Proceedings of the National Academy of Sciences of the United States of America *79*, 6098-6101.

174) Livingstone MS, and Hubel DH (1984). Anatomy and physiology of a color system in the primate visual cortex. Journal of Neuroscience *4*, 309-356.

175) Loffler G, and Orbach HS (1999). Computing feature motion without feature detectors: a model for terminator motion without end-stopped cells. Vision Research *39*, 859-871.

176) Loffler G, Wilson HR, and Wilkinson F (2003). Local and global contributions to shape discrimination. Vision Research *43*, 519-530.

177) Lorente de Nó R (1949). Cerebral cortex: architecture, intracortical connections, motor projections. In Physiology of the nervous system, JF Fulton, ed. (Oxford, Oxford University Press), pp. 288–330.

178) Lowel S, Schmidt KE, Kim DS, Wolf F, Hoffsummer F, Singer W, and Bonhoeffer T (1998). The layout of orientation and ocular dominance domains in area 17 of strabismic cats. Europena Journal of Neuroscience *10*, 2629-2643.

179) Lund JS (1973). Organization of neurons in the visual cortex, area 17, of the monkey (Macaca mulatta). Journal of Comparative Neurology *147*, 455-496.

180) Lund JS, Boothe RG, and Lund RD (1977). Development of neurons in the visual cortex (area 17) of the monkey (Macaca nemestrina): a Golgi study from fetal day 127 to postnatal maturity. Journal of Comparative Neurology *176*, 149-188.

181) Lund JS, Lund RD, Hendrickson AE, Bunt AH, and Fuchs AF (1975). The origin of efferent pathways from the primary visual cortex, area 17, of the macaque monkey as shown by retrograde transport of horseradish peroxidase. Journal of Comparative Neurology *164*, 287-303.

182) Lund JS, and Wu CQ (1997). Local circuit neurons of macaque monkey striate cortex: IV. Neurons of laminae 1-3A. Journal of Comparative Neurology *384*, 109-126.

183) Mach E (1865). Über die Wirkung der räumlichen Vertheilung des Lichtreizes auf der Netzhaut. Sitzungsberichte der mathematisch-naturwissenschaftlichen Classe der kaiserlichen Akademie der Wissenschaften *52*, 303-322.

184) Macknik SL, and Haglund MM (1999). Optical images of visible and invisible percepts in the primary visual cortex of primates. Proceedings of the National Academy of Sciences of the United States of America *96*, 15208-15210.

185) Macknik SL, Martinez-Conde S, and Haglund MM (2000). The role of spatiotemporal edges in visibility and visual masking. Proceedings of the National Academy of Sciences of the United States of America *97*, 7556-7560.

186) MacNeil MA, and Masland RH (1998). Extreme diversity among amacrine cells: implications for function. Neuron *20*, 971-982.

187) Maguire WM, and Baizer JS (1984). Visuotopic organization of the prelunate gyrus in rhesus monkey. Journal of Neuroscience *4*, 1690-1704.

188) Malach R, Amir Y, Harel M, and Grinvald A (1993). Relationship between intrinsic connections and functional architecture revealed by optical imaging and in vivo targeted biocytin injections in primate striate cortex. Proceedings of the National Academy of Sciences of the United States of America *90*, 10469-10473.

189) Mante V, Frazor RA, Bonin V, Geisler WS, and Carandini M (2005). Independence of luminance and contrast in natural scenes and in the early visual system. Nature Neuroscience *8*, 1690-1697.

190) Marks WB, Dobelle WH, and Macnichol EF, Jr. (1964). Visual Pigments Of Single Primate Cones. Science *143*, 1181-1183.

191) Marr D (1982). Vision (New York, W. H. Freeman and Company).

192) Marr D, and Hildreth E (1980). Theory of edge detection. Proceedings of the Royal Society of London Series B *207*, 187-217.

193) Martinez-Conde S, Cudeiro J, Grieve KL, Rodriguez R, Rivadulla C, and Acuna C (1999). Effects of feedback projections from area 18 layers 2/3 to area 17 layers 2/3 in the cat visual cortex. Journal of Neurophysiology *82*, 2667-2675.

194) Martinez-Conde S, and Macknik SL (2001). Junctions are the most salient visual features in the early visual system. Paper presented at: Society for Neuroscience 31st Annual Meeting (San Diego, CA).

195) Martinez LM, and Alonso JM (2001). Construction of complex receptive fields in cat primary visual cortex. Neuron *32*, 515-525.

196) Martinez LM, Wang Q, Reid RC, Pillai C, Alonso JM, Sommer FT, and Hirsch JA (2005). Receptive field structure varies with layer in the primary visual cortex. Nature Neuroscience *8*, 372-379.

197) Masland RH, and Ames A, 3rd (1976). Responses to acetylcholine of ganglion cells in an isolated mammalian retina. Journal of Neurophysiology *39*, 1220-1235.

198) Maunsell JH, and Newsome WT (1987). Visual processing in monkey extrastriate cortex. Annual Review of Neuroscience *10*, 363-401.

199) McArthur A, and Moulden B (1999). A two-dimensional model of brightness perception based on spatial filtering consistent with retinal processing. Vision Researchearch *39*, 1199-1219.

200) McGuire BA, Gilbert CD, Rivlin PK, and Wiesel TN (1991). Targets of horizontal connections in macaque primary visual cortex. Journal of Comparative Neurology *305*, 370-392.

201) Meadows JC (1974a). The anatomical basis of prosopagnosia. Journal of Neurology, Neurosurgery and Psychiatry *37*, 489-501.

202) Meadows JC (1974b). Disturbed perception of colours associated with localized cerebral lesions. Brain *97*, 615-632.

203) Meister M, and Berry MJ, 2nd (1999). The neural code of the retina. Neuron *22*, 435-450.

204) Meister M, Lagnado L, and Baylor DA (1995). Concerted signaling by retinal ganglion cells. Science *270*, 1207-1210.

205) Merigan WH, and Maunsell JH (1993). How parallel are the primate visual pathways? Annual Review of Neuroscience *16*, 369-402.

206) Miller RF, and Slaughter MM (1986). Excitatory amino acid receptors of the retina: Diversity and subtype and conductive mechanisms. TINS *9*, 211-213.

207) Milner PM (1974). A model for visual shape recognition. Psychological Review *81*, 521-535.

208) Mishkin M, and Ungerleider LG (1983). Object vision and spatial vision: two cortical pathways. Trends in Neuroscience *6*, 414-417.

209) Mollon JD, and Bowmaker JK (1992). The spatial arrangement of cones in the primate fovea. Nature *360*, 677-679.

210) Morgan MJ (1996). Visual Illusions. In Unsolved mysteries of the Mind, V Bruce, ed. (Hove, Earlbaum), pp. 29-58.

211) Morrone MC, and Burr DC (1988). Feature detection in human vision: a phase-dependent energy model. Proceedings of the Royal Society of London - Series B: Biological Sciences *235*, 221-245.

212) Morrone MC, Ross J, and Burr DC (1986). Mach bands are phase dependent. Nature *324*, 250-253.

213) Mota C, and Barth E (2000). On the uniqueness of curvature features. Proceedings in Artificial Intelligence *9*, 175-178.

214) Mountcastle VB (1957). Modality and topographic properties of single neurons of cat's somatic sensory cortex. Journal of Neurophysiology *20*, 408-434.

215) Mountcastle VB, Berman AL, and Davies PW (1955). Topographic organization and modality representation in first somatic area of cat's cerebral cortex by method of single unit analysis. American Journal of Physiology *183*, 646.

216) Movshon JA, Thompson ID, and Tolhurst DJ (1978a). Receptive field organization of complex cells in the cat's striate cortex. Journal of Physiology *283*, 79-99.

217) Movshon JA, Thompson ID, and Tolhurst DJ (1978b). Spatial summation in the receptive fields of simple cells in the cat's striate cortex. Journal of Physiology *283*, 53-77.

218) Muller JF, and Dacheux RF (1997). Alpha ganglion cells of the rabbit retina lose antagonistic surround responses under dark adaptation. Visual Neuroscience *14*, 395-401.

219) Murphy PC, Duckett SG, and Sillito AM (1999). Feedback connections to the lateral geniculate nucleus and cortical response properties. Science *286*, 1552-1554.

220) Murphy PC, and Sillito AM (1987). Corticofugal feedback influences the generation of length tuning in the visual pathway. Nature *329*, 727-729.

221) Nakayama K, and Silverman GH (1988). The aperture problem--II. Spatial integration of velocity information along contours. Vision Research *28*, 747-753.

222) Nawy S, and Copenhagen DR (1987). Multiple classes of glutamate receptor on depolarizing bipolar cells in retina. Nature *325*, 56-58.

223) Nelson JI, and Frost BJ (1978). Orientation-selective inhibition from beyond the classic visual receptive field. Brain Research *139*, 359-365.

224) Nelson R, Famiglietti EV, Jr., and Kolb H (1978). Intracellular staining reveals different levels of stratification for on- and off-center ganglion cells in cat retina. Journal of Neurophysiology *41*, 472-483.

225) Nelson R, and Kolb H (1983). Synaptic patterns and response properties of bipolar and ganglion cells in the cat retina. Vision Research *23*, 1183-1195.

226) Nichols JG, Martin AR, Wallace BG, and Fuchs PA, eds. (2001). From neuron to brain, 4 edn (Sunderland, Massachsetts, Sinauer Associates).

227) Norman JF, Phillips F, and Ross HE (2001). Information concentration along the boundary contours of naturally shaped solid objects. Perception *30*, 1285-1294.

228) Obermayer K, and Blasdel GG (1993). Geometry of orientation and ocular dominance columns in monkey striate cortex. Journal of Neuroscience *13*, 4114-4129.

229) Olavarria JF, and Van Essen DC (1997). The global pattern of cytochrome oxidase stripes in visual area V2 of the macaque monkey. Cerebral Cortex *7*, 395-404.

230) Østerberg G (1935). Topography of the layer of rods and cones in the human retina. Acta Ophthalmologica *6*, 1-103.

231) Pack CC, and Born RT (2001). Temporal dynamics of a neural solution to the aperture problem in visual area MT of macaque brain. Nature *409*, 1040-1042.

232) Pack CC, Gartland AJ, and Born RT (2004). Integration of contour and terminator signals in visual area MT of alert macaque. Journal of Neuroscience *24*, 3268-3280.

233) Pack CC, Livingstone MS, Duffy KR, and Born RT (2003). End-stopping and the aperture problem: two-dimensional motion signals in macaque V1. Neuron *39*, 671-680.

234) Paradiso MA, and Hahn S (1996). Filling-in percepts produced by luminance modulation. Vision Research *36*, 2657-2663.

235) Pasupathy A, and Connor CE (1999). Responses to contour features in macaque area V4. Journal of Neurophysiology *82*, 2490-2502.

236) Pasupathy A, and Connor CE (2001). Shape representation in area V4: position-specific tuning for boundary conformation. Journal of Neurophysiology *86*, 2505-2519.

237) Pasupathy A, and Connor CE (2002). Population coding of shape in area V4. Nature Neuroscience *5*, 1332-1338.

238) Pearlman AL, Birch J, and Meadows JC (1979). Cerebral color blindness: an acquired defect in hue discrimination. Annals of Neurology *5*, 253-261.

239) Peichl L, and Wassle H (1979). Size, scatter and coverage of ganglion cell receptive field centres in the cat retina. Journal of Physiology *291*, 117-141.

240) Peichl L, and Wassle H (1983). The structural correlate of the receptive field centre of alpha ganglion cells in the cat retina. Journal of Physiology *341*, 309-324.

241) Perkel DJ, Bullier J, and Kennedy H (1986). Topography of the afferent connectivity of area 17 in the macaque monkey: a double-labelling study. Journal of Comparative Neurology *253*, 374-402.

242) Perry VH, and Cowey A (1981). The morphological correlates of X- and Y-like retinal ganglion cells in the retina of monkeys. Experimental Brain Research *43*, 226-228.

243) Perry VH, Oehler R, and Cowey A (1984). Retinal ganglion cells that project to the dorsal lateral geniculate nucleus in the macaque monkey. Neuroscience *12*, 1101-1123.

244) Pessoa L, and De Weerd P, eds. (2003). Filling-in: from perceptual completion to cortical reorganization (Oxford, Oxford University Press).

245) Pillow JW, Paninski L, Uzzell VJ, Simoncelli EP, and Chichilnisky EJ (2005). Prediction and decoding of retinal ganglion cell responses with a probabilistic spiking model. Journal of Neuroscience *25*, 11003-11013.

246) Poggio GF, Doty RW, Jr., and Talbot WH (1977). Foveal striate cortex of behaving monkey: single-neuron responses to square-wave gratings during fixation of gaze. Journal of Neurophysiology *40*, 1369-1391.

247) Poggio T, and Edelman S (1990). A network that learns to recognize three-dimensional objects. Nature *343*, 263-266.

248) Polyak S (1941). The retina (Chicago, University of Chicago Press).

249) Powell TP, and Mountcastle VB (1959). Some aspects of the functional organization of the cortex of the postcentral gyrus of the monkey: a correlation of findings obtained in a single unit analysis with cytoarchitecture. Bulletin of Johns Hopkins Hospital *105*, 133-162.

250) Ramón y Cajal S (1893). La rétine des vertébrés. Cellule *9*, 17-257.

251) Rao RPN, Olshausen BA, and Lewicki MS (2002). Probabilistic models of the brain: perception and neural function (Cambridge, MA, MIT Press).

252) Ratcliff G, and Davies-Jones GA (1972). Defective visual localization in focal brain wounds. Brain *95*, 49-60.

253) Ratliff F (1965). Mach bands: Quantitative studies on neural networks in the retina (San Francisco, Holden-Day, Inc.).

254) Ratliff F, and Hartline HK (1959). The responses of Limulus optic nerve fibers to patterns of illumination on the receptor mosaic. Journal of General Physiology *42*, 1241-1255.

255) Regan D, Gray R, and Hamstra SJ (1996). Evidence for a neural mechanism that encodes angles. Vision Research *36*, 323-330.

256) Reich DS, Victor JD, and Knight BW (1998). The power ratio and the interval map: spiking models and extracellular recordings. Journal of Neuroscience *18*, 10090-10104.

257) Reid RC, and Alonso JM (1995). Specificity of monosynaptic connections from thalamus to visual cortex. Nature *378*, 281-284.

258) Resnikoff HL (1985). The illusion of reality: Topics in information science (New York, Springer-Verlag).

259) Ringach DL (2002a). Orientation selectivity in macaque V1: diversity and laminar dependence. Journal of Neuroscience *22*, 5639-5651.

260) Ringach DL (2002b). Spatial structure and symmetry of simple cell receptive fields in macaque primary visual cortex. Journal of Neurophysiology *88*, 455-463.

261) Rockland KS, and Lund JS (1983). Intrinsic laminar lattice connections in primate visual cortex. Journal of Comparative Neurology *216*, 303-318.

262) Rockland KS, Saleem KS, and Tanaka K (1994). Divergent feedback connections from areas V4 and TEO in the macaque. Visual Neuroscience *11*, 579-600.

263) Rodieck RW (1965). Quantitative analysis of cat retinal ganglion cell response to visual stimuli. Vision Research *5*, 583-601.

264) Rodieck RW (1998). The first steps in seeing (Sunderland, Massachusetts, Sinauer Associates).

265) Roorda A, and Williams DR (1999). The arrangement of the three cone classes in the living human eye. Nature *397*, 520-522.

266) Ross J, Morrone MC, and Burr DC (1989). The conditions under which Mach bands are visible. Vision Research *29*, 699-715.

267) Rubenstein BS, and Sagi D (1996). Preattentive texture segmentation: the role of line terminations, size, and filter wavelength. Perception and Psychophysics *58*, 489-509.

268) Sceniak MP, Hawken MJ, and Shapley R (2001). Visual spatial characterization of macaque V1 neurons. Journal of Neurophysiology *85*, 1873-1887.

269) Schiller PH, and Malpeli JG (1978). Functional specificity of lateral geniculate nucleus laminae of the rhesus monkey. Journal of Neurophysiology *41*, 788-797.

270) Schnitzer MJ, and Meister M (2003). Multineuronal firing patterns in the signal from eye to brain. Neuron *37*, 499-511.

271) Schultze M (1866). Zur Anatomie und Physiologie der Retina. Arch Mikrosk Anat Entwicklungsmech *2*, 165-286.

272) Sereno MI, Dale AM, Reppas JB, Kwong KK, Belliveau JW, Brady TJ, Rosen BR, and Tootell RB (1995). Borders of multiple visual areas in humans revealed by functional magnetic resonance imaging. Science *268*, 889-893.

273) Shadlen MN, and Newsome WT (1998). The variable discharge of cortical neurons: implications for connectivity, computation, and information coding. Journal of Neuroscience *18*, 3870-3896.

274) Shannon CE (1948). A mathematical theory of communication. Bell Systems Technical Journal *27*, 379-423, 623-656.

275) Shapley R, Hawken M, and Ringach DL (2003). Dynamics of orientation selectivity in the primary visual cortex and the importance of cortical inhibition. Neuron *38*, 689-699.

276) Shapley R, and Perry JS (1986). Cat and monkey retinal ganglion cells and their visual functional roles. Trends in Neuroscience 9, 229-235.

277) Shapley RM, and Victor JD (1978). The effect of contrast on the transfer properties of cat retinal ganglion cells. Journal of Physiology 285, 275-298.

278) Shapley RM, and Victor JD (1981). How the contrast gain control modifies the frequency responses of cat retinal ganglion cells. Journal of Physiology 318, 161-179.

279) Sherman SM, and Guillery RW (1998). On the actions that one nerve cell can have on another: distinguishing "drivers" from "modulators". Proceedings of the National Academy of Sciences of the United States of America 95, 7121-7126.

280) Sherman SM, and Guillery RW (2001). Exploring the thalamus (San Diego, Academic Press).

281) Sherrington CS (1906). The integrative action of the nervous system (New Haven, CT, Yale University Press).

282) Shevelev IA, Kamenkovich VM, and Sharaev GA (2003). The role of lines and corners of geometric figures in recognition performance. Acta Neurobiol Exp (Wars) 63, 361-368.

283) Shevelev IA, Lazareva NA, Sharaev GA, Novikova RV, and Tikhomirov AS (1998). Selective and invariant sensitivity to crosses and corners in cat striate neurons. Neuroscience 84, 713-721.

284) Shevelev IA, Lazareva NA, Sharaev GA, Novikova RV, and Tikhomirov AS (1999). Interrelation of tuning characteristics to bar, cross and corner in striate neurons. Neuroscience 88, 17-25.

285) Shipp S, and Zeki S (1985). Segregation of pathways leading from area V2 to areas V4 and V5 of macaque monkey visual cortex. Nature 315, 322-325.

286) Shipp S, and Zeki S (1989). The Organization of Connections between Areas V5 and V1 in Macaque Monkey Visual Cortex. Europena Journal of Neuroscience 1, 309-332.

287) Sigman M, Cecchi GA, Gilbert CD, and Magnasco MO (2001). On a common circle: natural scenes and Gestalt rules. Proceedings of the National Academy of Sciences of the United States of America *98*, 1935-1940.

288) Sillito AM, Grieve KL, Jones HE, Cudeiro J, and Davis J (1995). Visual cortical mechanisms detecting focal orientation discontinuities. Nature *378*, 492-496.

289) Slaughter MM, and Miller RF (1981). 2-amino-4-phosphonobutyric acid: a new pharmacological tool for retina research. Science *211*, 182-185.

290) Slaughter MM, and Miller RF (1983). An excitatory amino acid antagonist blocks cone input to sign-conserving second-order retinal neurons. Science *219*, 1230-1232.

291) Somers DC, Nelson SB, and Sur M (1995). An emergent model of orientation selectivity in cat visual cortical simple cells. Journal of Neuroscience *15*, 5448-5465.

292) Spillmann L, and Levine J (1971). Contrast enhancement in a Hermann grid with variable figure-ground ratio. Experimental Brain Research *13*, 547-559.

293) Steriade M, Jones EG, and McCormick DA, eds. (1997). Thalamus (New York, Elsevier).

294) Stone J, Dreher B, and Leventhal A (1979). Hierarchical and parallel mechanisms in the organization of visual cortex. Brain Research *180*, 345-394.

295) Suzuki W, Saleem KS, and Tanaka K (2000). Divergent backward projections from the anterior part of the inferotemporal cortex (area TE) in the macaque. Journal of Comparative Neurology *422*, 206-228.

296) Tadmor Y, and Tolhurst DJ (2000). Calculating the contrasts that retinal ganglion cells and LGN neurones encounter in natural scenes. Vision Research *40*, 3145-3157.

297) Tanaka K (1983). Cross-correlation analysis of geniculostriate neuronal relationships in cats. Journal of Neurophysiology *49*, 1303-1318.

298) Tomita T (1965). Electrophysiological study of the mechanisms subserving color coding in the fish retina. Cold Spring Harb Symp Quant Biol *30*, 559-566.

299) Touryan J, Lau B, and Dan Y (2002). Isolation of relevant visual features from random stimuli for cortical complex cells. Journal of Neuroscience *22*, 10811-10818.

300) Treisman AM, and Gelade G (1980). A feature-integration theory of attention. Cognit Psychol *12*, 97-136.

301) Trifonov YA (1968). Study of synaptic transmission between the photoreceptor and the horizontal cell using electrical stimulation of the retina. Biofizika *10*, 673-680.

302) Troncoso XG, Macknik SL, and Martinez-Conde S (2005). Novel visual illusions related to Vasarely's 'nested squares' show that corner salience varies with corner angle. Perception *34*, 409-420.

303) Troncoso XG, Macknik SL, and Martinez-Conde S (2006). Corner salience varies parametrically with corner angle during flicker-augmented contrast. Paper presented at: Visual Science Society 6th Annual Meeting (Sarasota, Florida, USA).

304) Troncoso XG, Tse PU, Macknik SL, Caplovitz, GP, Hsieh P-J, Schlegel AA, and Martinez-Conde S (2005a). fMRI correlates of corner-based illusions show that BOLD activation varies gradually with corner angle. Paper presented at: Society for Neuroscience 35th Annual Meeting (Washington DC, USA).

305) Troncoso XG, Tse PU, Macknik SL, Caplovitz, GP, Hsieh P-J, Schlegel AA, and Martinez-Conde S (2005b). fMRI correlates of corner-based illusions show that BOLD activation varies gradually with corner angle. Paper presented at: 28th European Conference on Visual Perception (A Coruña, Spain).

306) Troncoso XG, Tse PU, Macknik SL, Caplovitz, GP, Hsieh P-J, Schlegel AA, and Martinez-Conde S (2005c). fMRI correlates of corner illusions show that BOLD activation varies gradually with corner angle. Paper presented at: Optical Society of America Vision Meeting (Tucson, Arizona, USA).

307) Troyer TW, and Miller KD (1997). Physiological gain leads to high ISI variability in a simple model of a cortical regular spiking cell. Neural Computation *9*, 971-983.

308) Ts'o DY, Frostig RD, Lieke EE, and Grinvald A (1990). Functional organization of primate visual cortex revealed by high resolution optical imaging. Science *249*, 417-420.

309) Ts'o DY, Gilbert CD, and Wiesel TN (1986). Relationships between horizontal interactions and functional architecture in cat striate cortex as revealed by cross-correlation analysis. Journal of Neuroscience *6*, 1160-1170.

310) Tse PU (2002). A contour propagation approach to surface filling-in and volume formation. Psychological Review *109*, 91-115.

311) Ullman S (1989). Aligning pictorial descriptions: an approach to object recognition. Cognition *32*, 193-254.

312) Ungerleider LG, and Desimone R (1986a). Cortical connections of visual area MT in the macaque. Journal of Comparative Neurology *248*, 190-222.

313) Ungerleider LG, and Desimone R (1986b). Projections to the superior temporal sulcus from the central and peripheral field representations of V1 and V2. Journal of Comparative Neurology *248*, 147-163.

314) Ungerleider LG, and Mishkin M (1982). Two cortical visual systems. In Analysis of visual behavior, DG Ingle, MA Goodale, and JQ Mansfield, eds. (Cambridge, Massachusetts, MIT Press), pp. 549-586.

315) Usrey WM, Alonso JM, and Reid RC (2000). Synaptic interactions between thalamic inputs to simple cells in cat visual cortex. Journal of Neuroscience *20*, 5461-5467.

316) Van Essen DC, Anderson CH, and Felleman DJ (1992). Information processing in the primate visual system: an integrated systems perspective. Science *255*, 419-423.

317) Van Essen DC, and Gallant JL (1994). Neural mechanisms of form and motion processing in the primate visual system. Neuron *13*, 1-10.

318) Van Essen DC, and Zeki SM (1978). The topographic organization of rhesus monkey prestriate cortex. Journal of Physiology *277*, 193-226.

319) Vasarely V (1970). Vasarely II (Neuchâtel, Éditions du Griffon).

320) Vasarely V (1982). Gea (Paris, Editions Hervas).

321) Versavel M, Orban GA, and Lagae L (1990). Responses of visual cortical
neurons to curved stimuli and chevrons. Vision Research *30*, 235-248.

322) Verweij J, Dacey DM, Peterson BB, and Buck SL (1999). Sensitivity and
dynamics of rod signals in H1 horizontal cells of the macaque monkey retina.
Vision Research *39*, 3662-3672.

323) von Békésy G (1960). Neural inhibitory units of the eye and the skin.
Quantitative description of contrast phenomena. Journal of the Optical
Society of America *50*, 1060-1070.

324) von Békésy G (1968). Brightness distribution across the Mach bands measured
with flicker photometry, and the linearity of sensory nervous interaction.
Journal of the Optical Society of America *58*, 1-8.

325) Walker GA, Ohzawa I, and Freeman RD (1999). Asymmetric suppression
outside the classical receptive field of the visual cortex. Journal of
Neuroscience *19*, 10536-10553.

326) Wandell BA (1995). Foundations of vision (Sunderland, Massachusetts, Sinauer
Associates).

327) Wässle H, and Boycott BB (1991). Functional architecture of the mammalian
retina. Physiological Reviews *71*, 447-480.

328) Watanabe M, and Rodieck RW (1989). Parasol and midget ganglion cells of the
primate retina. Journal of Comparative Neurology *289*, 434-454.

329) Watt RJ (1984). Further evidence concerning the analysis of curvature in human
foveal vision. Vision Research *24*, 251-253.

330) Watt RJ (1985). Psychophysics. Structured representation in low-level vision.
Nature *313*, 266-267.

331) Watt RJ (1986). Feature-based image segmentation in human vision. Spatial
Vision *1*, 243-256.

332) Watt RJ (1988). Visual processing: computational, psychophysical and cognitive
research (Hove, Lawrence Erlbaum Associates).

333) Watt RJ, and Andrews DP (1982). Contour curvature analysis: hyperacuities in the discrimination of detailed shape. Vision Research *22*, 449-460.

334) Wehmeier U, Dong D, Koch C, and Van Essen D (1989). Modeling the visual system. In Methods in neuronal modeling, C Koch, and I Segev, eds. (Cambridge, MA, MIT Press), pp. 335-359.

335) Werblin FS, and Dowling JE (1969). Organization of the retina of the mudpuppy, Necturus maculosus. II. Intracellular recording. Journal of Neurophysiology *32*, 339-355.

336) Werner H (1935). Studies on countour: I. Qualitative analyses. American Journal of Psychology *47*, 40-64.

337) Wichmann FA, and Hill NJ (2001). The psychometric function: I. Fitting, sampling, and goodness of fit. Perception and Psychophysics *63*, 1293-1313.

338) Wiesel TN, Hubel DH, and Lam DM (1974). Autoradiographic demonstration of ocular-dominance columns in the monkey striate cortex by means of transneuronal transport. Brain Research *79*, 273-279.

339) Wilson JR, and Sherman SM (1976). Receptive-field characteristics of neurons in cat striate cortex: Changes with visual field eccentricity. Journal of Neurophysiology *39*, 512-533.

340) Wiser AK, and Callaway EM (1996). Contributions of individual layer 6 pyramidal neurons to local circuitry in macaque primary visual cortex. Journal of Neuroscience *16*, 2724-2739.

341) Wolfe JM, Yee A, and Friedman-Hill SR (1992). Curvature is a basic feature for visual search tasks. Perception *21*, 465-480.

342) Worgotter F, and Koch C (1991). A detailed model of the primary visual pathway in the cat: comparison of afferent excitatory and intracortical inhibitory connection schemes for orientation selectivity. Journal of Neuroscience *11*, 1959-1979.

343) Yang Z, and Purves D (2003). Image/source statistics of surfaces in natural scenes. Network *14*, 371-390.

344) Zeki SM (1974a). Cells responding to changing image size and disparity in the cortex of the rhesus monkey. Journal of Physiology *242*, 827-841.

345) Zeki SM (1974b). Functional organization of a visual area in the posterior bank of the superior temporal sulcus of the rhesus monkey. Journal of Physiology *236*, 549-573.

346) Zeki SM (1978a). Functional specialisation in the visual cortex of the rhesus monkey. Nature *274*, 423-428.

347) Zeki SM (1978b). Uniformity and diversity of structure and function in rhesus monkey prestriate visual cortex. Journal of Physiology *277*, 273-290.

348) Zetzsche C, and Barth E (1990). Fundamental limits of linear filters in the visual processing of two-dimensional signals. Vision Research *30*, 1111-1117.

349) Zhaoping L (2005). The primary visual cortex creates a bottom-up saliency map. In Neurobiology of Attention, L Itti, G Rees, and JK Tsotsos, eds. (Elsevier), pp. 570-575.

350) Zihl J, von Cramon D, and Mai N (1983). Selective disturbance of movement vision after bilateral brain damage. Brain *106 (Pt 2)*, 313-340.